การพัฒนาซิลิกอนไนไตรด์เซรามิกที่มีต้นทุนการผลิตต่ำ

นายนิรุติ หวังหมู่กลาง

วิทยานิพนธ์นี้เป็นส่วนหนึ่งของการศึกษาตามหลักสูตรปริญญาวิทยาศาสตรมหาบัณฑิต
สาขาวิชาเทคโนโลยีเซรามิก ภาควิชาวัสดุศาสตร์
คณะวิทยาศาสตร์ จุฬาลงกรณ์มหาวิทยาลัย
ปีการศึกษา 2546
ISBN 974-17-4721-7

DEVELOPMENT OF LOW COST Si_3N_4 CERAMICS

Mr. Nirut Wangmooklang

A Thesis Submitted in Partial Fulfillment of the Requirements
for the Degree of Master of Science in Ceramic Technology

Department of Materials Science

Faculty of Science

Chulalongkorn University

Academic Year 2003

ISBN 974-17-4721-7

Thesis Title	Development of low cost Si_3N_4 ceramics
By	Mr. Nirut Wangmooklang
Field of study	Materials Science
Thesis Advisor	Chair Professor Shigetaka Wada, Ph.D.
Thesis Co-advisor	Kuljira Sujirote, Ph.D.

Accepted by the Faculty of Science, Chulalongkorn University in Partial Fulfillment of the Requirements for the Master's Degree

…….. Dean of Faculty of Science
(Professor Piamsak Menasveta, Ph.D.)

THESIS COMMITTEE

…….. Chairman
(Associate Professor Saowaroj Chuayjuljit)

…….. Thesis Advisor
(Chair Professor Shigetaka Wada, Ph.D.)

…….. Thesis Co-advisor
(Kuljira Sujirote, Ph.D.)

…….. Member
(Associate Professor Supatra Jinawath, Ph.D.)

…….. Member
(Sirithan Jiemsirilers, Ph.D.)

นิรุติ หวังหมู่กลาง : การพัฒนาซิลิกอนไนไตรด์เซรามิกที่มีต้นทุนการผลิตต่ำ.
(DEVELOPMENT OF LOW COST Si_3N_4 CERAMICS) อ. ที่ปรึกษา : ศ. ดร. ชิเกตากะ วาดะ,
อ.ที่ปรึกษาร่วม : ดร. กุลจิรา สุจิโรจน์, จำนวนหน้า 106 หน้า. ISBN 974-17-4721-7

งานวิจัยนี้เป็นการศึกษาการพัฒนาซิลิกอนไนไตรด์ที่มีต้นทุนการผลิตต่ำ โดยใช้สารตั้งต้นและวิธีการซินเทอร์ที่มีต้นทุนต่ำ คือใช้ผงเบต้าซิลิกอนไนไตรด์ แมกนีเซีย และอะลูมินา เป็นสารตั้งต้น และทำการซินเทอร์ในเตาเผาบรรยากาศปกติ การขึ้นรูปทำโดยการบดผสมวัสดุผง 90wt%Si_3N_4 + 5wt%MgO + 5wt%Al_2O_3 เป็นเวลา 4 ถึง 16 ชั่วโมง จากนั้นนำผงผสมอัดในแม่พิมพ์ เครื่องอัดทุกทิศทาง นำชิ้นตัวอย่างซิลิกอนไนไตรด์มาซินเทอร์ในเบ้าอะลูมินาและกลบทับด้วยผงซิลิกอนไนไตรด์และอะลูมินาในเตาเผาบรรยากาศปกติ ที่อุณหภูมิ 1500 °C ถึง 1700 °C เป็นเวลา 2 ชั่วโมง และมีการซินเทอร์ผงซิลิกอนไนไตรด์ที่บดผสมกับสารปรับปรุงสมบัติเป็นเวลา 4 ถึง 8 ชั่วโมง ในเตาเผาบรรยากาศก๊าซไนโตรเจนที่อุณหภูมิ 1750 °C ถึง 1800 °C ที่ความดันก๊าซไนโตรเจน 1 บรรยากาศ เป็นเวลา 2 ชั่วโมงเพื่อเปรียบเทียบสมบัติของชิ้นงานหลังการซินเทอร์กับการซินเทอร์ในเตาเผาบรรยากาศปกติชิ้นงานซิลิกอนไนไตรด์หลังการซินเทอร์ในเตาเผาบรรยากาศปกติทุกตัวอย่างมีค่าความหนาแน่นทางทฤษฎีมากกว่า 96 เปอร์เซ็นต์ที่อุณหภูมิ 1700 °C และชิ้นงานที่ได้จากการซินเทอร์ผงตัวอย่างที่ใช้เวลาในการบดผสมเป็นเวลา 4 ถึง 8 ชั่วโมง มีความแข็ง ความต้านทานต่อการแตกหัก และความต้านทานแรงดัดอยู่ในช่วง 12.7 ถึง 13.0 GPa 5.5 ถึง 6.1 MPa.$m^{1/2}$ และ 238 ถึง 263 MPa ตามลำดับ ซึ่งมีค่าน้อยกว่าชิ้นงานที่ได้จากการซินเทอร์ของผสมชนิดเดียวกันในเตาเผาบรรยากาศก๊าซไนโตรเจนที่มีความแข็ง ความต้านทานต่อการแตกหัก และความต้านทานแรงดัดอยู่ในช่วง 13.3 ถึง 13.8 GPa 6.1 ถึง 6.8 MPa.$m^{1/2}$ และ 327 ถึง 406 MPa ตามลำดับ อย่างไรก็ตามความต้านทานแรงดัดยังมีค่าต่ำเมื่อเทียบกับทางการค้าซึ่งมีค่า 500 ถึง 600 MPa.

ภาควิชาวัสดุศาสตร์ ลายมือชื่อนิสิต.....
สาขาเทคโนโลยีเซรามิก ลายมือชื่ออาจารย์ที่ปรึกษา.....
ปีการศึกษา 2546 ลายมือชื่ออาจารย์ที่ปรึกษาร่วม.....

4472527823 : MAJOR CERAMIC TECHNOLOGY

KEYWORD : β-Si_3N_4 / AIR ATMOSPHERE FURNACE / SINTERING / MAGNESIA /ALUMINA

NIRUT WANGMOOKLANG : DEVELOPMENT OF LOW COST Si_3N_4 CERAMICS.

THESIS ADVISOR : CHAIR PROF. SHIGETAKA WADA, Ph.D., THESIS CO-ADVISOR : KULJIRA SUJIROTE, Ph.D., 106 pp. ISBN 974-17-4721-7

Development of low cost Si_3N_4 ceramics is studied by using low cost starting materials, β-Si_3N_4 powder with MgO and Al_2O_3 additives, and sintering in air atmosphere furnace. Fabrication processes were performed by mixing and grinding 90wt%Si_3N_4 + 5wt%MgO + 5wt%Al_2O_3 powders for 4 to 16 hours. Then, the mixture was uniaxially and isostatically pressed into specimens. The specimens were placed in a set of specially designed alumina crucibles with silicon nitride and alumina packing powders and sintered in air atmosphere furnace at temperature ranging from 1500 to 1700°C for 2 hours. Sintering of β-Si_3N_4 powder in N_2 gas furnace at a temperature of 1750 to 1800 °C for 2 hours with N_2 gas pressure of 0.1 MPa was also operated in order to compare with the specimens sintered in air furnace. The theoretical densities of all specimens sintered in air furnace were over 96 % at the sintering temperature of 1700 °C. Vickers hardness, fracture toughness, and flexural strength of specimens sintered from mixed powder for 4 to 8 hours were from 12.7 to 13.0 GPa, 5.5 to 6.1 MPa.$m^{1/2}$, and 238 to 263 MPa, respectively. These values were less than the specimens sintered from the same powder in N_2 gas furnace of which the Vickers hardness, fracture toughness, and flexural strength are 13.3 to 13.8 GPa, 6.1 to 6.8 MPa.$m^{1/2}$, and 327 to 406 MPa, respectively. However, the values of flexural strength are relatively low, when compared with 500-600 MPa of commercial Si_3N_4 ceramics.

Department Materials Science — Student's signature……

Field of study Ceramic Technology — Advisor's signature……..

Academic year 2003 — Co-advisor's signature……

Acknowledgements

This work was accomplished under the supervision of my thesis advisor, Professor Dr. Shigetaka Wada, Chair Professor of the Department of Materials Science, Faculty of Science, Chulalongkorn University. I would like to gratefully thank for his guidance, and invaluable suggestion throughout this research. My sincere appreciation is expressed to my thesis co-advisor, Dr. Kuljira Sujirote, National Metal and Materials Technology Center (MTEC), for her kindness understanding and valuable advice. I also would like to thank Associate Professor Dr. Supatra Jinawath for her suggestion and grammar proofreading of my thesis.

I also wish to express my appreciation to Mr. Thanakorn Wasanapienpong for his help and suggestions. Special thanks to the staff of Department of Geology, Faculty of Science, Chulalongkorn University for the kind support of phase analysis in this experiment. My thank is also extended to the staff of Scientific and Technological Research Equipment Center, Chulalongkorn University (STREC) for the help in hardness and fracture toughness investigation.

Many thanks are due to my friends and faculty members in the Department of Materials Science for friendship and support. Finally, I would like to express my deep appreciation to my family for their love, patience and understanding and I also would like to gratefully acknowledge MTEC for granting me the TGIST scholarship during my M.S. study.

CONTENTS

Page

CONTENTS (Cont.)

LIST OF TABLES

Page

LIST OF FIGURES

Page

LIST OF FIGURES (Cont.)

Page

CHAPTER I
INTRODUCTION

1.1 Introduction

Silicon nitride ceramics have been intensively studied for many years because of their great potential for structural applications at room and elevated temperatures. This due to their excellent mechanical properties in combination with good corrosion and thermal shock resistance.[1-3] Silicon nitride is a covalent ceramic and is difficult to consolidate by solid state sintering because of a low diffusivity.[1,4] Hence, sintering additives such as MgO, Y_2O_3, CeO_2, Y_2O_3-Al_2O_3 must be used to enhance densification.[4-7]

An α-Si_3N_4 powder with Y_2O_3-Al_2O_3 additives is one of the most popular system for densification of Si_3N_4 because the resulted ceramics show excellent mechanical properties [8-9]. However, α-Si_3N_4 powder and Y_2O_3 are so expensive and must be sintered in a furnace with applied N_2 gas pressure.[6-9] As a result, the production cost of silicon nitride ceramics rises so high.

Sintering of β-Si_3N_4 powder has been investigated by several researchers. However, they used high gas pressure sintering at high temperature with Y_2O_3-Al_2O_3, Y_2O_3-Nd_2O_3 sintering additives [10-17] and the experimental results of them such as mechanical properties were satisfied. The results are still uneconomical because of the high costs incurred by the sintering methods and expensive sintering additives. Therefore, in this research we focus on the sintering of β-Si_3N_4 powder (SN-F2) with MgO-Al_2O_3 additives, because β-Si_3N_4 powder (SN-F2) and MgO are less expensive than α-Si_3N_4 and Y_2O_3 powders, respectively. And sintering in air atmosphere furnace, invented by Prof. Dr. Shigetaka Wada et al., was promising.[18] According to this system, we expect to get low production cost of Si_3N_4 ceramics.

The scope of this experiment is to study the sintering of β-Si_3N_4 powder with MgO-Al_2O_3 additives, which is sintered in a temperature range between 1500 °C to 1700 °C at an interval of 50 °C, in air atmosphere furnace. Also sintering in N_2 gas furnace at a temperature range between 1750 °C and 1800 °C was performed as the reference to the result of sintering in air.

1.2 The objectives of this research

1. To get the optimal condition for grinding and mixing of Si_3N_4 powder with sintering additives.

2. To study the sinterability of β-Si_3N_4 powder with MgO-Al_2O_3 additives and mechanical properties of sintered β-Si_3N_4 ceramic.

3. To pursue the technological knowledge on the sintering of low cost Si_3N_4 powder and sintering additives.

CHAPTER II

LITERATURE REVIEW

2.1 Crystal structure, properties and applications of Si_3N_4 ceramics

2.1.1 Crystal structure of Si_3N_4

The tetrahedra structure (SiN_4) is the basis of crystalline Si_3N_4 (Fig. 2.1a) [19]. The silicon atoms are in the center site of irregular nitrogen tetrahedral and each nitrogen atom belongs to three tetrahedra as shown in Fig 2.1a and 2.1b. [20] It is indicated that the SiN_4 tetrahedra introduces an open structure with large voids.

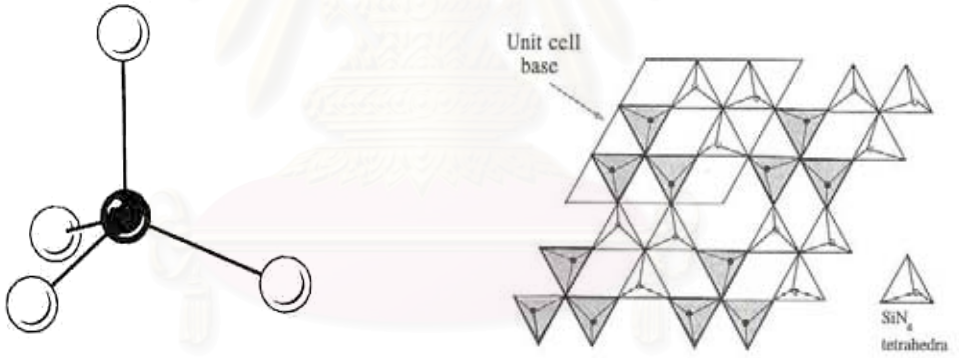

(a) (b)

Fig 2.1 (a) The basis of crystalline Si_3N_4 tetrahedra[19]. (b) Outline of silicon nitride crystal structure [20]

Silicon nitride occurs in two polytypes, the α and β phases[19,21]. Both are hexagonal, but differ in the sequence in which Si-N layers are arranged in the c-axis direction. The β-Si_3N_4 has an ABAB stacking sequence of layers with a unit cell of formula Si_6N_8, while α-Si_3N_4 has an ABCD stacking sequence of layers and twice the unit cell formula, $Si_{12}N_{16}$. Since in α-Si_3N_4 the stacking repeats after twice the number of layers, it has approximately twice the c-axis lattice parameter of the β phase (see Table 2.1).[22]

Fig 2.2a shows the atomic arrangement in a single AB layer sequence. The N atoms indicated by the filled triangles and the layer of Si atoms shown as filled circles lie in a plane forming the base of the unit cell. The Si atoms in this layer are indicated by "0" in the schematic in Fig. 2.2b. The next layers of N and Si atoms are shown as open circles and triangles, and are located at the "1/2" position in Fig. 2.2b. Noticed that a ring-like configuration of Si-N-Si-N bonds exists, with either 8 or 12 membered rings (similar configuration exists in the crystalline silicates). In β-Si_3N_4 the next AB layer is superimposed directly over the first, so that a continuous interstitial channel parallel to the c-axis forms around the site surrounded by 12 Si-N bonds. In α-Si_3N_4 the CD layer shown in Fig. 2.2c is superimposed on the AB layer. This isolates the large interstices formed by the 12-membered ring. The height of Si atoms above the base of the unit cell in the α phase is shown in Fig.2.2d. The availability of large interstitial sites in both structures facilitates the formation of oxynitride solid solutions.

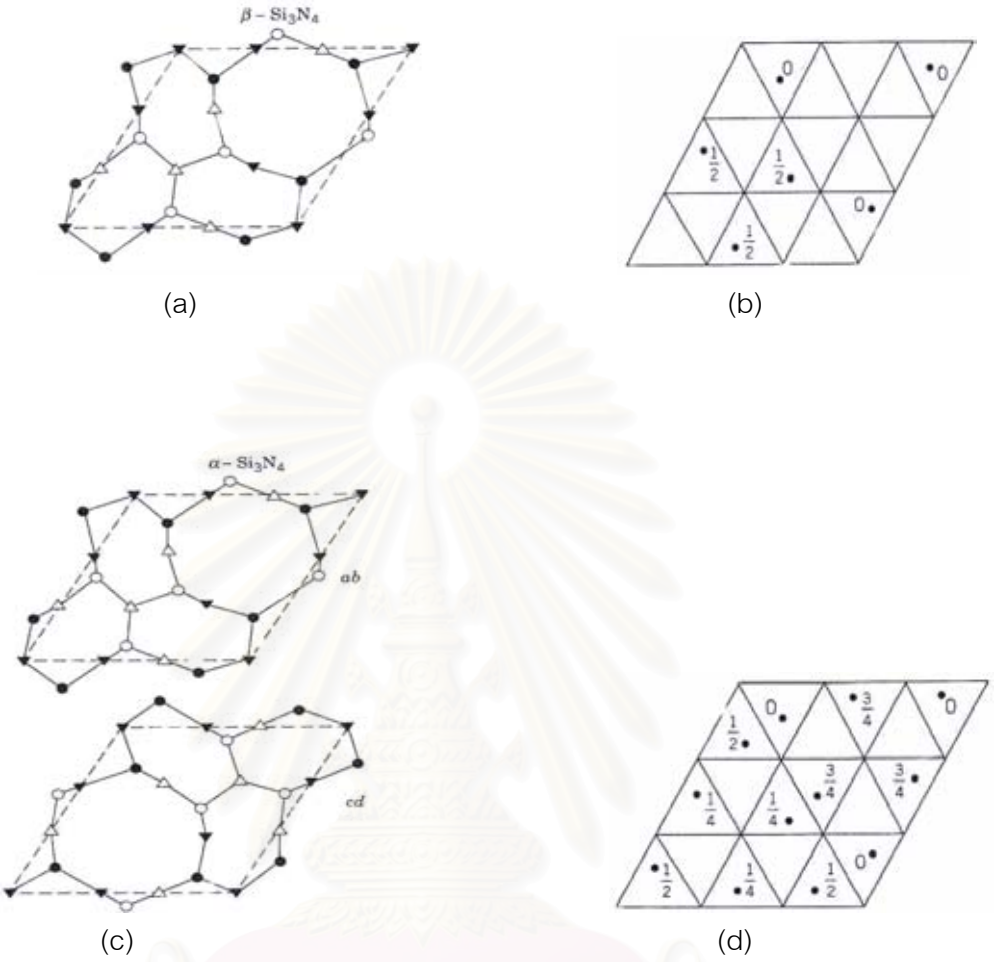

Fig. 2.2 (a) AB layer, which is repeated in the stacking sequence of β-Si_3N_4. (b) Positions of Si atoms above the base of the unit cell in β-Si_3N_4. (c) AB and CD layers, which are alternated in the stacking sequence of α-Si_3N_4. (d) Positions of Si atoms above the base of the unit cell in α-Si_3N_4. [19)]

2.1.2 Properties of Si_3N_4

The properties of Si_3N_4 ceramics are shown in Table 2.1.

Table 2.1 Properties of silicon nitride ceramics [22)]

Decomposition temperature (°C)	1900
Theoretical density (g cm^{-3})	
α-phase	3.168-3.188
β-phase	3.19-3.202
Density (g cm^{-3}):	
dense Si_3N_4	90-100 % th.d.*
Coefficient of thermal expansion	
(20-1500 °C) (10^{-6} °C^{-1})	2.9-3.6
Thermal conductivity (RT) (W m^{-1} K^{-1}):	
dense Si_3N_4	15-50
Thermal diffusivity (RT) (cm^2 sec^{-1}):	
dense Si_3N_4	0.08-0.29
Specific heat (J kg^{-1} °C^{-1})	700
Electrical resistivity (RT) (Ωcm)	~ 10^{13}
Microhardness (Vickers, MN m^{-2})	1600-2200
Young's modulus, (RT) (GN m^{-2}):	
dense Si_3N_4	300-330
Flexural strength (RT) (MN m^{-2}):	
dense Si_3N_4	400-95
Fracture toughness (MN $m^{-3/2}$):	
dense Si_3N_4	3.4-8.2
Thermal stress resistance	
Parameter $R = \sigma_F(1-\nu)/\alpha E$ (°C)	
and $R' = R\lambda(10^3-\nu)$ W m^{-1}):	
dense Si_3N_4	R = 300-780 R' = 7-32

* Theoretical density is dependent on the type and composition of consolidation aids (t.d. of pure Si_3N_4 = 3.2 g cm^{-3})

2.1.3 Applications of Si_3N_4 ceramics

Silicon nitride has better high temperature properties, such as strength, creep and oxidation resistance, than metals. In addition, its low thermal expansion coefficient gives good thermal shock resistance compared with most other ceramic materials.

Table 2.2 and Fig. 2.3 show typical Si_3N_4 components, for several application fields. Heat or wear resistant components, such as mechanical seals, cutting tools and glow plugs, are shown. [20,23)]

Table 2.2 Expected fields of application of silicon nitride ceramics [23)]

Application fields	Components
Wear-and corrosion-resistant components	Bearings, mechanical seals, blast honing nozzles, vane pump parts, chemical pump parts
Metal treatment components	Aluminum diecast parts (metal melt guides, plungers, cylinders, and piston cylinders); wire-drawing roller pulleys and dies; steel forming parts
Tools	Cutting tolls
Heat-resistant jigs:	
Heat-protecting parts	Thermal-insulation ceramic tiles, heat-shielding plates, plasma insulators
High-temperature test jigs	Strength test jigs (bend and tensile)

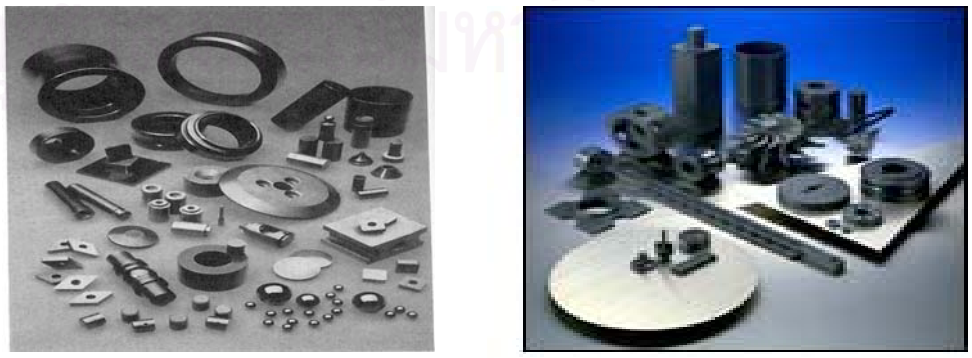

Fig. 2.3 Sintered Si_3N_4 components [20,24)]

2.2 Silicon nitride powders

There are four main technologies to produce Si_3N_4 powder.[25-28] Si_3N_4 powders synthesized by the method a) and d) are commercially produced.

a) Nitridation of silicon powder :

$$3Si + 2N_2 \square Si_3N_4 \qquad \text{----------(1)}$$

b) Gas-phase deposition :→

$$3SiCl_4 + 4NH_3 \rightarrow Si_3N_4 + 12HCl \uparrow \qquad \text{----------(2)}$$

c) Carbo-thremal reduction of SiO_2 in notrogen atmosphere :

$$3SiO_2 + 6C + 2N_2 \square Si_3N_4 + 6CO \square \qquad \text{----------(3)}$$

d) Precipitation of silicon diimide and thermal decomposition :

$$SiCl_4 + 6NH_3 \square Si(NH)_2 + 4NH_4Cl \square \qquad \text{----------(4)}$$

$$3Si(NH)_2 \square Si_3N_4 + 2NH_3 \square \qquad \text{----------(5)}$$

There are marked differences in the type and amount of impurities, in the size and morphology of the powder particles and the phase composition of powders obtained from these techniques. By varying the processing conditions, however, the properties of powders produced by any of these techniques may be changed, particularly the phase composition, degree of crystallinity and particle morphology.

The prices of Si_3N_4 powders depend on the characteristic of powders such as □/□ ratio, purity and mean particle size or specific surface area.

2.3 Sintering mechanism of Si_3N_4 ceramics

Pure Si_3N_4 is difficult to densify because of the high covalent nature of the Si-N bonds. [29] The self-diffusion coefficient is very low in comparison to other ceramic materials. Usually the densification of Si_3N_4 is achieved through the acceleration of mass transport by the formation of a liquid phase during sintering. The liquid phase used for sintering is an oxynitride liquid formed by the reaction of sintering additives with the SiO_2 existing on the surface of the Si_3N_4 powder particles. The most commonly used additives are Al_2O_3 in combination with Y_2O_3, La_2O_3, lanthanoids or MgO. [6,9,30]

The polymorphic forms of the starting powders (α or β) have a definite influence on the morphology of the consolidated structure. When the starting powder contains mainly α phase material, the particles first dissolute into grain boundary liquid and precipitate as long rod like acicular grains of β. When the starting powder is β phase, the β phase particles merely coalesce and grow.

The dissolution-precipitation mechanisms of both α and β phase powders during liquid phase sintering are shown in Fig 2.4.

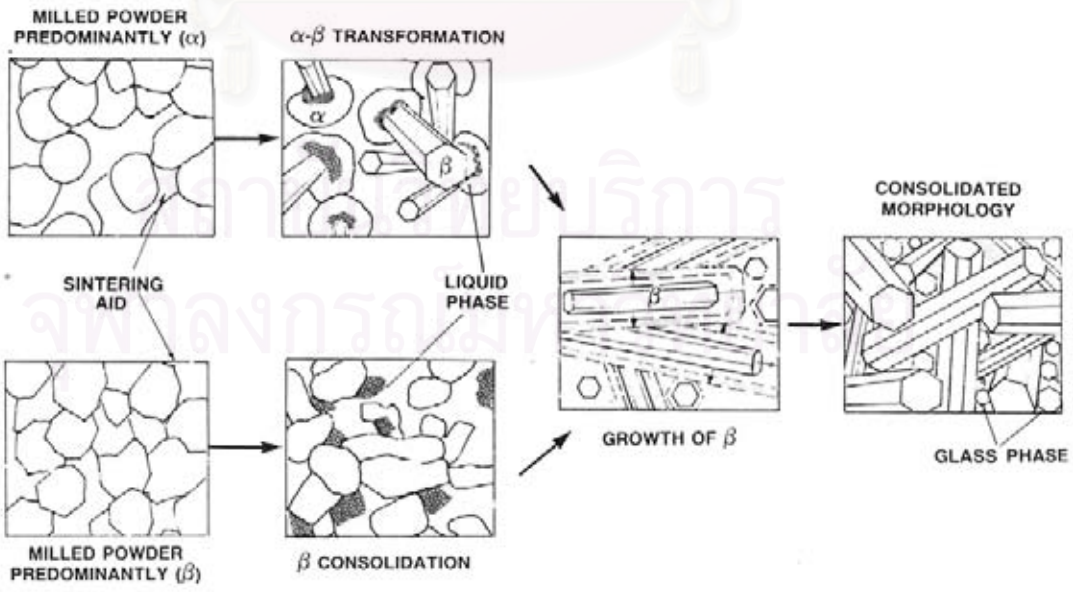

Fig 2.4 Schematic diagram illustrating the morphological development of β-Si_3N_4 grains during consolidation [31]

2.4 Instability of Si_3N_4 and Si_3N_4 ceramics

Si_3N_4 is thermodynamically unstable with respect to oxidation. Moreover, Si_3N_4 decomposes at high temperature and Si_3N_4 ceramics show mass loss reaction during sintering.

2.4.1 Oxidation of Si_3N_4

The oxidation occurs by two mechanisms, passive oxidation and active oxidation as shown in reaction (1) and (2), respectively. [32)]

$$Si_3N_4\ (s) + 3O_2\ (g) \longrightarrow 3SiO_2\ (l) + 2N_2\ (g) \qquad \text{----------(6)}$$

$$2Si_3N_4\ (s) + 3O_2\ (g) \longrightarrow 6SiO\ (g) + 4N_2\ (g) \qquad \text{----------(7)}$$

Silicon nitride and silicon nitride ceramics are easily oxidized in air at elevated temperature above 1000 °C. The oxidation mechanisms are passive oxidation in the atmosphere of $PO_2 \geq 10^2$ and active oxidation at less than 10^2 Pa. [32)] A SiO_2 protective layer is formed on a surface of specimen by passive oxidation and active oxidation occurs with formation of volatile SiO.

2.4.2 Decomposition of Si_3N_4

Fig 2.5 shows the stability diagram of Si_3N_4, silicon nitride does not have a melting point but decomposes under 0.1 MPa N_2 at 1900 °C. From the thermodynamic viewpoint, Si_3N_4 (s) decomposes to Si (l) and N_2 (g) at the sintering temperature in vacuum according to the reaction (8).[33)]

$$Si_3N_4\ (s) \longrightarrow 3Si\ (l) + 2N_2\ (g) \qquad \text{----------(8)}$$

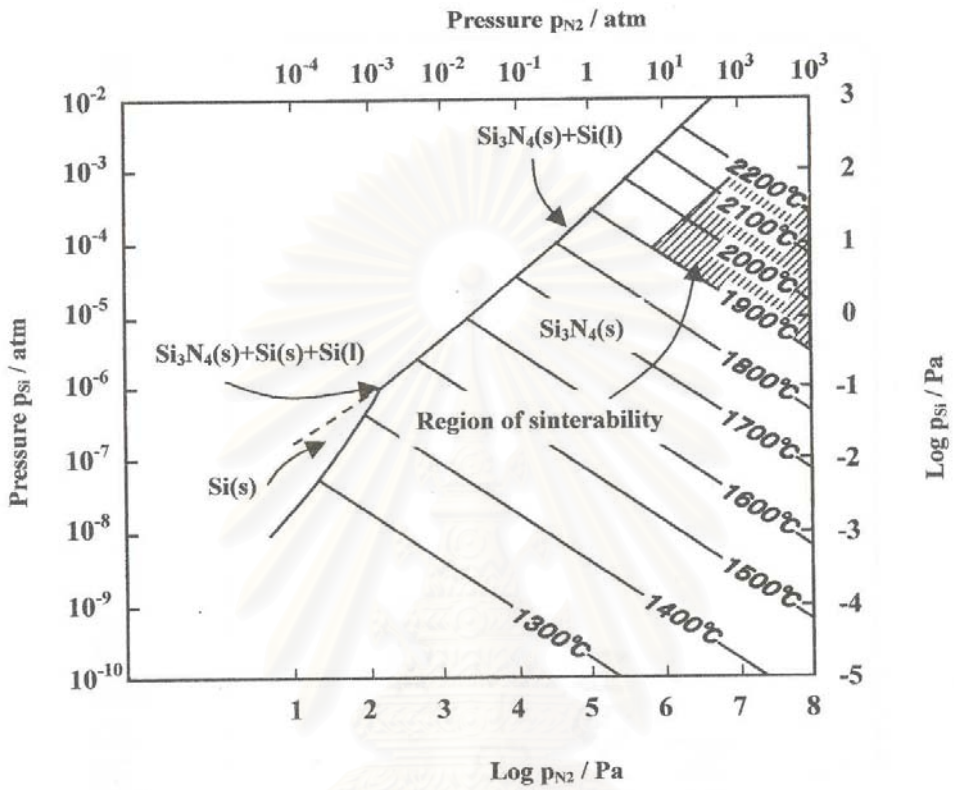

Fig 2.5 Stability diagram for Si_3N_4, where Si vapor is in equilibrium with Si_3N_4 as a function of N_2 pressure and temperature

From the stability diagram, N_2 gas pressure as high as $P_{N2} > 10^6$ Pa is essential to obtain dense Si_3N_4 ceramics at high sintering temperature. In other words, high N_2 gas pressure in the furnace effectively suppresses the mass loss during sintering.

2.5 Sintering of Si_3N_4 ceramic in air furnace

Non-pressurized sintering of Si_3N_4 ceramic in N_2 gas furnace is thought to be a low cost fabrication. But N_2 gas furnace is still special comparing to air furnace. According to Wada et al. in 2001, Si_3N_4 ceramic could be sintered without serious oxidation in air atmosphere furnace.[18] To isolate Si_3N_4 specimen from air, it is set in two Al_2O_3 crucibles that are filled with Si_3N_4 powder in the inner crucible and Al_2O_3 powder in the outer crucible. When Si_3N_4 ceramics are sintered in the mentioned sagger, there are two different sources of oxygen: one is the oxygen in the sagger, the other is the oxygen diffusing into the sagger through a gap. The amount of oxygen calculated from the volume of the sagger is not so large. When the sagger is filled with Si_3N_4 powder, the powder consumes oxygen in the sagger via Reaction (6) and then, when PO_2 in the sagger decreases to below 10^2 Pa, Reaction (7) occurs, three moles of O_2 (g) change to 6 mol of SiO (g) and 4 mol of N_2 (g). Therefore, once active oxidation occurs, the generated gas increases in volume and flows out through the gap of the sagger, thereby decreasing the oxygen partial pressure in the sagger and disturbing the diffusion of air from outside of the sagger. After most of the oxygen in the sagger has reacted with Si_3N_4, the generated gas flow stops and air will again diffuse into the sagger. However, since the sagger is filled with Si_3N_4 powder, oxygen diffusing into the sagger reacts with Si_3N_4 powder near the gap of the sagger and these will not reach the Si_3N_4 specimen. Therefore, Si_3N_4 ceramics could be sintered without serious oxidation and mass loss in air atmosphere furnace.

2.6 Literature survey of sintering of β-Si_3N_4 powder

Sintering of β-Si_3N_4 powder with Y_2O_3-Al_2O_3 or Y_2O_3-Nd_2O_3 sintering additives by using N_2 gas atmosphere furnace was investigated by several researchers. The experimental conditions and mechanical properties are shown in Table 2.3.

Table 2.3 Literature survey of sintering of β-Si_3N_4 powder with various additives, sintering temperature and gas pressure

Authors	Sintering additives	β phase content in powder (%)	Sintering conditions	Flexural strength (MPa) / Fracture toughness (MPa $m^{1/2}$)	References
Mitomo et al.	Y_2O_3-Al_2O_3	>99	1950 °C, N_2 10 MPa	467 / 5.8	17
Hirosaki et al.	Y_2O_3-Nd_2O_3	95	1900-2000 °C, N_2 10-30 MPa	515-689 / 8.5-10.3	34
Hirosaki et al.	Y_2O_3-Al_2O_3	95	1800-1900 °C, N_2 1-10 MPa	358-900 / 3.1-7.1	12
Hirosaki et al.	Y_2O_3-Nd_2O_3	>99	1900 °C, N_2 10 MPa	600-843 / 5.3-7.1	13
Ogasawa et al.	Y_2O_3-Nd_2O_3	>99	1900-2000 °C, N_2 10-30 MPa	678-746 / 7.2-9.0	15
Okamoto et al.	Y_2O_3-Al_2O_3	>99	1900 °C, N_2 1 MPa	689 / 6.4	16

In 1990, Mamoru Mitomo et al., [17] investigated in the topic of "Grain growth during gas-pressure sintering of β-silicon nitride". This work was performed using over 99 mass % of β-Si_3N_4 powder and Y_2O_3-Al_2O_3 as sintering additives. The sample was sintered at 1950 °C under N_2 gas pressure of 10 MPa.

In 1993, Naoto Hirosaki et al.,[34] investigated the effect of grain growth of β-silicon nitride on strength, Weibull modulus, and fracture toughness using 95 mass % of β-Si_3N_4 powder with Y_2O_3 and Nd_2O_3 additives. The sintering process was performed using the temperature range of 1900 °C to 2000 °C at N_2 gas pressure of 10-30 MPa. Then, after one and two years, they studied in the titles, "Sintering of Y_2O_3-Al_2O_3-doped β-Si_3N_4 powder and mechanical properties of sintered materials"[12], and "Effect of purification of β-Si_3N_4 powder on the strength of sintered materials"[13], respectively. Both of research work were performed using β-Si_3N_4 powder with Y_2O_3, Al_2O_3 and Nd_2O_3 additives, and sintering at the temperature range of 1800 °C to 1900 °C under the N_2 gas pressure of 1-10 MPa.

In 1995, Toshio Ogasawara et al,[15] and Yusuke Okamoto et al [16] investigated in the topics of "Fatigue behavior of silicon nitride ceramics prepared from β-phase powder" and "Mechanical properties and oxidation resistance of silicon nitride produced from low purity β-powder", respectively. In the work of Ogasawara and Okamoto works, high β-phase content of Si_3N_4 powder and Y_2O_3, Al_2O_3 and Nd_2O_3 additives were used. The sintering processes were operated at the temperature range of 1900 °C to 2000 °C under N_2 gas pressure of 10-30 MPa for Ogasawara work. In the case of Okamoto, the sintering temperature of 1900 °C at 1 MPa of N_2 gas pressure was used.

All of the mechanical properties obtained by these researchers are shown in Table 2.3. Most of the experimental results show satisfactory mechanical properties. However, expensive sintering additives and the high cost sintering processes are used.

CHAPTER III

EXPERIMENTAL PROCEDURE

3.1 Instrument and equipment

Instruments and equipments used for this experiment are shown in Table 3.1.

Table 3.1 List of instrument and equipment used in this experiment

Instrument and equipment	Trademarks	Types/Models
Attrition mill	Szegvari Attritor	-
Roller (for ball mill)	U.S. Stoneware	CZ-02003
Electrical balance	Sartorius	BP 221S
Particle size analyzer	Shimadzu	SA-CP2
Drying oven	Bulglin	DICF
Oxygen/Nitrogen determinator	LECO	TC-436 DR
Pressing machine	-	NT-100H
Cold isostatic press	Cobe Steel	Dr. CIP
Vernier caliper	Mitutoyo	-
Alumina crucible	Nikkato	SSA-S
Electrical furnace	Lindberg	LCC256PCOMC (1700 ºC)
High temperature furnace (N_2 atmosphere)	Fujidempa	FVP HP-R-5, FRET-20
X-ray diffractometer	Bruker	D8-Advance
Grinding/Polishing machine	Buehler	Phoenix 4000
Optical microscope	Olympus	BX60M
Scanning electron microscope	JEOL	JSM-5410L
Hardness tester	Zwick GmbH	Zwick 3212
Biaxial bending tester	Intro enterprise	LLOYD 500

3.2 Starting materials and chemicals

Silicon nitride powder, sintering additives, packing powder and grinding medium as listed in Table 3.2 were used. The properties of SN-F2, MJ-30, AKP-30 and A-11 are shown in Table A-1, A-2, A-3 and A-4 in appendices.

Table 3.2 List of raw materials and chemicals used in this experiment

Raw materials / Chemicals	Trademarks / Manufactures	Grades	Chemical compositions (%)
Silicon nitride powder	Denki Kagaku Kogyo	SN-F2	β phase = 100
Magnesium oxide	Iwatani Chemicals	MJ-30	MgO = 99.9
Aluminium oxide	Taimei Chemicals	AKP-30	Al_2O_3 = 99.99
	Fuji Kasei	A-11	Al_2O_3 = 99.7
Ethanol (C_2H_5OH)	Carlo Erba	AR	Purity = 99.8
n-hexane (C_6H_{14})	Fisher Chemicals	AR	Purity = 99.9
Sodium hexametaphosphate	Fluka chemicals	AR	-

3.3 Process flow chart and experimental conditions

The process flow chart is shown in Fig. 3.1. Raw Si_3N_4 powder (SN-F2) and sintering additives were ground and mixed by attrition mill using ZrO_2 pot (1100 cm^3) and Si_3N_4 balls (diameter 5 mm) for 4, 6, 8, 10 and 16 h. Ethanol and n-hexane were used as solvent. In case of using n-hexane as the solvent, grinding time was only 10 and 16 h, and it was evaporated at room temperature before drying at 100 °C. When the solvent was ethanol, the slurry was dried at a temperature around 80 °C. The dried powder was sieved through 100 mesh. The sieved powders were formed into tablets of 20 mm in diameter and 5 mm in thickness.

Initially, the mixed powders without binder were compacted by a uniaxial press at 20 MPa. Then the specimens were cold isostatic pressed (CIP) to obtain higher density of green compacts with a pressure of 200 MPa. The specimens were set in an Al_2O_3 crucible with Si_3N_4 (SN-F2) and Al_2O_3 (A-11) packing powders. Sintering was performed in an air atmosphere furnace at a temperature range between 1500 °C to 1700 °C at the interval of 50 °C. Some specimens were sintered in N_2 gas furnace at a temperature range between 1750 °C and 1800 °C under a N_2 gas pressure of 0.1 MPa by with a heating and cooling rates of 10 °C/min, and a soaking time of 2 h. Bulk density, and mass change were determined for all specimens. Phase composition, microstructure, Vickers hardness, fracture toughness and flexural strength of selected specimens were measured and observed. All grinding and sintering conditions are shown in Table 3.3 and Table 3.4, respectively.

Bulk density, water absorption and apparent porosity were measured by Archimedes' method.[35] Crystalline phase compositions were identified by X-ray diffractometer (XRD). The morphology of polished surface was observed by scanning electron microscope (SEM). Vickers hardness and fracture toughness were measured by indentation method.[36-37] Then, the flexural strength was determined by a biaxial-bending test in conformity with ASTM-F394-78.[38]

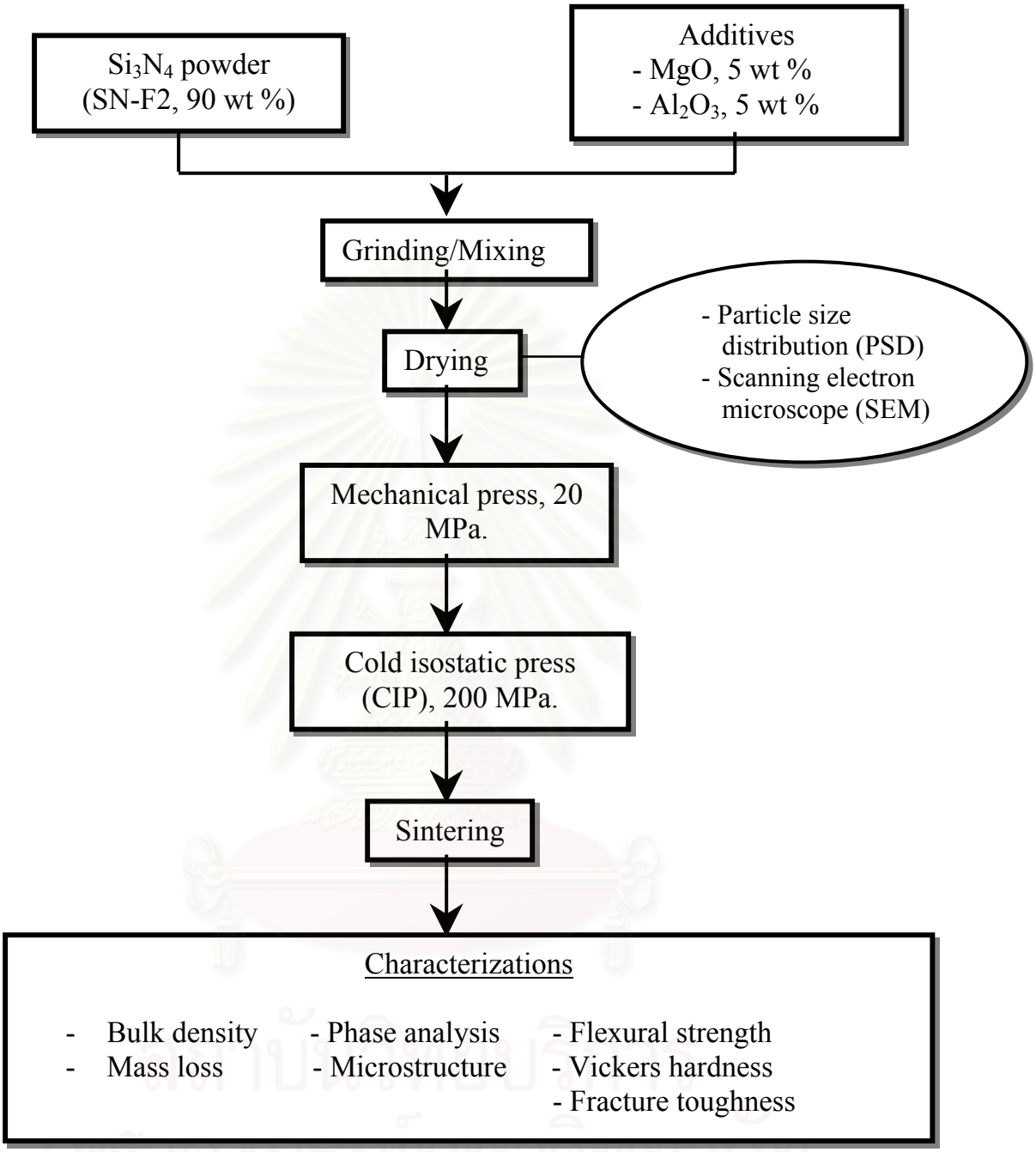

Fig. 3.1 Flow chart of specimen preparation and characterization

Table 3.3 Grinding and mixing conditions of Si_3N_4 mixtures by attrition mill

Powder codes	Grinding/mixing mediums	Grinding/mixing times (h)	Grinding/mixing speed (rpm)
E4H	ethanol	4	550
E6H	ethanol	6	550
E8H	ethanol	8	550
E10H	ethanol	10	550
E16H	ethanol	16	550
H10H	n-hexane	10	550
H16H	n-hexane	16	550

Table 3.4 Sintering conditions of this experiment

Powder codes	Temperature(°C)		Heating/Cooling rate (°C/min)	Soaking time (hr)
	Air furnace	N_2 gas furnace[1)]		
E4H	1500-1700	1750-1800	10/10 (10/10)[2)]	2 (2)[3)]
E6H	1500-1700	1750-1800	10/10 (10/10)[2)]	2 (2)[3)]
E8H	1500-1700	1750-1800	10/10 (10/10)[2)]	2 (2)[3)]
E10H	1500-1700	-	10/10	2
E16H	1500-1700	-	10/10	2
H10H	1500-1700	-	10/10	2
H16H	1500-1700	-	10/10	2

[1)] = N_2 gas pressure is 0.1 MPa with flow rate of 2 lit/min.

[2)] = Heating and cooling rate of sintering in N_2 gas furnace.

[3)] = Soaking time of sintering in N_2 gas furnace.

3.4 Sample preparations

3.4.1 Particle size reduction of Si_3N_4 powder

The commercial Si_3N_4 powder (SN-F2) was used as the raw Si_3N_4 powder. The powder was composed of 100 % β-phase content and small amount of impurities (Fe and Na). The oxygen content is around 1.18 wt %. However, the mean particle size of SN-F2 quite large and difficult to get high density of sintered bodies.[39)]

In order to reduce the size of Si_3N_4 particles, two methods for grinding and mixing Si_3N_4 powder were used, ball mill and attrition mill were used in this experiment.

3.4.1.1 Grinding Si_3N_4 powder by ball mill

The commercial Si_3N_4 powder were ground by ball milling in a Si_3N_4 pot, using Si_3N_4 balls with 150 cm^3 of ethanol and 40 g of powder for 192 h, and the rotation speed was 150 rpm. At every 24 h the slurry was sampled and dried in the oven at 80 $^{\circ}C$, for particle size analysis. Then, the particle size distributions of powder were measured by particle size analyzer. Grinding conditions of Si_3N_4 powder are shown in Table 3.5.

Table 3.5 Grinding conditions of Si_3N_4 powder by ball mill

Pot and balls	Si_3N_4 pot (500 cm^3), Si_3N_4 balls (ϕ 5 mm) 250 cm^3 (Half a volume of pot)
Medium	150 cm^3 of ethanol[40)]
Powder	Si_3N_4 powder (40 g of the mixed powder)[40)]
Rotation speed	150 rpm[40)]
Time	192 h

3.4.1.2 Grinding Si_3N_4 powder by attrition mill

Table 3.6 shows the grinding conditions and the ratio of Si_3N_4 powder, Si_3N_4 balls and grinding medium (ethanol). At 1, 3, 5, 7 and 10 h, the slurry was sampled and dried in the oven at 80 °C, for particle size analysis.

Table 3.6 Grinding conditions of Si_3N_4 powder by attrition mill

Pot and balls	ZrO_2 pot (1100 cm^3), Si_3N_4 balls (ϕ 5 mm)
Medium	ethanol
Ratio of raw powder : solvent : balls	100 g : 300 g : 1200 g (1:3:12)[40]
Rotation speed	550 rpm
Time	10 h

3.4.2 Grinding and mixing of Si_3N_4 powder with additives

Table 3.7 shows the grinding/mixing conditions Si_3N_4 mixture of with composition 90 wt% Si_3N_4 powder, 5 wt% MgO and 5 wt% Al_2O_3.

Table 3.7 Grinding/mixing conditions of Si_3N_4 mixture by attrition mill

Pot and balls	ZrO_2 pot (1100 cm^3), Si_3N_4 balls (ϕ 5 mm)
Medium	ethanol and n-hexane
Ratio of raw powder : solvent : balls	100 g* : 300 g** : 1200 g (1:3:12)[40] 100 g* : 225 g*** : 1200 g (1:2.25:12)
Rotation speed	550 rpm
Times	(4, 6, 8, 10, and 16 h)**, (10 and 16 h)***

* = Si_3N_4 powder 90 g + MgO 5 g + Al_2O_3 5 g

** = ethanol *** = n-hexane

3.4.3 Sintering of Si_3N_4

3.4.3.1 Sintering in air atmosphere furnace

Al_2O_3 is a candidate material for crucible as described in previous paper.[18] Crucible structure is shown in Fig.3.2 the specimens were set in the small Al_2O_3 crucible (50 cm^3) with Si_3N_4 packing powder of which particle size was larger than 75 μm. Then, the small crucible was set in a larger crucible (280 cm^3), which was filled with Al_2O_3 packing powder (A-11).

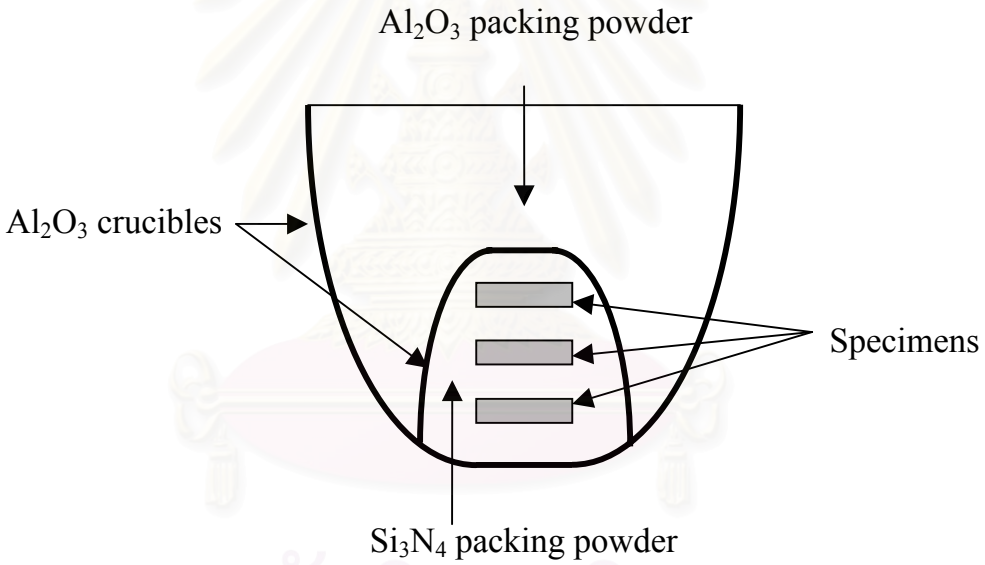

Fig. 3.2 Schematic of the crucible structure

3.4.3.2 Sintering in N_2 gas furnace

The specimens were embedded in the powder mixture of Si_3N_4 and BN, in a BN sagger as shown in Fig. 3.3. Sintering was performed using N_2 gas furnace (HIGH MULTI-5000) at a temperature range between 1750 °C and 1800 °C for 2 h under a N_2 gas pressure of 0.1 MPa and a flow rate of 2 lit/min.

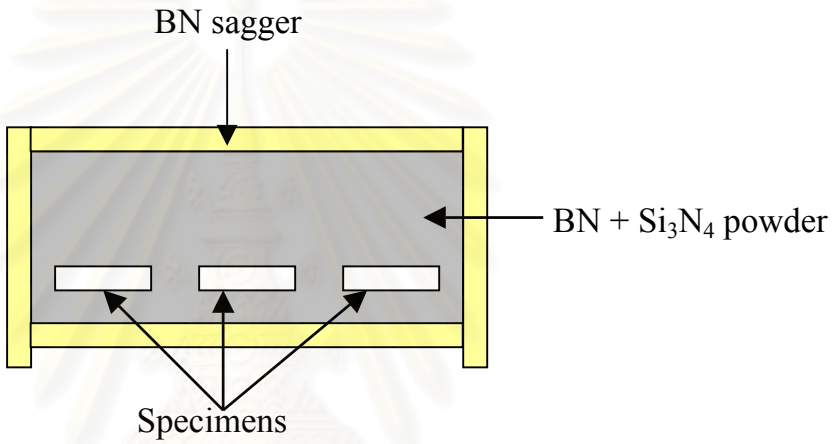

Fig. 3.3 Schematic of specimens setting for sintering in N_2 gas furnace

3.5 Property measurements and characterizations

3.5.1 Particle size distribution of starting materials and mixed powders

Sedimentation method (Shimadzu SA-CP2) was used for investigation of particle size distribution of raw Si_3N_4 powder (SN-F2) and ground or mixed powders.

Approximately 0.5 g of the powder was dispersed in 50 cm^3 water, which was 0.2 wt% aqueous solution of sodium hexametaphosphate. Sample particles were completely dispersed by magnetic stirrer, at least for 20 min.

Then, sample slurry was de-agglomerated in an ultrasonic bath. Gravity or centrifugal mode was selected for powder with diameter larger than 10 μm or smaller than 8 μm, respectively. Sedimentation depth No.3 and rotation speed of 500 or 1000 rpm were used as the condition for analysis depending on the fineness of powders.

3.5.2 Oxygen analysis and theoretical density calculation of mixed powder

Oxygen contents in raw powder and mixed powder were measured by using Nitrogen/Oxygen determinator (LECO TC-436 DR) at the Siam Research and Development Co.,Ltd.

In this experiment, the contents of oxygen before and after milling of mixed powder are analyzed. The analyzed amount of oxygen in the mixed powder includes oxygen from MgO and Al_2O_3. Therefore, the oxygen belongs to MgO and Al_2O_3 is subtracted from the analyzed amount. Then oxygen belongs to SiO_2 is determined.

One example of theoretical density calculation of mixed powder is as follows:

For the composition, 90 wt% Si_3N_4, 5 wt% MgO and 5 wt% Al_2O_3 at a milling time for 6 h, oxygen content of raw Si_3N_4 (SN-F2) and mixed powder are 1.18 wt% and 7.24 wt% , respectively.

a) Calculation of wt% oxygen in raw powder.

Oxygen (wt %) = Si_3N_4 wt% × (1.18/100)

= 90 × 0.0118

= 1.06

b) Calculation of % SiO_2 in raw powder

SiO_2 (wt%) = [(60.08/2×16)] × 1.06

= 1.99

c) Calculation of wt % of oxygen in MgO and Al_2O_3.

Wt % of oxygen in oxide M_aO_b can be calculated as follows:

$$\text{Wt \% O } (M_aO_b) = \left(100 \times \frac{b \times MW_O}{MW_{M_aO_b}}\right) \times [\text{wt\% oxide}] \quad \text{----------(1)}$$

Wt % Oxygen of (5 wt% Al_2O_3) = (3×16/101.96) × 5

= 2.35 Where :

a = Mole of metal

b = Mole of oxygen

MW_o = Molecular weight of oxygen

MW_{MaOb} = Molecular weight of oxide

From equation (1) :

Wt % Oxygen of (5 wt% MgO) = (16/40.31) × 5

= 1.98

d) Calculation of the incremental oxygen content in mixed powder.

The analyzed oxygen content of mixed powder is 7.24 wt%

Therefore : Oxygen (increased) = 7.24 - 1.98 - 1.18 - 2.35

= 1.73 wt%

From 1.73 wt% of oxygen, wt% of SiO_2 in Si_3N_4 is :

SiO_2 (wt%) = [(60.08)/(2×16)] × 1.73

= 3.25

Total SiO_2 in mixed Si_3N_4 powder is 1.99 + 3.25 = 5.24 wt%

e) Theoretical density of glassy phase is calculated from SiO_2, MgO and Al_2O_3 compositions, because the glassy phase containing in Si_3N_4 is made from them, using theoretical density value of 2.2 g/cm^3, 3.64 g/cm^3 and 4.0 g/cm^3 for SiO_2, MgO and Al_2O_3, respectively.

The density of glass could be estimated as follows:

Glass density = $\sum$ (Weight fraction of oxide × density of oxide)

= [(5.24/15.24)×2.2] + [(5/15.24)×3.64] + [(5/15.24)×4]

= 0.76 + 1.19 + 1.31

= 3.26 g/cm^3

f) The theoretical density of mixed powder is the sum of the theoretical density of Si_3N_4 and glassy phase. The theoretical density of mixed powder is calculated as 3.22 g/cm^3.

Table 3.8 Calculated theoretical density of mixed powder for 6 h

Powder composition	Real composition	Theoretical density (g/cm^3)	Density (g/cm^3)
Si_3N_4	84.76	3.21	2.72
Glass	15.24	3.26	0.50
Total	100	-	3.22

All results calculated for mixed powders at various grinding time are shown in Table 3.9.

Table 3.9 Calculated theoretical density of mixed powder from various grinding conditions

Grinding medium	Grinding time (h)	Analyzed oxygen content (wt%)	Real composition (wt%)				Calculated theoretical density (g/cm^3)
			Si_3N_4*	SiO_2*	MgO	Al_2O_3	
-	0	1.18	88.01	1.99	5	5	3.26
ethanol	4	6.92	85.36	4.64	5	5	3.22
	6	7.24	84.76	5.24	5	5	3.22
	8	7.88	83.56	6.44	5	5	3.20
	10	8.97	81.51	8.49	5	5	3.19
	16	9.54	80.44	9.56	5	5	3.17
n-hexane	10	10.00	79.58	10.42	5	5	3.16
	16	11.30	77.14	12.86	5	5	3.15

* = the value from calculation

3.5.3 Mass change measurement

The mass loss of each specimen was calculated from the weight measurement of specimens before (W_B) and after sintering (W_A). The mass loss is calculated as follows:

$$\text{Mass change (\%)} = ((W_B - W_A)/ W_B) \times 100$$

3.5.4 Bulk density and relative density

Bulk density was measured by Archimedes' method.[35] The detail was omitted. Relative density was calculated from bulk density and theoretical density which is shown in Table 3.9.

3.5.5 Identification of material and determination of phase content in Si_3N_4 by X-ray diffraction analysis

The qualitative analyses of raw Si_3N_4 (SN-F2) and sintered specimens were determined by X-ray diffraction (D8-Advance, Bruker Co., Ltd.). The value of 2θ around 10-70°, and the scanning speed of 2°/min were used as conditions. The specimens analyzed by X-ray diffraction analysis are shown in Table 3.10.

Sample preparation

The sintered specimen was ground in an Al_2O_3 mortar. Then, the powder was screen through sieve number 230 (70 μm). Then, about 1-2 grams of powder was used for X-ray diffraction analysis.

Table 3.10 Sintered Si_3N_4 specimens selected for XRD analysis

Samples	Sintering in air furnace		Sintering in N_2 gas furnace	
	1500 °C	1700 °C	1750 °C	1800 °C
E4H	O	O		
E6H	O	O	O	O
E8H	O	O		
E10H	O	O		
E16H	O	O		
H10H	O	O		
H16H	O	O		

3.5.6 Observation of microstructure by scanning electron microscope (SEM)

The microstructures of polished surface were characterized by SEM. Sintered Si_3N_4 specimens selected for SEM analysis are shown in Table 3.11. The procedure of sample preparation for polished surface analysis is shown in Fig 3.4.

Table 3.11 Sintered Si_3N_4 specimens selected for SEM analysis

Samples	Sintering in air furnace					Sintering in N_2 gas furnace	
	1500 °C	1550 °C	1600 °C	1650 °C	1700 °C	1750 °C	1800 °C
E4H						○	○
E6H						○	○
E8H	○	○	○	○	○	○	○
H16H	○	○	○	○	○		

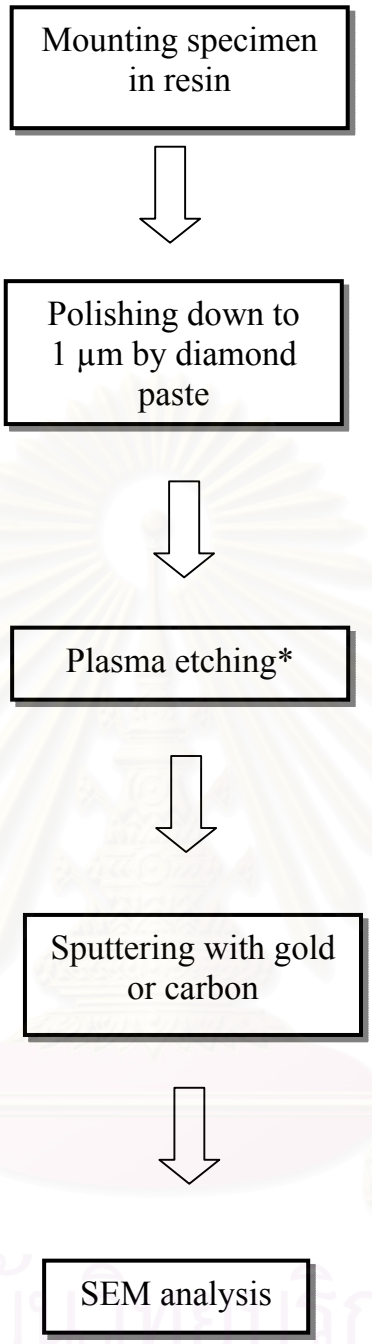

Fig 3.4 Sample preparation flow chart for SEM analysis

*Plasma etching and SEM analysis were performed by Mr.Thanakorn Wasanapienpong at Tokyo Institute of Technology (TIT), Japan.

3.5.7 Vickers hardness and fracture toughness

Sample preparation:

The Vickers hardness and fracture toughness of the sintered specimens were measured by Vickers indentation method and calculated according to JIS-R1610[36] and JIS-R1607, [37] respectively. For this experiment, sintered specimens that are selected for Vickers hardness and fracture toughness testing are shown in Table 3.12.

Test specimen was ground with 200 grit diamond wheel and then polished with 400, 800 and 1,200 grit SiC papers (Buehler grinding paper) down to 15.30 μm, and followed by 6, 3 and 1 μm diamond paste. The surface was examined at intervals using optical microscope. After polishing, specimens were washed with alcohol in an ultrasonic bath to remove dirt and debris from the surfaces. Vickers indentation was applied at a load of 98.07 N(10 kgf) in conformity with JIS standard (Designation R 1610-1991) using microhardness tester.(Zwick 3212, Zwick GmbH & Co.)

Calculation:

Vickers hardness, (Hv) is calculated by the following equation:

$$Hv = 1.8544 \left(\frac{P}{(d)^2} \right)$$

Where: P = Load (N)

d = Diagonal length (mm)

Fracture toughness, (K_{IC}) is calculate by the following equation in conformity with JIS R1607-1995

$$K_{1C} = 0.018 \left(\frac{E}{Hv} \right)^{1/2} \left(\frac{P}{C^{3/2}} \right)$$

Where: C = Crack length (mm)

E = Young' modulus ~ 300 GPa

Hv = Vickers hardness

Table 3.12 Specimens for Vickers hardness (Hv), fracture toughness (K_{IC}) and flexural strength test

Samples	Sintering in air furnace	Sintering in N_2 gas furnace	
	1700 °C	1750 °C	1800 °C
E4H	○	○	○
E6H	○	○	○
E8H	○	○	○

3.5.8 Flexural strength test by biaxial bending test at room temperature

Flexural strength was measured by a biaxial-bending test in conformity with ASTM F : 394-78. [38] The figure of testing equipment is shown in Fig. 3.5.

Sample preparation:

The selected specimens for flexural strength tests are shown in Table 3.12. The specimens were ground to flat surface by # 170 diamond wheel. Next, their tensile surfaces were ground with 200 and 400 grit diamond wheel followed by polishing with 800 and 1200 grit SiC papers (Buehler grinding paper), respectively. Then, the finished surfaces were polished using 6, 3 and 1 μm diamond paste, respectively. All tests were performed using LLOYD 500, Intro enterprise Co., Ltd. The crosshead speed was constant at 0.5 mm/min.

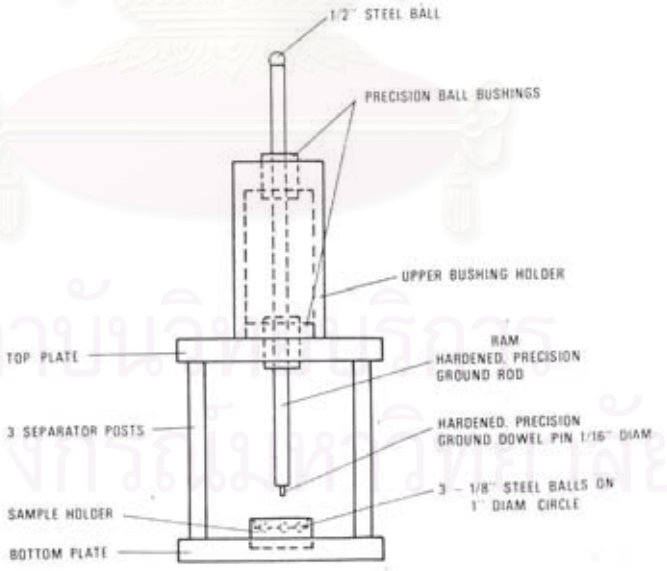

Fig. 3.5 Biaxial-Flexure Strength Fixture

Calculation:

Flexural strength is calculated by the following equations.

$$S = \frac{-0.2387P \times (X - Y)}{d^2} \quad \text{----------(1)}$$

$$X = \left\{(1-\nu) \times \ln\left(\frac{B}{C}\right)^2\right\} + \left\{\frac{(1-\nu)}{2} \times \left(\frac{B}{C}\right)^2\right\} \quad \text{----------(2)}$$

$$Y = \left\{(1-\nu) \times \left(1 + \ln\left(\frac{A}{C}\right)^2\right)\right\} + \left\{(1-\nu) \times \left(\frac{A}{C}\right)^2\right\} \quad \text{----------(3)}$$

Where:

S = Maximum center tensile stress (MPa)

P = Total load causing fracture (N)

μ = Poisson's ratio, 0.23

A = Radius of support circle (12.5 mm)

B = Radius of loaded area or ram tip (2.5 mm)

C = Radius of specimen (mm)

d = Specimen thickness at fracture origin (mm)

The relation between X and B, when C = 13.5, is shown in Fig 3.6.

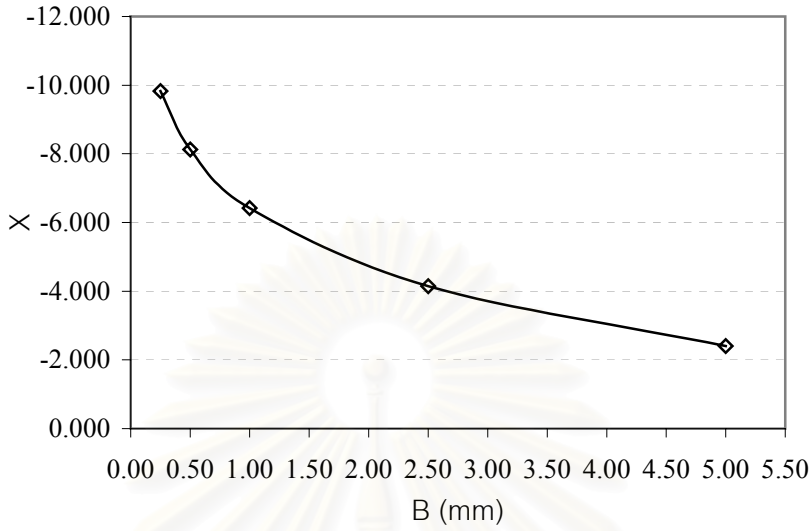

Fig 3.6 Relationship between X and B value for 3-point bending strength test

Miss. Bongkoch [41] used the Si_3N_4 ball of 2.5 mm. radius as the ram tip for her master thesis. The contact radius of the ball was 0.125 mm. From Fig 3.6, it was understood that X value changed much when contact radius B changed just a little at the range of B < 0.5 mm. The ram tip radius of 2.5 mm was thought to be not so sensitive to the deviation of B. Considering this fact, the ram tip radius of 2.5 mm was selected.

CHAPTER IV

RESULTS AND DISCUSSION

4.1 Particle size distribution of Si_3N_4 and mixed powder

4.1.1 Characteristics of Si_3N_4 (SN-F2) powder

Figure 4.1 shows the SEM image of Si_3N_4 powder, SN-F2 grade. Its particle size distribution is shown in Figure 4.2 and 4.3. As shown in Figure 4.1, this starting powder consists of wide distribution, large agglomerated particles, large acicular shaped particle and small particles. The particle size distributions measured by sieve analysis are shown in Appendix B. The mean particle size about 22 μm was measured from the particle size distribution curve (Figure 4.2 or 4.3, as-received powder). Therefore, in order to get high density of sintered materials this powder must be crushed.[22,39)]

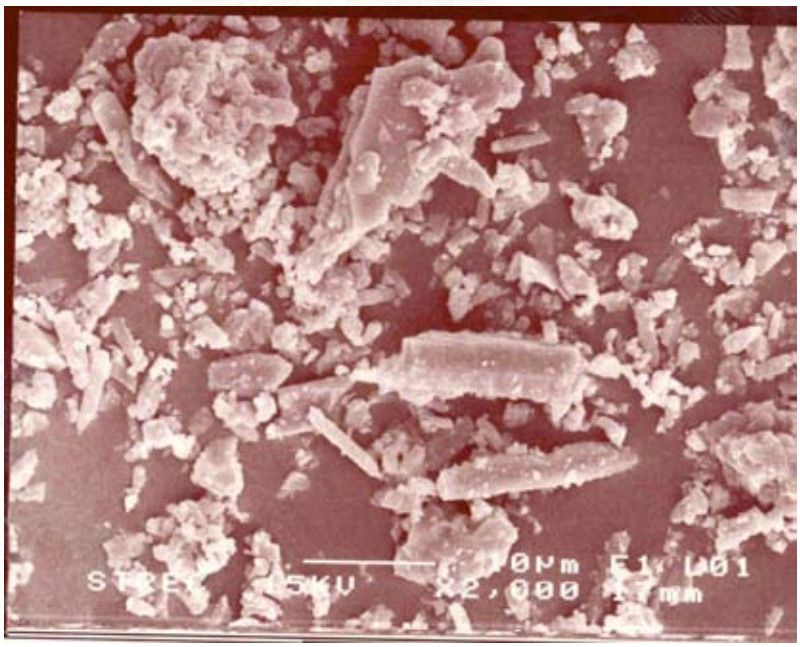

Fig 4.1 SEM image of Si_3N_4 powder, SN-F2 grade

4.1.2 Particle size distribution of Si_3N_4 powder

Two kinds of grinding method, which are ball mill and attrition mill, were used to investigate the reduction of Si_3N_4 powder. The particle size distribution curves of milled SN-F2 powder by ball mill and attrition mill are shown in Figure 4.2 and 4.3, respectively.

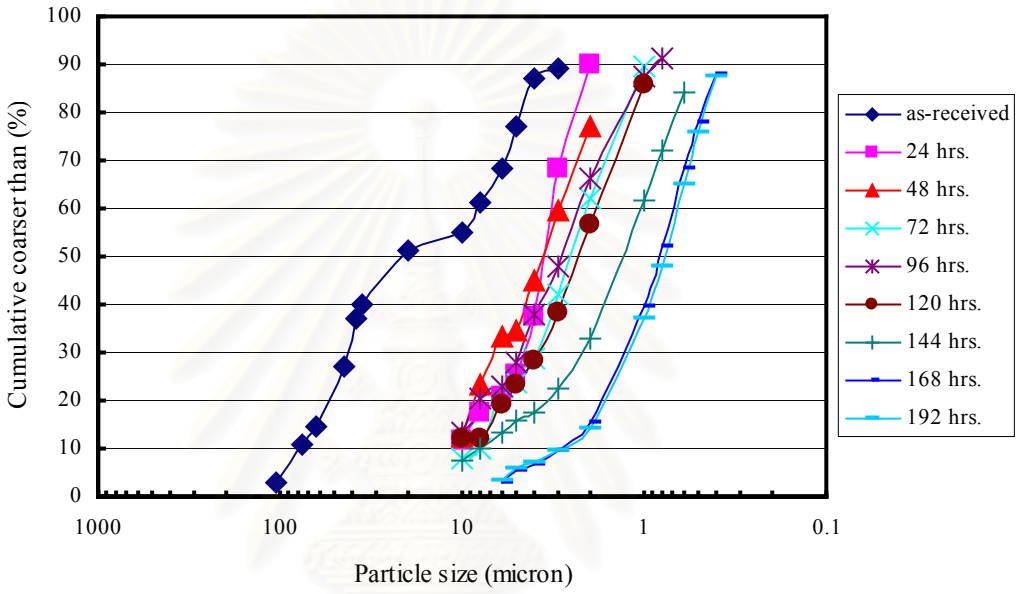

Fig 4.2 Particle size distributions of milled Si_3N_4 powder (SN-F2) by ball mill at various milling times

The mean particle size of milled Si_3N_4 powder by ball mill for 192 h and attrition mill for 10 h are 0.78 μm and 0.73 μm, respectively. The particle morphology of milled powder is shown in Figure 4.4. The particle shapes after ground are equiaxed small grains size, hence acicular grains were crushed. Both ball mill and attrition mill grinding methods could reduced the particle size down to sub-micrometer size. However, in the case of attrition mill was more time economical than ball mill. Therefore, the attrition mill method was more suitable for grinding and mixing of Si_3N_4 powder with sintering additives than ball mill.

Attrition mill method was selected for mixing of Si_3N_4 powder with additives, MgO and Al_2O_3. The particle size distribution curves of mixed powder are shown in Figure 4.5.

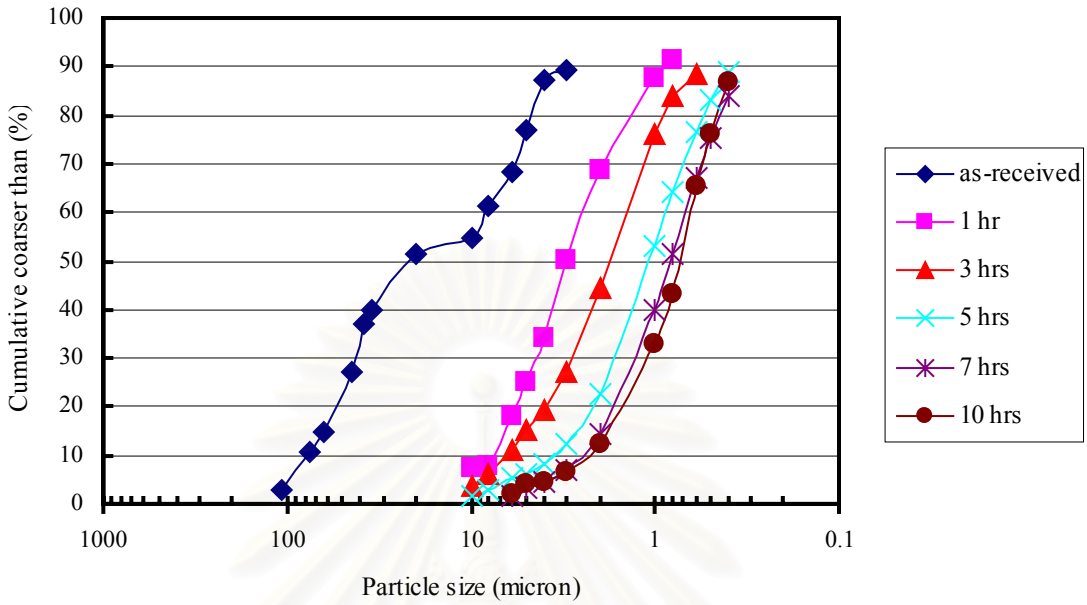

Fig 4.3 Particle size distributions of milled Si_3N_4 powder by attrition mill at various milling times

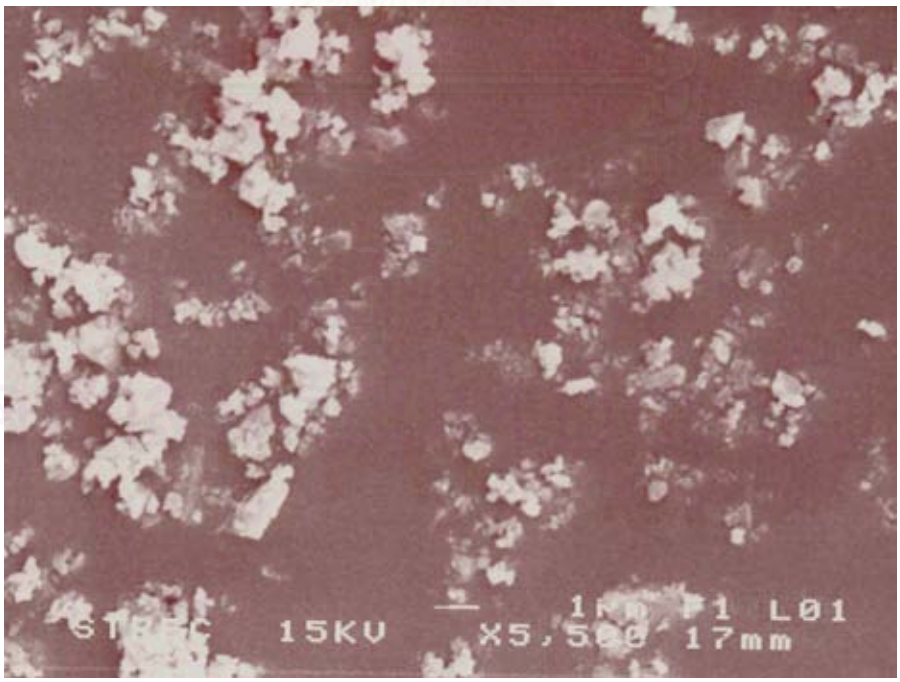

Fig 4.4 SEM image of milled Si_3N_4 powder by attrition mill for 10 h (E10H)

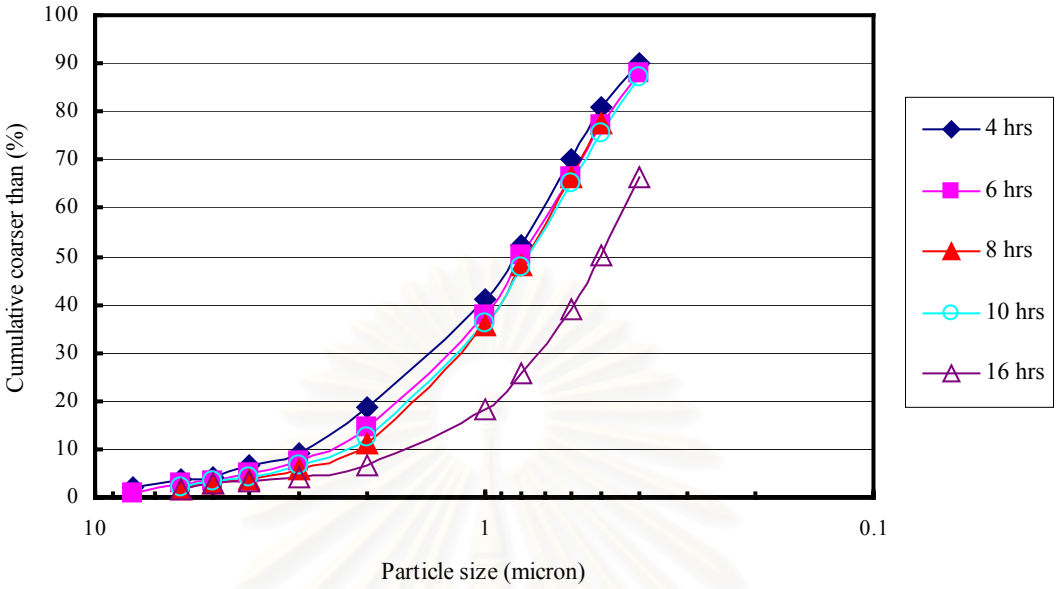

Fig 4.5 Particle size distributions of mixed Si_3N_4 powder by attrition mill at various milling times

4.2 Oxygen content of mixed Si_3N_4 powders

Two kinds of solvents, ethanol and n-hexane, were used as grinding and mixing medium. The oxygen content of mixed Si_3N_4 powder was measured by Oxygen/Nitrogen determinator. The results of analysis are shown in Table 3.9. The Increment of total oxygen content caused by increasing the mixing times is shown in Figure 4.6.

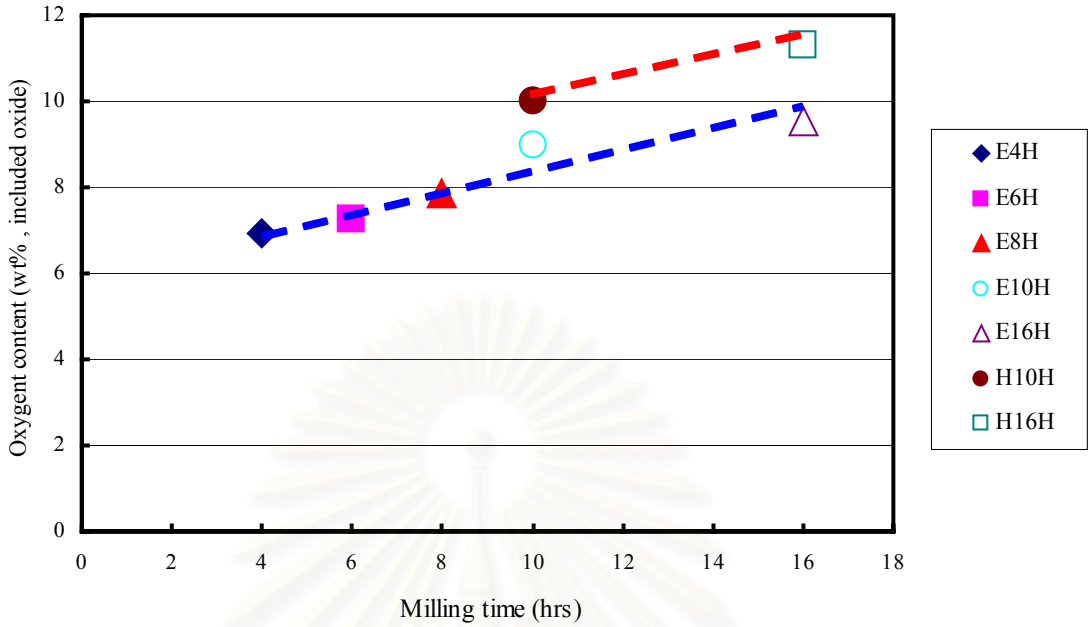

Fig 4.6 Oxygen contents of mixed Si_3N_4 powder as a function of mixing time

The oxygen content is increased with increasing mixing time in both ethanol and n-hexane as mixing mediums. In case of ethanol as a solvent, Prof. Dr. Shigetaka Wada reported that,[40] the most of increment of oxygen content came from two main reactions, which are the reaction of Si_3N_4 with moisture in the air and the mechanochemical reaction between Si_3N_4 and ethanol. The reaction of H_2O and Si_3N_4 was considered to be as follows:

$$6H_2O\ (l) + Si_3N_4\ (s) \rightarrow 3SiO_2\ (s) + 4NH_3\ (g) \qquad \text{----------(1)}$$

The mechanochemical reaction was complicated reaction, Hirano et al. quoted.[42-43] that the Si-O-R bond was formed on the surface of the Si_3N_4 powder according to the reaction in equation (2).

$$Si\text{-}OH + R\text{-}OH \rightarrow Si\text{-}O\text{-}R + H_2O \qquad \text{----------(2)}$$

Considering that this reaction may take place in the attrition mill, it can naturally be conceived that the H_2O generated acts according to equation (1).

In the case of n-hexane as a solvent (H10H, H16H), in this experiment the author did not exactly examine the process of the reaction between Si_3N_4 and n-hexane. The oxygen content of milled powder is higher than that ethanol at the same mixing time. The reason for this may be supposed that n-hexane more active than ethanol. The reaction of n-hexane with the moisture in air may happen easier than the reaction in an ethanol, because this experiment was performed in an open system.

4.3 Mass loss

The relationship between mass loss and sintering temperature of both specimens sintered in air and N_2 atmosphere furnace are shown in Figure 4.7. The original data are shown in Appendix Table D-1 and Table D-3, respectively.

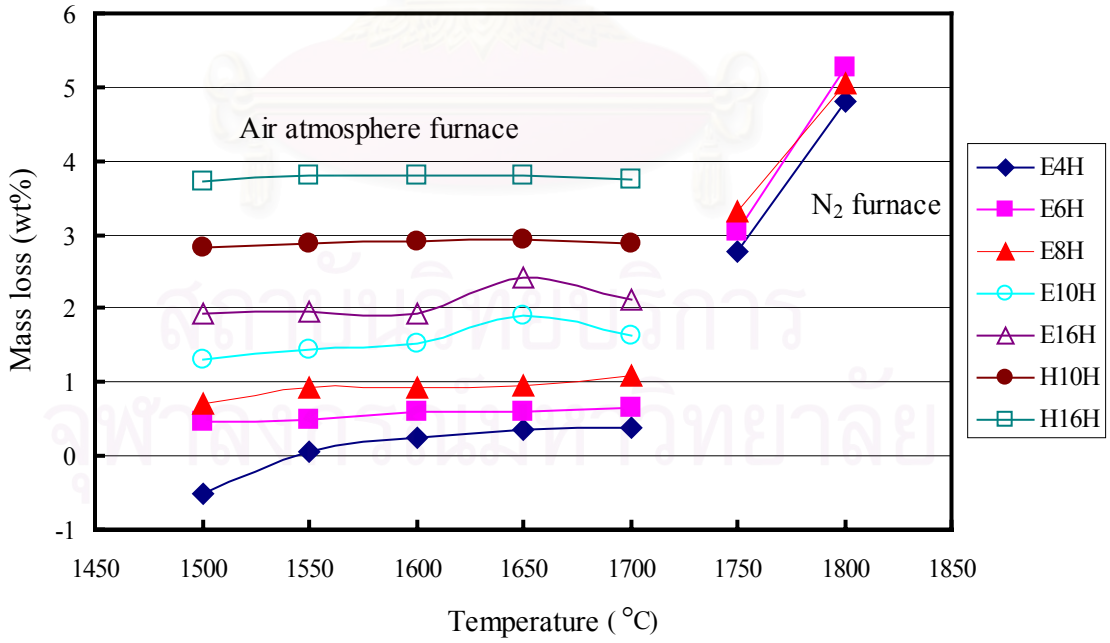

Fig 4.7 Mass loss of specimens sintered in air atmosphere and N_2 atmosphere furnaces as a function of temperature

In case of sintering in N_2 gas furnace, the major mass loss reaction was presumed to be reaction (3). [50] Since the SiO (g) partial pressure increases by increasing temperature, as shown in Fig C-1 in Appendix C, the mass loss values increased as a function of temperature.

$$Si_3N_4\ (s) + 3SiO_2\ (l) \rightarrow 6SiO\ (g) + 2N_2\ (g) \qquad \text{----------(3)}$$

In the case of sintering in air furnace, mass loss of specimens was not increased so much even when increased the sintering temperature, but increased as a function of oxygen content in Si_3N_4 powder. The major mass loss will be resulted from the same reaction as sintering in N_2 gas furnace (reaction (3)). However, there are big atmosphere difference in the partial pressure of O_2 (g) and N_2 (g) in these two sintering methods. It might be caused the difference of mass loss phenomenon.

Moreover, the mass loss might occur according to the decomposition of MgO additive to Mg (g) and O_2 (g), because MgO is not stable at high temperature. The MgO (g) and Mg (g) partial pressures are shown in Appendix Fig C-1.

4.4 Bulk density and relative density

Figure 4.8 and 4.9 show bulk density and relative density of the specimens sintered in air atmosphere compared with specimens sintered in N_2 gas furnace, respectively. The original data are shown in Appendix Table D-2 and D-4.

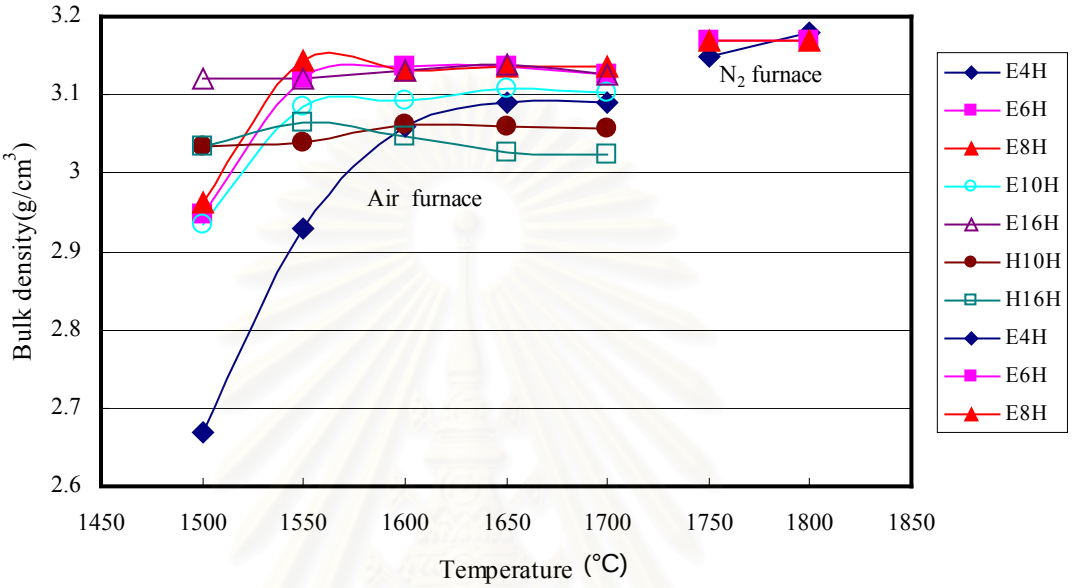

Fig 4.8 Bulk density of sintered specimens with various kinds of milling conditions as a function of sintering temperature

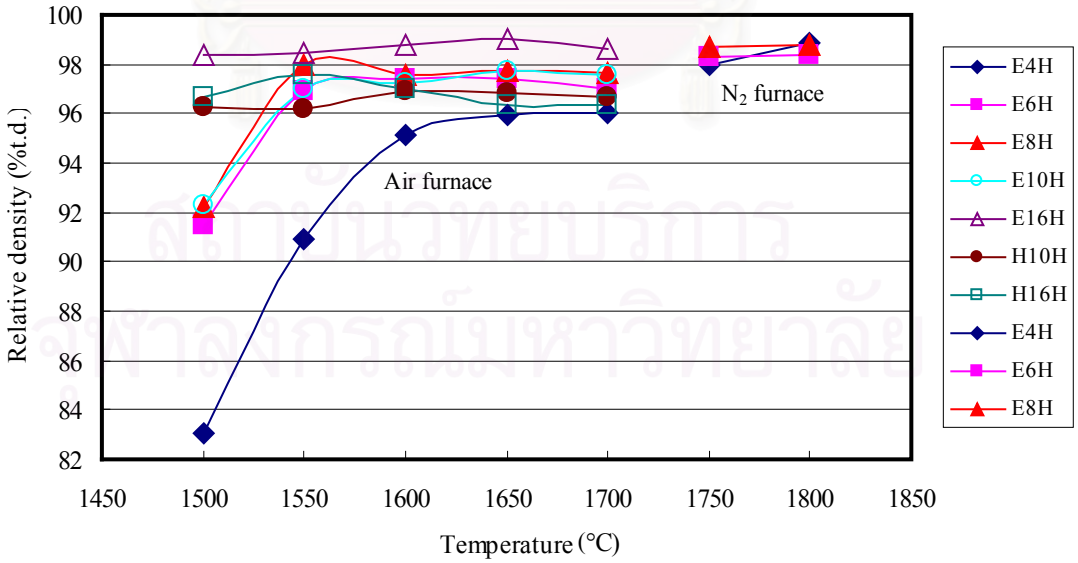

Fig 4.9 Relative density of sintered specimens with various kinds of milling conditions as a function of sintering temperature

Figure 4.8 shows changes of bulk density with sintering temperature. For the specimens sintered in air atmosphere furnace, E4H, E6H, E8H, E10H, and E16H could achieve almost full density at the temperature over 1650 °C. However, at the lowest temperature (1500 °C), we found that the relative densities of sintered specimens except E4H were over 92 % of theoretical density (see Fig 4.9). The high densities at the low sintering temperature were caused by the formation of liquid phase. Because, MgO and Al_2O_3 additives, and surface silica of Si_3N_4 powder could form as liquid phase at low temperature.[46)]

In the case of MgO addition, the eutectic temperature of the mixture MgO-SiO_2 is about 1540 °C [46)] and this can be lowered by addition of Al_2O_3, as shown in Figure 4.10. With increasing temperature, the viscosity of the liquid is decreased. As a result, rearrangement and subsequently the solution-diffusion-precipitation processes are enhanced. [22)] Thus, the specimens could be sintered at low temperature. However, in the case of E4H, the specimens did not achieve high density because of its larger mean particle size than other ones and smaller amount of glassy phase.

The densities of specimens sintered in air furnace of over 96 % of theoretical density. The high density was achieved at the sintering temperature of 1650 °C and 1700 °C, which was the same as specimens sintered in N_2 atmosphere, because the compositions of specimens consist of much amount of additives and oxidized SiO_2 in this experiment. Therefore, the specimens could be sintered at low sintering temperature. However, densities of specimens sintered in air furnace were less than the specimens sintered in N_2 gas furnace, because of sintering temperature of N_2 gas furnace was higher than that of the air furnace. In the other word, the higher densities were attributed to the higher sintering temperature.

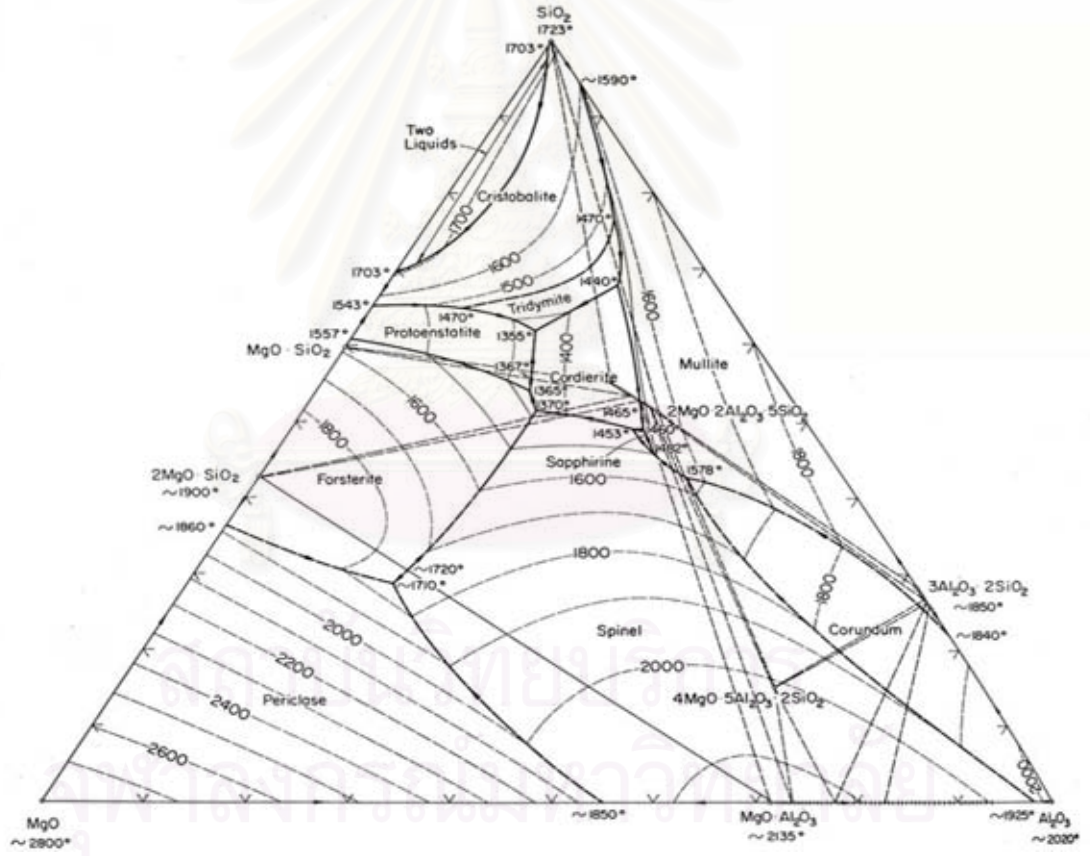

Fig 4.10 Phase diagram of MgO-Al_2O_3-SiO_2 system

4.5 Deterioration of Al_2O_3 crucible

After sintering for several times, the whole color of the inside wall of Al_2O_3 crucible changed from white to gray and became swollen. It was alter confirmed that some powder reacted with the wall of Al_2O_3 crucible and formed layer of porous product. Its phase contents were measured by Piyaporn.[47] Phase analysis by X-ray diffraction revealed three types of materials, Si_3N_4, corundum, and aluminum silicon oxide nitride ($Si_{12}Al_{18}O_{39}N_8$). Figure 4.11 shows the outlook observation of Al_2O_3 crucible after sintering for several times.

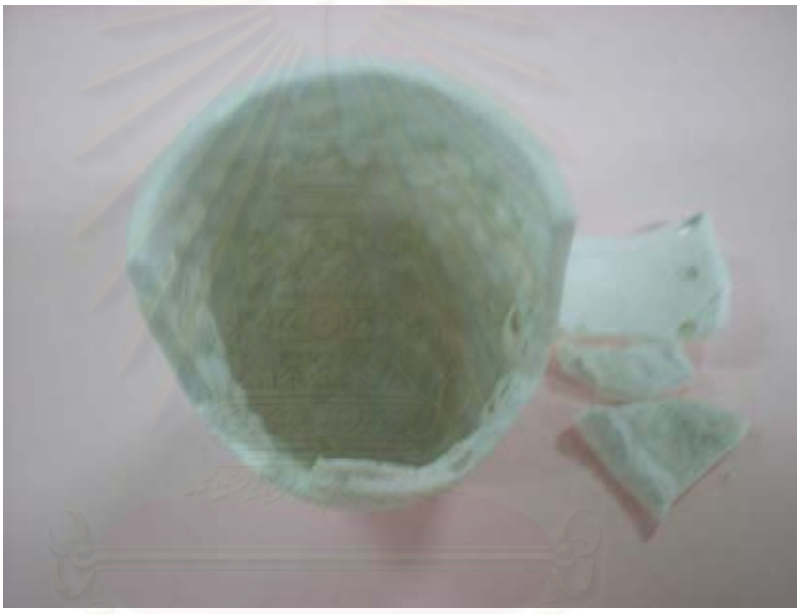

Fig 4.11 Aspect of inside wall of Al_2O_3 crucible after sintering

Piyaporn reported that, the phase content on reacted surface of Al_2O_3 crucible is aluminum silicon oxide nitride ($Si_{12}Al_{18}O_{39}N_8$). Aluminum silicon oxide nitride was supposed to come from either of the following reactions.

$$6SiO_2\ (l) + 2Si_3N_4\ (s) + 9Al_2O_3\ (s) = Si_{12}Al_{18}O_{39}N_8\ (s) \quad \text{----------(1)}$$

$$12SiO\ (g) + 9Al_2O_3\ (s) + 4N_2\ (g) = Si_{12}Al_{18}O_{39}N_8\ (s) \quad \text{----------(2)}$$

On the surface of Al_2O_3 crucible, there was not so much SiO_2 (l) so it must be difficult thinking that it was the reaction between solid (Si_3N_4) and solid (Al_2O_3). On the contrary, SiO and N_2 are both gases. Then, reaction (2) might be more possible. Al_2O_3 crucible cracked after using for several times. The difference of thermal expansion between $Si_{12}Al_{18}O_{39}N_8$ (s) and Al_2O_3 may cause those cracks.

4.6 Phase compositions of Si_3N_4 raw powder and specimens

4.6.1 Si_3N_4 raw powder

Phase compositions of Si_3N_4 raw powder were confirmed by X-ray diffractometer (XRD). The XRD pattern is shown in Figure 4.12, Si_3N_4 raw powder consists of β-Si_3N_4 and small amount of silicon oxynitride. That is, the powder is almost 100% β phase.

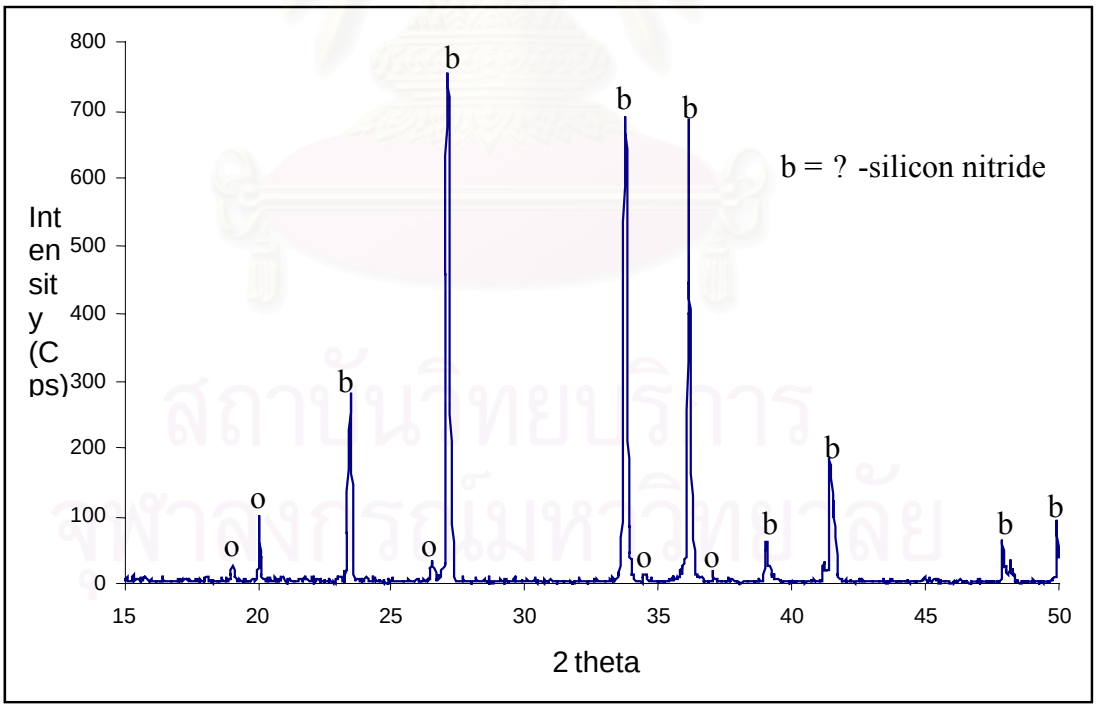

Fig 4.12 X-ray diffraction pattern of Si_3N_4 raw powder (SN-F2)

4.6.2 Sintered specimens

Phase compositions of sintered specimens were measured by XRD. Phase contents of sintered specimens are show in Table 4.1. Figure 4.13 and 4.14 show the XRD patterns of the specimens sintered in air atmosphere furnace at the temperature of 1500 °C and 1700 °C, respectively. The original data are shown in Appendix E.

Table 4.1 Phase content of specimens sintered in air atmosphere furnace and in N_2 gas furnace

Samples	Sintering in air furnace		Sintering in N_2 gas furnace	
	1500 °C	1700 °C	1750 °C	1800 °C
E4H	β	β		
E6H	β + Z	β + Z	β	β
E8H	β + O + Z	β + Z		
E10H	β + O + Z	β + Z		
E16H	β + O + Z	β + O + Z		
H10H	β + O	β + O		
H16H	β + O	β + O		

Note : β = β-Si_3N_4

O = Sinoite (Si_2N_2O)

Z = Baddeleyite, ZrO_2

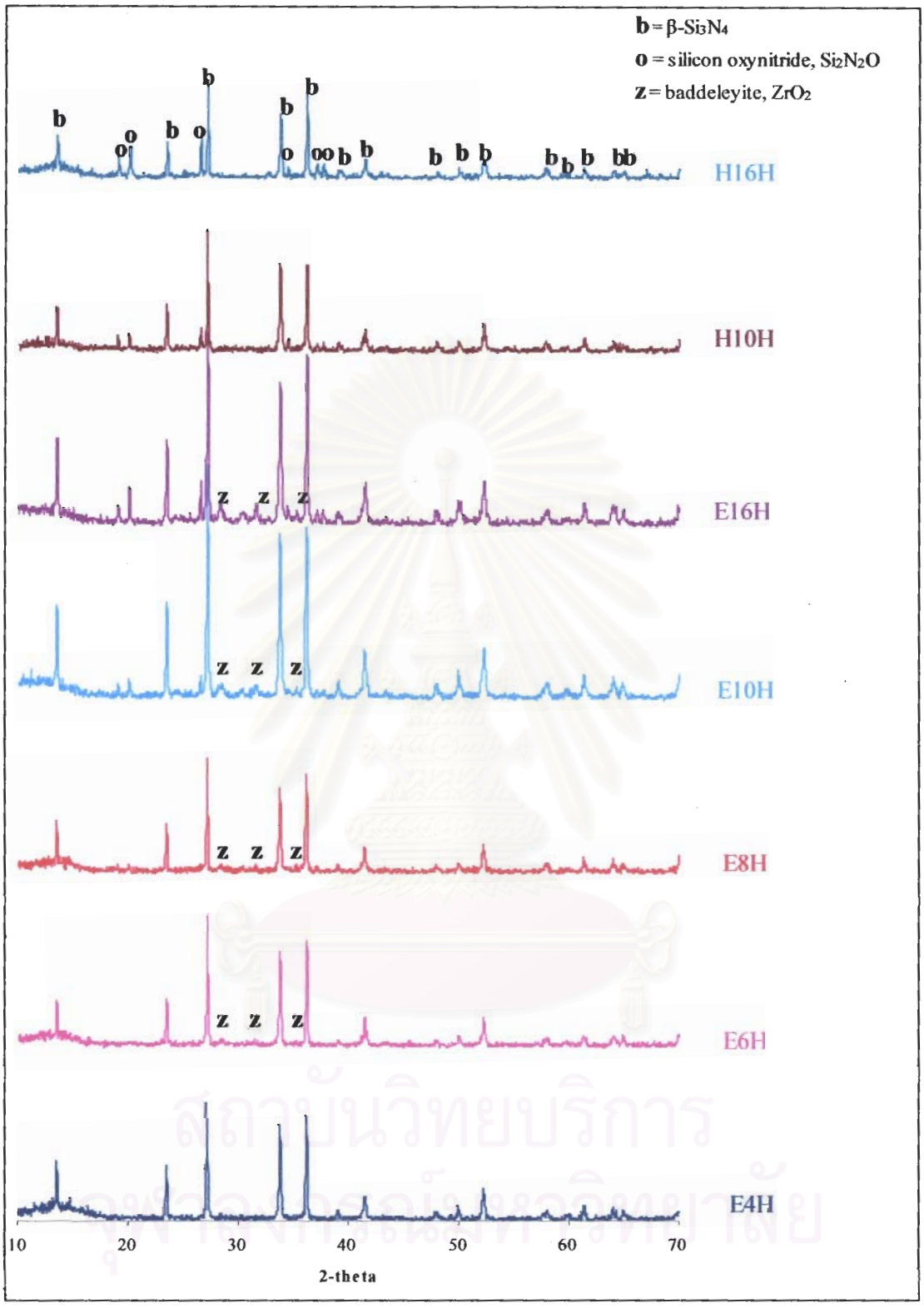

Fig 4.13 XRD patterns of specimens sintered in air atmosphere furnace at 1500 °C

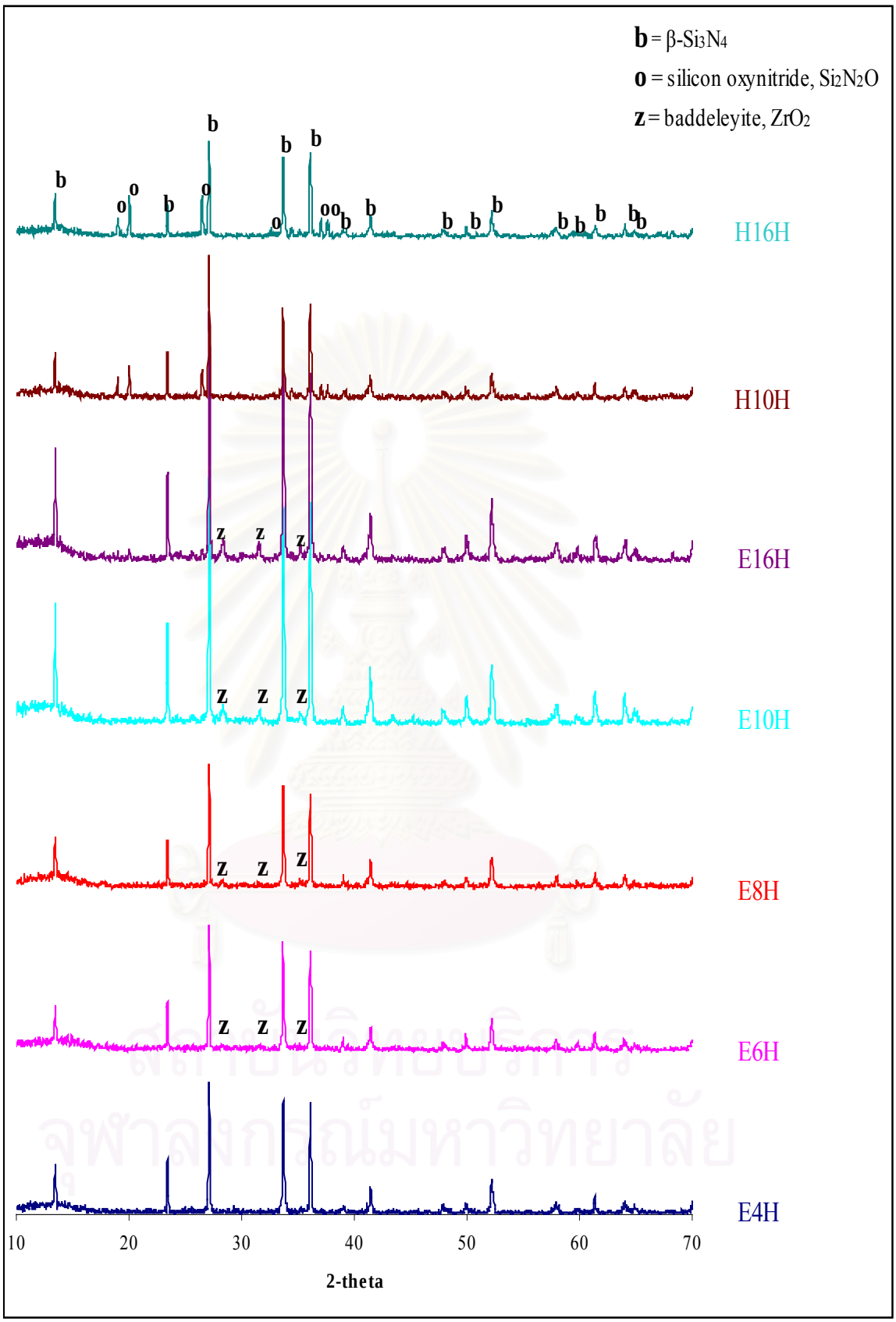

Fig 4.14 XRD patterns of specimens sintered in air atmosphere furnace at 1700 °C

Silicon oxynitride can be formed by reaction between Si_3N_4 and surface SiO_2.[48-49] The reaction is shown in equation (4).

$$Si_3N_4\ (s) + SiO_2\ (s) \longrightarrow 2Si_2N_2O\ (s) \qquad \text{----------(4)}$$

From the X-ray diffraction patterns of sintered specimens, it is shown that Si_2N_2O phase is present in the specimens that contain much amount of SiO_2 (long milling time). At the sintering temperature of 1500 °C, Si_2N_2O phase is found as a trace in E8H and could be obviously observed in the specimens with higher SiO_2 content (E10H, E16H, H10H, and E16H). In the specimen of 1700 °C, Si_2N_2O phase can not be seen in E8H and E10H. However, in the specimens E16H, H10H, and H16H Si_2N_2O still appeared, because their SiO_2 content are high.[48] However, the content of Si_2N_2O was not analyzed quantitative in this work. In case of sintering in N_2 gas furnace, only β-Si_3N_4 phase is presented as shown in Figure 4.15.

In addition, baddeleyite phase (ZrO_2) was seen in some specimens. It was a contaminant from the wearing of ZrO_2 pot of the attrition mill.

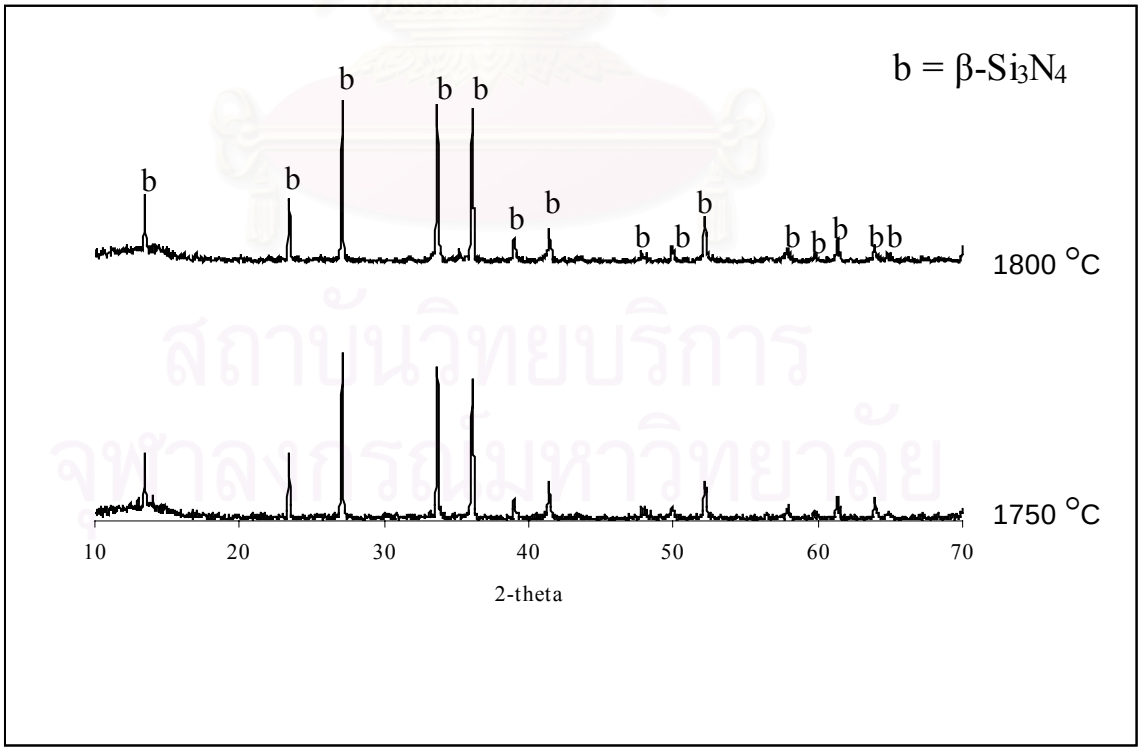

Fig 4.15 XRD patterns of specimens sintered in N_2 gas furnace, E6H

4.7 Microstructures

Microstructures of sintered specimens were observed by scanning electron microscope (SEM). Figure 4.16 shows polished surface of E8H specimens sintered in air furnace at 1500 °C and 1650 °C. The micrograph reveals the development of grain growth. With increasing temperature, the solution-diffusion-precipitation process starts and superimpose on the rearrangement process. The driving force for this second stage is the higher solubility at the contact points of the particle caused by capillary forces as well as the differences in the chemical potentials between small and large particles, which leads to an enhanced solution of small particles.[22] Therefore, when increasing the sintering temperature, the grain growth of the β grains occurs.

Figure 4.17 shows polished surface of H16H (highest amount glass phase) specimens sintered in air furnace at 1500 °C and 1650 °C. It is analyzed by XRD that these specimens are composed of β-Si_3N_4 and Si_2N_2O. From these micrographs, it is concluded that small needle-like crystal in Figure 4.17 might be Si_2N_2O. Moreover, grain growth is developed as a function of temperature as well.

Microstructures of specimens sintered in N_2 gas furnace are shown in Figure 4.18. In the case of sintering in N_2 furnace, the microstructures are also mainly equiaxed grains and grain size is slightly increased by increasing sintering temperature.

In this work, β-Si_3N_4 powder were used. Thus, in this case no α-to-β conversion occur. Both of specimens sintered in air and N_2 gas furnace show mostly equiaxied small grain, because the sintering temperature and time are not high enough to accelerate the grain growth of β-Si_3N_4. V.K. Sarin reported that the large elongated grains of Si_3N_4 from β powder appear at the sintering temperature over 1800 °C and sintering time over 4 hrs. [31] The SEM micrographs of other specimens are attached in Appendix F.

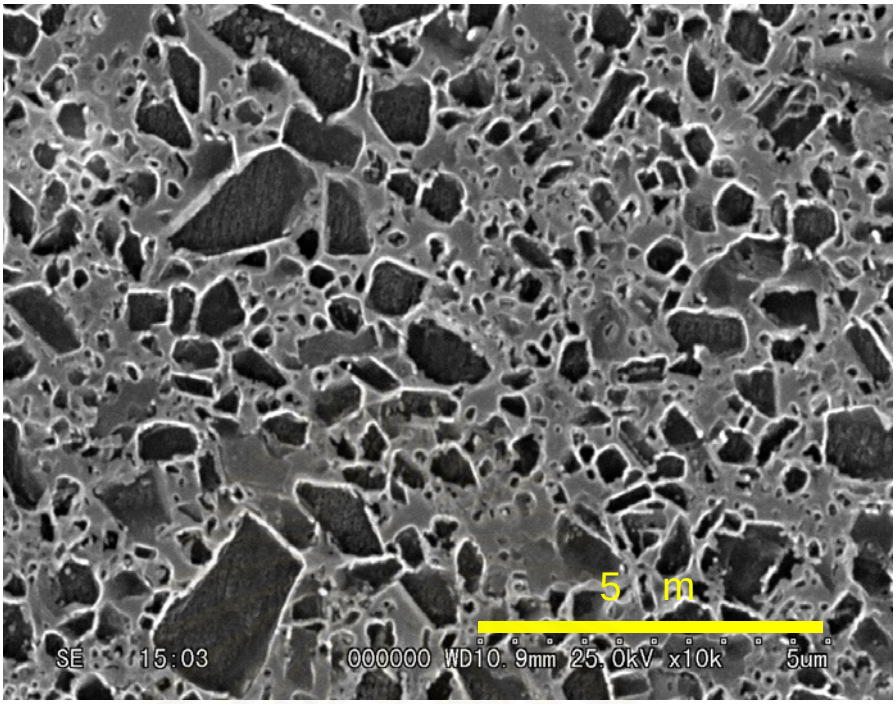

(a)

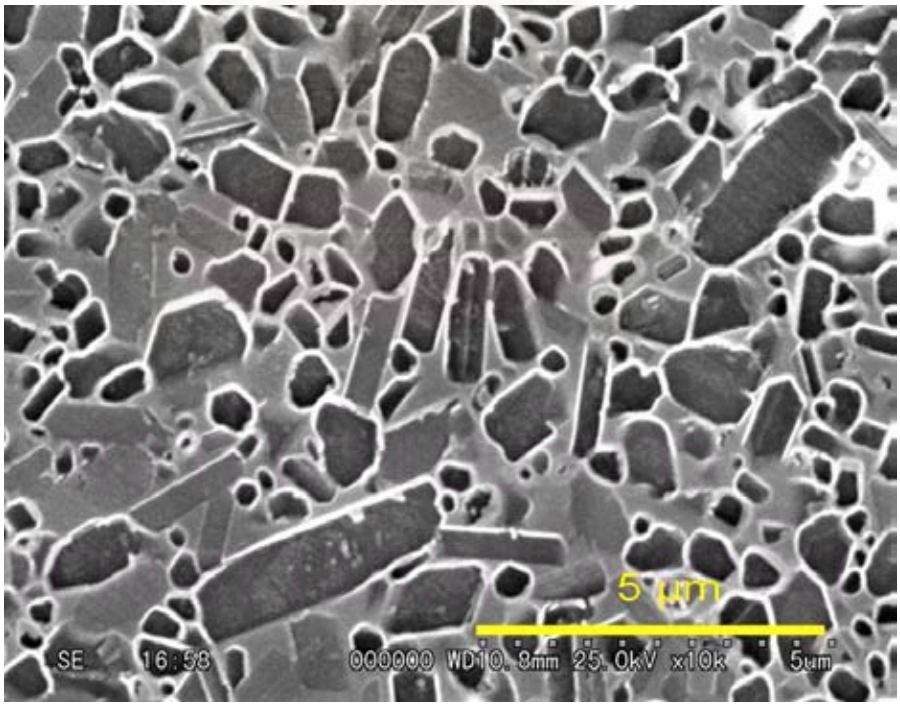

(b)

Fig 4.16 SEM micrographs of plasma etched E8H specimens sintered in air furnace at various temperature for 2 h; (a) 1500 °C, (b) 1650 °C

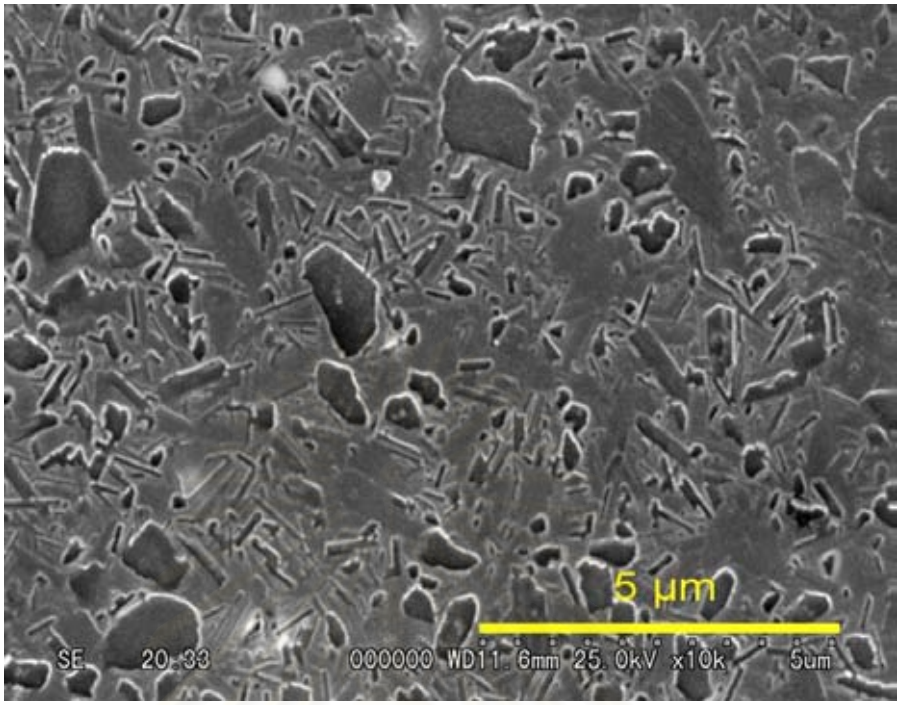

(a)

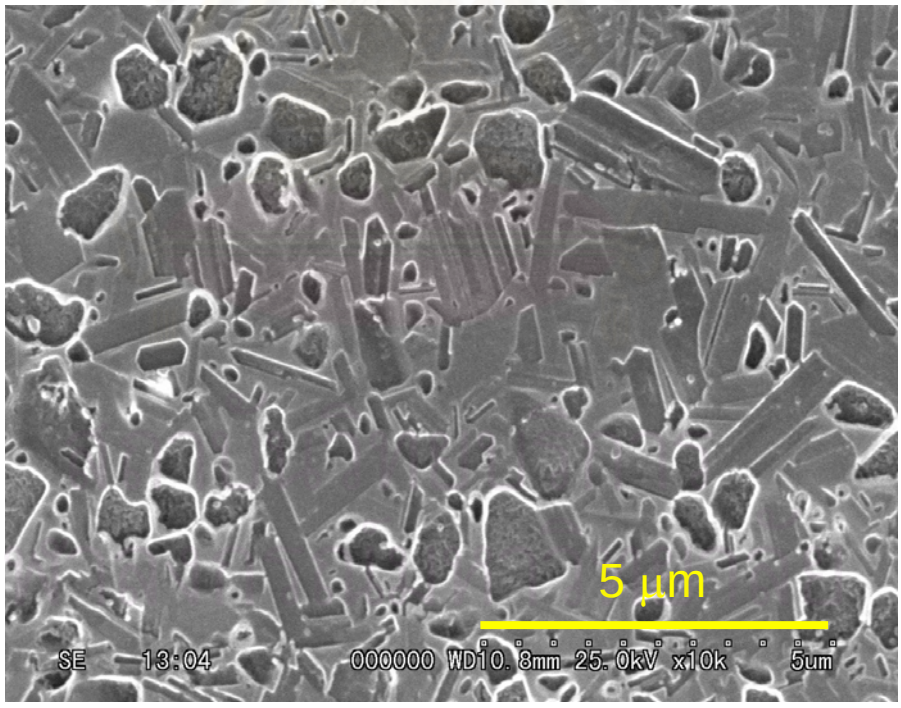

(b)

Fig 4.17 SEM micrographs of plasma etched H16H specimens sintered in air furnace at various temperature for 2 h; (a) 1500 °C, (b) 1650 °C

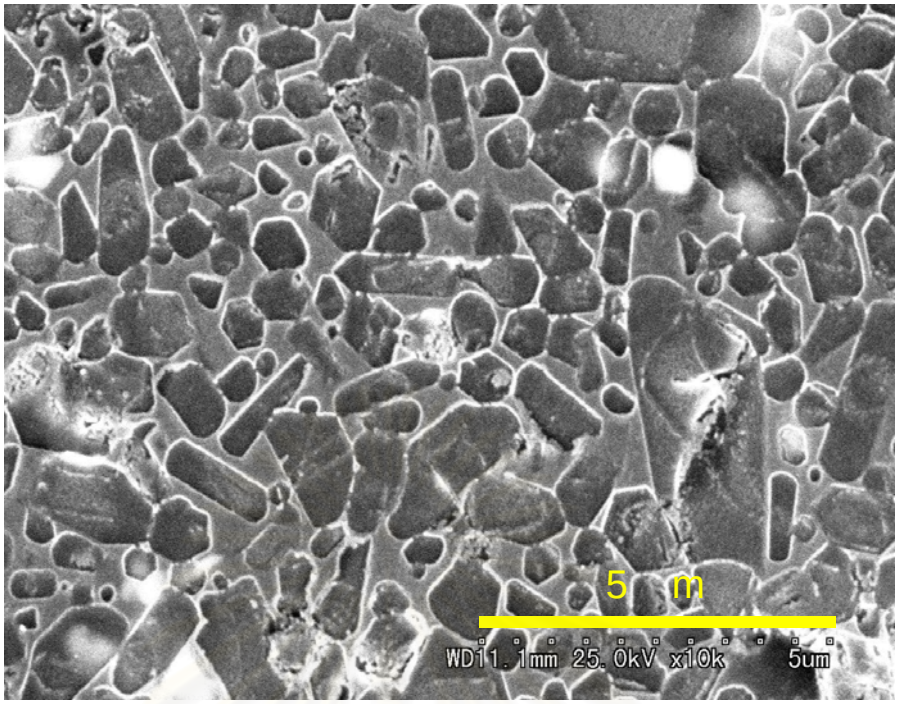

(a)

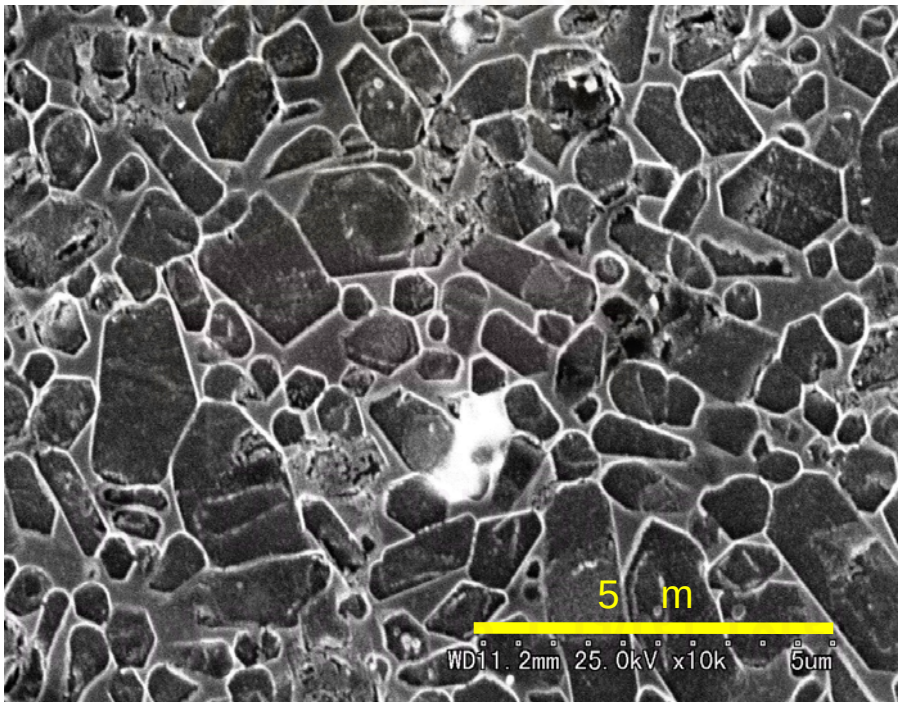

(b)

Fig 4.18 SEM micrographs of plasma etched E8H specimens sintered in N_2 furnace for 2 h; (a) 1750 °C and (b) 1800 °C

4.8 Mechanical properties

4.8.1 Vickers hardness and fracture toughness

Top view of indent is shown in Figure 4.19. The size of the indent and crack was measured, and the Vickers hardness (Hv) and fracture toughness (K_{IC}) were calculated by the equation in 3.5.7. The calculation results are shown in Appendix G.

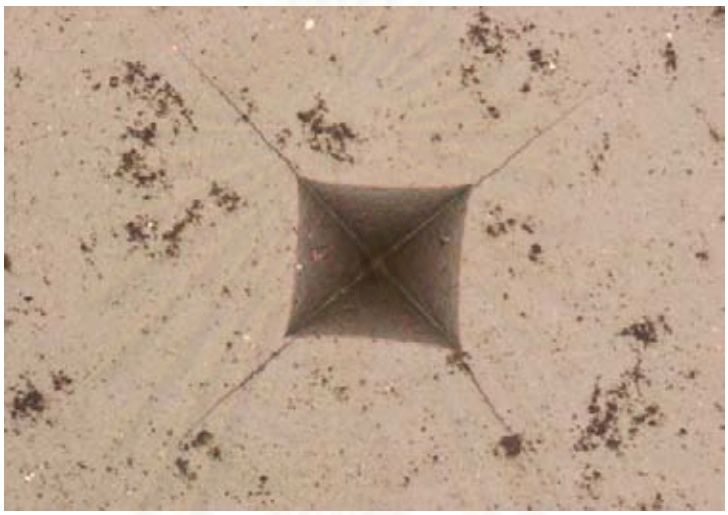

Fig 4.19 Top view of indent of E8H specimen sintered in air furnace at 1700 ^{O}C for 2 h

Table 4.2 Hv and K_{IC} of Si_3N_4 sintered in air furnace at 1700 ^{O}C for 2 h

Samples	Hv (GPa)	K_{IC} (MPa $m^{1/2}$)	Bulk density (g/cm^3)
E4H	12.7 ± 0.2	5.9 ± 0.4	3.09
E6H	13.0 ± 0.3	6.1 ± 0.3	3.13
E8H	12.7 ± 0.2	5.5 ± 0.1	3.14

The specimens of E4H, E6H, and E8H sintered at 1700 °C were selected for the measure of Vickers hardness (Hv) and fracture toughness (K_{IC}), because of their low oxygen contents. As shown in Table 4.2, both of Hv and K_{IC} values are not so different, in the compositions.

In Appendix H, properties of TOSHIBA's specimen are shown. Comparing its Hv, 16.8 GPa and K_{IC}, 5.4 MPa.$m^{1/2}$ to the results of our specimens, Hv, 12.7-13.0 GPa and K_{IC}, 5.5-6.1 MPa.$m^{1/2}$, the K_{IC} values of our specimens are similar to that of TOSHIBA's specimen. However, hardness of our specimens are lower than the commercial one. The reason for this might be due to the much amount of glassy phase in our specimens.

Vickers hardness and fracture toughness of specimens sintered in N_2 gas furnace are shown in Table 4.3. The K_{IC} values are higher than the specimens sintered in air furnace. The reason for this might be come from the larger grain in the specimens sintered in air (see Fig 4.16 and 4.15 (e)). Peillon and Thevenot reported that the fracture toughness is proportional to the grain diameter square root [51] and it increases with the fraction of the large grains.

Table 4.3 Hv and K_{1C} of specimens sintered in N_2 gas furnace at 1700 ^{O}C and 1800 ^{O}C for 2 h

Temperature (°C)	Samples	Hv (GPa)	K_{IC} (MPa $m^{1/2}$)	Bulk density (g/cm^3)
1750	E4H	13.3 ± 0.1	6.8 ± 0.7	3.15
	E6H	13.7 ± 0.2	6.5 ± 0.3	3.17
	E8H	13.4 ± 0.1	6.1 ± 0.3	3.17
1800	E4H	13.6 ± 0.3	6.6 ± 0.7	3.18
	E6H	13.8 ± 0.1	6.4 ± 0.7	3.17
	E8H	13.5 ± 0.6	6.8 ± 0.2	3.17

Moreover, the Vickers hardness values of specimens sintered in N_2 furnace are a little higher than the ones in an air furnace, because of the higher densities. However, Vickers hardness values are still lower than TOSHIBA's specimen.

Comparison of Vickers hardness and fracture toughness of specimens sintered in air furnace with different starting Si_3N_4 powder (α-powder and β-powder) are compared. In case of Piyaporn's thesis experiment [47], using α-Si_3N_4 powder as raw material, hardness and fracture toughness of sintered specimens are 16.0 GPa and 5.0 MPa $m^{1/2}$, respectively. The hardness of Piyaporn's specimens is higher than that of our specimens. It is come from the fact that α phase, which hardness is higher that that of β phase, remained in her specimen. On the contrary, fracture toughness of our specimens is higher than the specimens from α-powder, which is attributed to grain diameter of specimens produced from β-powder are larger than the α-powder as seen in Figure 4.20.

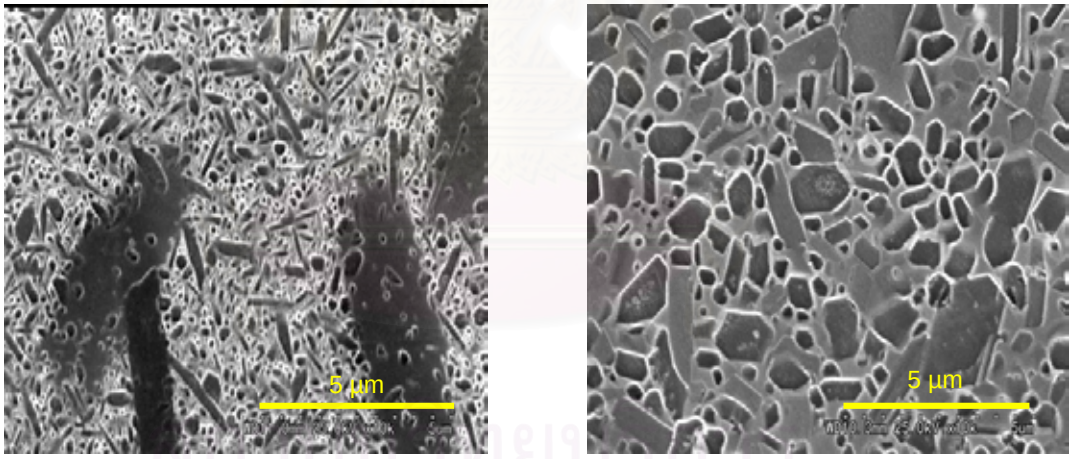

(a) (b)

Fig 4.20 SEM micrographs of specimens sintered in air furnace at 1700 °C for 2 h; (a) α-Si_3N_4 powder and (b) β-Si_3N_4 powder

4.8.2 Flexural strength

The averages biaxial flexural strength of specimens sintered both in air and N_2 gas furnace are shown in Table 4.4 and 4.5, respectively. The calculation results are attached as Table G-4, G-5, and G-6 in appendix G. In case of sintering in air furnace, the minimum strength value was 219 MPa and maximum was 263 MPa. The minimum and maximum values of specimens sintered in N_2 gas furnace were 261 MPa and 406 MPa, respectively.

Table 4.4 Biaxial flexural strength of specimens sintered in air atmosphere furnace

Sintering temperature (°C)	Strength (MPa)			
	E4H	E6H	E8H	E10H
1650				219 ± 36
1700	238 ± 25	263 ± 45	252 ± 42	

Table 4.5 Biaxial flexural strength of specimens sintered in N_2 gas furnace

Sintering temperature (°C)	Strength (MPa)		
	E4H	E6H	E8H
1750	406 ± 14	327 ± 49	328 ± 79
1800	307 ± 46	261 ± 34	390 ± 63

The difference in flexural strength of specimens sintered in air furnace with different mixing time were not significant. The strength values were lower than that those the specimens sintered in N_2 gas furnace. The causes are thought as follows:

1) Much amount of glass phase

As seen in Table 3.6, the oxygen content in the mixed powder increased with the mixing times. That cause the increase in the quantity of SiO_2 in mixed powder. As a result, the total content of glassy phase increased. It is reported that increasing the glassy phase lowered the strength lower.[52)]

2) Low aspect ratio of β-grains

Generally, the structures with elongated grains show better mechanical properties than that with equiaxed ones. Since the elongated grains cause linking each other, crack deflection and pull out of crystal increase. These cracks deflection and pull out crystals absorb energy and lead to an enlarged fracture surface. [53)] In this experiment, the grain morphology of specimens sintered both in air and N_2 gas furnace show small equiaxed grains, almost no elongated grains. Therefore, the flexural strength of specimens become low.

CHAPTER V

CONCLUSION

1. β-Si_3N_4 powder (SN-F2) could be ground down to 1 μm by both ball mill and attrition mill. However, attrition mill was selected for mixing raw powder with sintering additives due to high efficiency.
2. β-Si_3N_4 (SN-F2) was successfully sintered in air furnace. The relative densities after sintering at 1700 ^{O}C for 2 h were over 96 % of theoretical density. It was very close to the density of Si_3N_4 sintered in N_2 gas furnace. Mass losses of sintered specimens do not depend on sintering temperature, but depend on the quantity of glassy phase. Mass loss is presumed to be the reaction of Si_3N_4 and SiO_2.

$$Si_3N_4\ (s) + 3\ SiO_2\ (l) \longrightarrow 6\ SiO\ (g) + 2\ N_2\ (g)$$

However, the tendency mass loss phenomenon of the specimens sintered in air furnace differed from that of sintered in N_2 gas furnace.

3. The materials of both specimens sintered in air and N_2 gas furnace consisted of mostly small equiaxed grains of β-Si_3N_4 and much amount of glassy phase, the average grain size of β-Si_3N_4 was less than 5 μm.
4. Vickers hardness and fracture toughness of Si_3N_4 sintered in air furnace were in the range of 12.7 to 13.0 GPa and 5.5 to 6.1 MPa.m$^{1/2}$, respectively. These values were a little lower than the specimens sintered in N_2 gas furnace. Comparing with commercial Si_3N_4 (TOSHIBA's standard bar) the hardness values are lower but fracture toughness were a little higher.
5. The flexural strength values of specimens sintered in air and N_2 gas furnaces were in the range of 219 to 263 MPa and 261 to 406 MPa, respectively. These values were relatively low compared to ~ 600 MPa of commercial Si_3N_4.

CHAPTER VI

FUTURE WORK

1. In this experiment, the oxygen content of mixed powder was increased with mixing time. As a result, SiO_2 content increased too much by the long time milling. The much amount of SiO_2 degrades the mechanical properties. Therefore, it is important to develop a crushing technology without increasing SiO_2.

2. Al_2O_3 crucible reacted with Si_3N_4 and SiO and deteriorated or cracked after several times of usage. It causes high cost in production. Therefore, it is essential to find a technology or material, which delays the deterioration of crucible.

3. The mechanical strength of sintered specimens was not so high comparing with the commercial silicon nitride ceramics, because of the much amount of glassy phase. Therefore, we should improve the mechanical properties of these materials by reduction of the glassy phase in the future work.

References

1. M. Herrmann, H. Klemm, and C. Schubert. Silicon nitride based hard materials. Handbook of Ceramic Hard Materials. Dresden: WILEY-VCH Verlag GmbH, 2000.
2. Chihiro Kawai and Akira Yamakawa. Effect of Porosity and Microstructure on the Strength of Si_3N_4: Designed Microstructure for High Strength, High Thermal Shock Resistance, and Facile Machining. J. Am. Ceram. Soc. Vol.80, No.10 (1997) : 2705-2708.
3. G. R. Terwilliger. Properties of Sintered Si_3N_4. J. Am. Ceram. Soc. Vol.57, No.1(1974) : 48-49.
4. Randall M. German. Liquid Phase Sintering. New York and London : Plenum press, 1985.
5. S. Hampshire and K. H. Jack. The Kinetics of Densification and Phase Transformation of Nitrogen Ceramics. Proc. Bri. Ceram. Soc. 31, (1981) : 37-48.
6. Pavol Sajgalik and Miroslav Haviar. Pressureless Sintering of Si_3N_4 with Y_2O_3 and Al_2O_3 Additives-Compatibility of Powder Beds. Ceramics International. 18, (1992) : 279-283.
7. H. Yang, G. Yang and R. Yuan. Pressureless Sintering of Silicon Nitride with Magnesia and Ceria. Materials research Bulletin. Vol.33, No.10 (1998) : 1467-1473.
8. M. Yoshimura et al. Grain Size Controlled High-Strength Silicon Nitride Ceramics. J. Ceram. Soc. Japan. Vol.103, No.4 (1995) : 407-408.
9. E. Tani et al. Gas-Pressure Sintering of Si_3N_4 with Concurrent Addition of Al_2O_3 and 5 wt% Rare Earth Oxide: High fracture Toughness Si_3N_4 with Fiber-Like Structure. Am. Ceram. Soc. Bull. Vol65, No.9 (1986) : 1311-1315.
10. N. Hirosaki et al. Gas-Pressure Sintering of β-Si_3N_4 Containing Y_2O_3 and Nd_2O_3. J. Ceram. Soc. Japan. Vol.100, No.6 (1992) : 826-829.
11. N. Hirosaki et al. Gas-Pressure Sintering of Low-Purity β-Si_3N_4 powder. J. Ceram. Soc. Japan. Vol.100, No.11 (1992) : 1366-1370.

12. N. Hirosaki et al. Sintering of Y_2O_3-Al_2O_3-Doped β-Si_3N_4 Powder and Mechanical Properties of Sintered Materials. J. Ceram. Soc. Japan. Vol.102, No.8 (1994) : 790-794.
13. N. Hirosaki et al. Effect of Purification of β-Si_3N_4 Powder on the Strength of Sintered Materials. J. Ceram. Soc. Japan. Vol.103, No.6 (1995) : 639-643.
14. N. Hirosaki et al. Sintering of β-Si_3N_4 Powder Made by the Imide-Decomposition Method. J. Ceram. Soc. Japan. Vol.103, No.9 (1995) : 977-978.
15. T. Ogasawara et al. Fatigue Behavior of Silicon Nitride Ceramics Prepared from β-Phase Powder. J. Ceram. Soc. Japan. Vol.103, No.7 (1995) : 709-712.
16. Y. Okamoto et al. Mechanical Properties and Oxidation Resistance of Silicon Nitride Produced from Low Purity β-Powder. J. Ceram. Soc. Japan. Vol.103, No.7 (1995) : 720-723.
17. M. Mitomo et al. Grain Growth During Gas-Pressure Sintering of β-silicon nitride. J. Am. Ceram. Soc. Vol.73, No.8 (1990) : 2441-2445.
18. S. Wada et al. Sintering of Si_3N_4 Ceramics in Air Atmosphere Furnace. J. Ceram. Soc. Japan. Vol.109, No.3 (2001) : 281-283.
19. Yet-Ming Chiang, Dunbar P. Birnie, and W. David Kingery. Physical Ceramics. New York : Jonh Wiley & Sons. Inc., 1997.
20. F. L. Riley. Silicon nitride and related materials. J. Am. Ceram. Soc. Vol.83, No.2 (2000) : 245-265.
21. D. Hardie and K. H. Jack. Nature. Vol.180 (1957) : 332.
22. G. Ziegler, J. Heinrich, and G. Wotting. Relationships between processing, microstructure and properties of dense and reaction-bonded silicon nitride. J. Mater.Sci. Vol.22 (1987) : 3041-3086.
23. S. Saito. Fine Ceramics. New York : Elsevier, 1988.
24. www.kyocera.com/kicc/industrial/types/index.htm
25. G. Schwier. Keramische Komponenten fur Fahrzeug-Gasturbinen. Vol. 3, edited by W. Bunk, M. Bohmer and H. Kissler (Springer-Verlag, Berlin. (1984) : 55.
26. S. T. Buljan and P. E. Stermer. United State Patent. Patent Number : 4073845, 1978.

27. M. Mori, H. Inoue and T. Ochiai, Progress in Nitrogen Ceramics, edited by F.L. Riley, (1983) : 149.

28. T. Yamate, T. Kawahito and T. Iwai. Proceedings of the International Symposium on Ceramic Components for Engines, edited by S. Somiya, E. Kanai and K. Ando. Tokyo, (1983) : 333.

29. C. Grekovich, J. H. Rosolowski. Sintering of covalent Solid. J. Am. Ceram. Soc. Vol.59, No.7-8 (1976) : 336-343.

30. E. Proverbio, D. Rossi and R. Cigna. Influence of Water Vapour on High-temperature Oxidation of Al_2O_3-MgO doped Hot-pressed Silicon Nitride. J. Euro. Ceram. Soc. Vol.9 (1992) : 453-458.

31. V. K. Sarin. On the α-to-β Phase Transformation in Silicon Nitride. Mater. Sci. Eng. A105/106 (1988) : 151-159.

32. S. Wada. Control of Instability of Si_3N_4 during Pressureless Sintering. J. Ceram. Soc. Japan. Vol.109, No.10 (2001) : 803-808

33. C. Greskovich and S. Prochazka. Stability of Si_3N_4 and Liquid Phase (s) During Sintering. J. Am. Ceram. Soc. Vol.63 (1981) : C96-C97.

34. N. Hirosaki, Y. Akimune. Effect of Grain Growth of β-Silicon Nitride on Strength, Wiebull Modulus, and Fracture Toughness. J. Am. Ceram. Soc. Vol.76, No.7 (1993) : 1892-1894.

35. American Society for Testing and Material (ASTM). Standard test method for apparent porosity, liquid absorption, apparent specific gravity, and bulk density of refractory shapes by vacuum pressure. ASTM C: 830-893. New York : ASTM,1998.

36. Japanese Industrials Standards (JIS). Testing method for Vicker hardness of high performance ceramic, JIS R 1610, 1991.

37. Japanese Industrials Standards (JIS). Testing method for toughness of high performance ceramic, JIS R 1607, 1995.

38. American Society for Testing and Material (ASTM). Standard test method for biaxial flexure strength (Modulus of rupture) of ceramic substrates. ASTM F : 394-78. New York : ASTM, 1991.

39. T. P. Herbell, Marc R. Freedman, and James D. Kiser. Particle-Size Reduction of Si_3N_4 Powder with Si_3N_4 Milling Hardware. Ceram. Eng. Sci. Proc. Vol.7, No.7-8 (1986).

40. S. Wada. Increase of oxygen content in Si_3N_4 powder during ball milling using alcohol as solvent. J. Ceram. Soc. Japan. Vol.104 (1996) : 1092-1094.

41. Bongkoch Piempermpoon. Improvement of thermal conductivity of alumina for Peltier element. Master of science thesis, Department of Materials Science, Faculty of Science, Chulalongkorn University, 2002.

42. H. Scholze, Glastech. Ber.Vol.63 (1990) : 141-147.

43. R.G. Azrak and C.L. Angell, J. Phys. Chem. Vol.77 (1973) : 3048-3052.

44. Michel W. Barsoum. Fundamentals of ceramics. New York : McGraw-Hill Companies, Inc., 1997.

45. JANAF Thermochemical Table,2nd ed. U.S. Government printing office, Washington DC.,1971.

46. E.M. Levin, C.R. Lobbins, and H.F. Mcmurdie. Phase Diagrams for Ceramists. New York : Am. Ceram. Soc, 1964.

47. Piyaporn Chaiyapuck. Sintering of Silicon Nitride Ceramic in Air Furnace. Master of science thesis, Department of Materials Science, Faculty of Science, Chulalongkorn University, 2003.

48. H. Wada, M.J. Wang, and T.Y. Tien. Stability of Phase in the Si-C-N-O System. J. Am. Ceram. Soc. Vol.71, No.10 (1988) : 837-840.

49. M. Mitomo et al. Effect of Atmosphere on the Reaction Sintering of Si_2N_2O. Ceramics International. Vol.15 (1989) : 345-350.

50. K. Yokoyama and S. Wada. Solid-Gas Reaction during Sintering of Si_3N_4 Ceramics (Part 3) : Mass losses in a Carbon Heater Furnace. J. Ceram. Soc. Japan. Vol.108, No.3 (2000) : 230-235.

51. F.C. Peillon and F. thevenot. Microstructural designing of silicon nitride related to toughness. J. Eur. Ceram. Soc. Vol.22 (2002) : 271-278.

52. N. Hirosaki, and H. Matsubara. Effect of heat treatment of Si_3N_4 on grain growth behavior and grain boundary structure. J. Ceram. Soc. Japan. Vol.105 (1996) : 234 - 238.

53. G. Himsolt et al. Mechanical Properties of Hot-Pressed Silicon Nitride with Different Grain Structures. J. Am. Ceram. Soc. Vol.62, No.1-2 (1979) : 29 -32.

Appendices

Appendix A

Table A-1 Properties of Si_3N_4 powder

Grade	SN-F2
Beta-phase	100 %
Chemical composition	Fe = 0.2 %
	Na^+ = 5 ppm
	Cl^- = 1 ppm
	Fe^{++} = 2010 ppm
pH	9
Particle size	+150 μm < 0.01 %
	- 96 μm = 93 %
	- 48 μm = 66 %
	D_{50} = 29 μm

Table A-2 Properties of MgO used as additive

Grade	MJ-30
Chemical composition (%)	MgO = 99.9
	Fe = 0.0015
	Si = 0.0031
	Al = 0.0011
	Ca = 0.0001
Mean particle size (μm)	0.35

Table A-3 Properties of Al_2O_3 used as an additive

Grade	AKP-30
Chemical composition	Al_2O_3 = 99.99 %
	Fe ≤ 20 ppm
	Si ≤ 40 ppm
	Na ≤ 10 ppm
	Mg ≤ 10 ppm
	Cu ≤ 10 ppm
Packed bulk density	1.1~1.5 g/cm^3
Loose bulk density	0.7~1.1 g/cm^3
Mean particle size	0.4~0.6 μm
Specific surface area	4 ~ 6 m^2/g

Table A-4 Properties of Al_2O_3 used as packing powder

Grade	A-11
Chemical composition	L.O.I = 0.01 %
	Fe_2O_3 = 0.01 %
	SiO_2 = 0.01 %
	Na_2O = 0.30 %
	Al_2O_3 = 99.7 %
	H_2O = 0.06 %
True specific gravity	3.93 g/cm^3
Mean particle size	63 μm

Appendix B

Table B-1 Particle size of SN-F2 packing powder measured by sieve analysis

Sieve number (mesh)	Particle size (μm)	Weight of powder on sieve (%)	Accumulate weight (%)
50	300	0.03	0.03
100	150	14.86	14.89
140	106	7.15	22.04
200	75	11.43	33.47
230	63	6.16	39.63
325	45	9.46	49.09
400	38	5.00	54.09
Pan	< 38	45.91	100.00
Total		100.00	

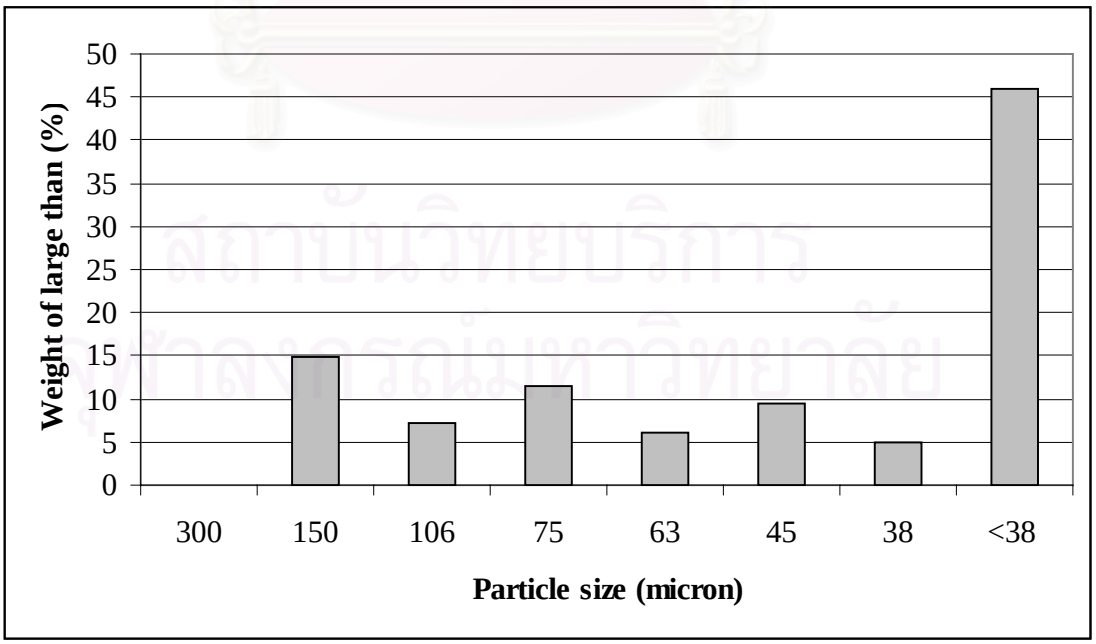

Fig B-1 Particle size distribution of SN-F2 packing powder measured by sieve analysis

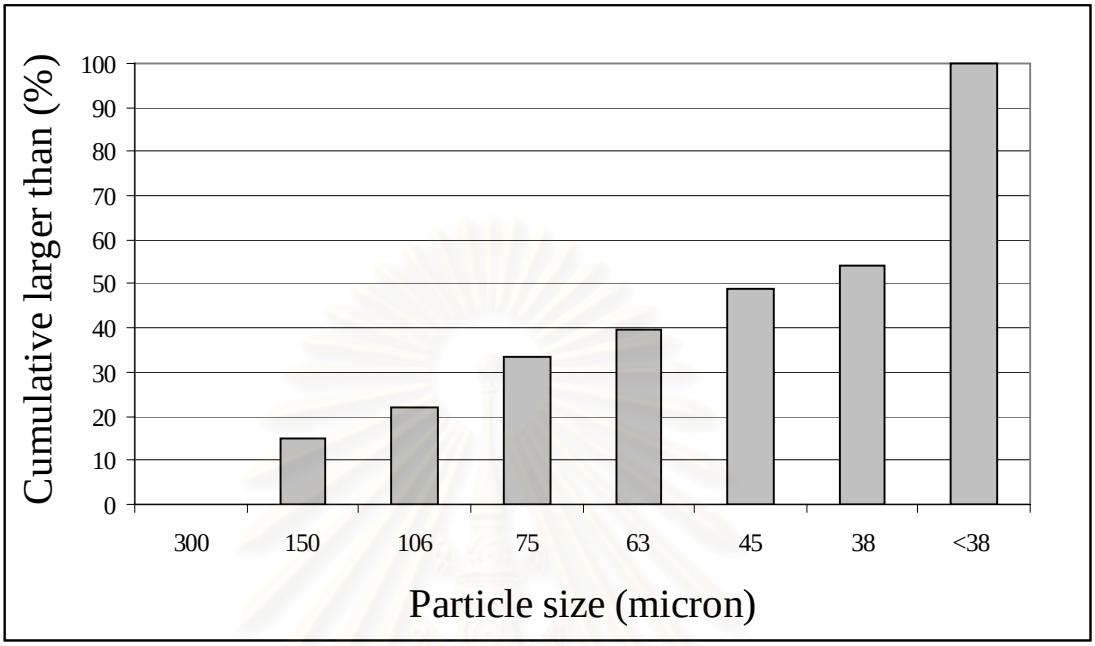

Fig B-2 Accumulate weight of SN-F2 packing powder measured by sieve analysis

Appendix C

Calculation of equilibrium $P_{SiO\ (g)}$, $P_{Mg\ (g)}$, $P_{MgO\ (g)}$, $P_{Al2O(g)}$ and $P_{AlO\ (g)}$ as a function of temperature

In the previous work, it has been reported that the mass loss of Si_3N_4 during sintering comes from the reaction between Si_3N_4 (s) and SiO_2 (l) according to reaction (1).[32)]

$$Si_3N_4\ (s) + 3\ SiO_2\ (l) = 6\ SiO\ (g) + 2\ N_2\ (g) \qquad \text{-------(1)}$$

The equilibrium constant of the reaction, K_p, is calculated from the equation (2).

$$K_p = \frac{P_{SiO}^{\ 6} . P_{N2}^{\ 2}}{a_{Si3N4(s)} . a_{SiO2(l)}^{\ 3}} \qquad \text{-------(2)}$$

As the activity of a solid and liquid is 1.[44)] Thus, the activity of Si_3N_4, ($a_{Si3N4(s)}$) and SiO_2, ($a_{SiO2(l)}$) is 1. Then:

$$K_p = P_{SiO\ (g)}^{\ 6} . P_{N2(g)}^{\ 2} \qquad \text{-------(3)}$$

From equation (3), the partial pressure of the SiO (g) that is in equilibrium of equation (1) is determined by equation (4):

$$\Delta G = \Delta G^O + RT\ \ln K_p \qquad \text{-------(4)}$$

The other extreme occurs when the driving force for the reaction is zero, that is $\Delta G = 0$ then :

$$0 = \Delta G^O + RT\ \ln K_p$$

$$\ln K_p = -(\Delta G^O/RT)$$

$$\log K_P = \frac{-\Delta G^0}{2.302RT}$$

$$\log K_P = \frac{-\Delta G^0}{4.576T} \qquad \text{-------(5)}$$

As equation (6), ΔG^O is the free energy changes that calculate from the free energy of each compound i (ΔG_i^O). All ΔG_i^O of each compound, which is Si_3N_4 (s), SiO_2 (l), N_2 (g) and SiO (g), are seen in the JANAF thermodynamic Table. [45)]

$$\Delta G^O_{rxn} = \Delta G_i^O(\text{products}) - \Delta G_i^O(\text{reactants}) \text{ -------(6)}$$

In this case, assuming Partial pressure of N_2 gas, $P_{N2(g)}$ is approximate 0.8 atm, because air includes 80 % of nitrogen. [18)] And R = 1.9872 Kcal.mol^{-1}.K^{-1} is used. [44)]

Partial pressure of SiO gas, $P_{SiO\ (g)}$ calculate from take equation (3) into equation (5) Thus:

$$\log P_{SiO\ (g)}^{\ 6} \cdot P_{N2(g)}^{\ 2} = \frac{-\Delta G^0}{4.576T}$$

$$\log P_{SiO\ (g)}^{\ 6} + \log P_{N2(g)}^{\ 2} = \frac{-\Delta G^0}{4.576T}$$

$$6 \log P_{SiO\ (g)} = \frac{-\Delta G^0}{4.576T} - 2 \log (0.8)$$

$$\log P_{SiO\ (g)} = \left(\frac{\frac{1}{4.576T} \times \left(-\Delta G^O + 0.88T \right)}{6} \right)$$

$$P_{SiO\ (g)} = 10^{\left(\frac{1}{27.45T} \times \left(-\Delta G^O + 0.88T \right) \right)}$$

As the same way, the gas partial pressure of Mg (g), MgO (g), Al_2O (g) and AlO (g) could be calculated from respectively reaction (7), (8), (9) and (10) by taken on equation (5). All of the calculation results are shown in Table C-1. In addition, the relationship between temperature (°C) and P_{SiO} (g), Mg (g), MgO (g), Al_2O (g) and AlO (g) are shown in Fig 1.

$MgO\ (s) = Mg\ (g) + 1/2O_2\ (g)$ -------(7)

$MgO\ (s) = MgO\ (g)$ -------(8)

$Al_2O_3\ (s) = Al_2O\ (g) + O_2\ (g)$ -------(9)

$2Al_2O_3\ (s) = 4AlO\ (g) + O_2\ (g)$ -------(10)

TableC- 1 Calculation results of SiO (g), Mg (g), MgO (g), Al_2O (g) and AlO (g) partial pressure in equilibrium over Si_3N_4 at temperature range1500 °C to 1700 °C (1773 K to 1973 K)

T (°C)	T (K)	Gases partial pressure (Pa)				
		$P_{SiO\ (g)}$	$P_{Mg\ (g)}$	$P_{MgO\ (g)}$	$P_{Al2O\ (g)}$	$P_{AlO\ (g)}$
1500	1773	7.8×10^{2}	3.38×10^{-6}	1.12×10^{-5}	4.98×10^{-20}	4.28×10^{-10}
1550	1823	1.85×10^{3}	1.32×10^{-5}	3.41×10^{-5}	8.69×10^{-19}	2.30×10^{-9}
1600	1873	4.14×10^{3}	4.73×10^{-5}	1.42×10^{-4}	1.23×10^{-17}	1.09×10^{-8}
1650	1923	8.92×10^{3}	1.61×10^{-4}	4.28×10^{-4}	1.51×10^{-16}	4.75×10^{-8}
1700	1973	1.84×10^{4}	5.07×10^{-4}	1.20×10^{-3}	1.62×10^{-15}	1.93×10^{-7}

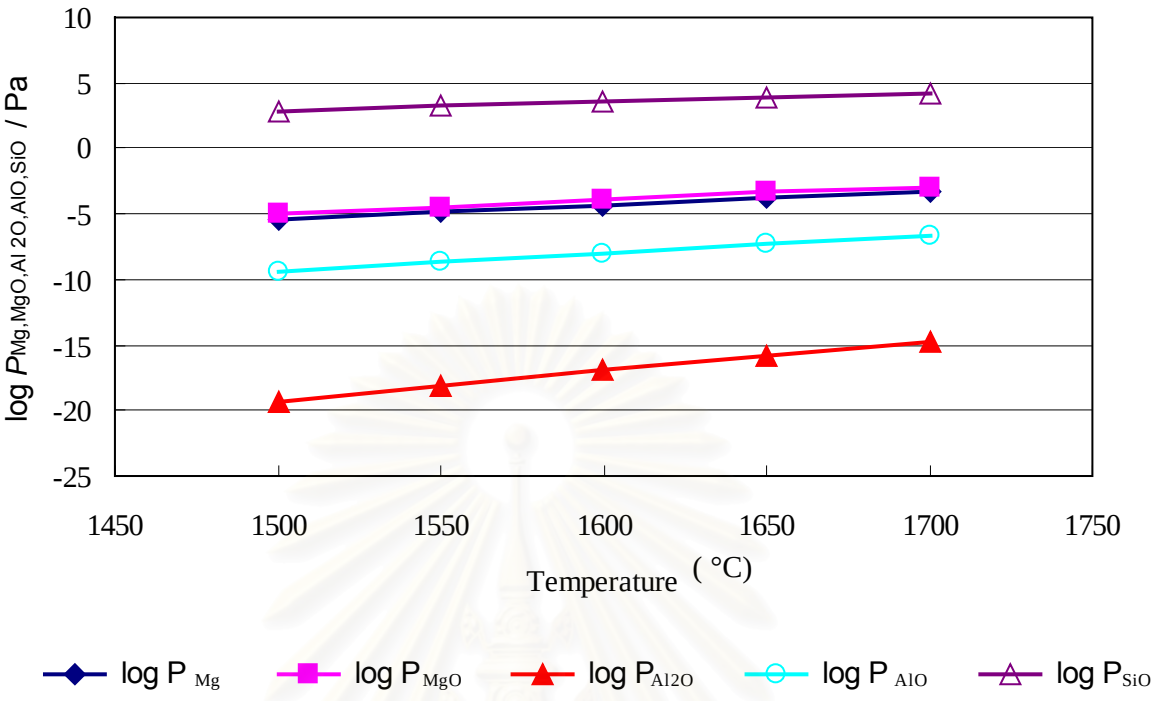

Fig C-1 Relationship between partial pressure of SiO (g), Mg (g), MgO (g), Al_2O (g) and AlO (g) as a function of temperature.

Appendix D

Table D-1 Mass loss of Si_3N_4 specimens sintered in air atmosphere furnace at 1500, 1550, 1600, 1650 and 1700 °C for 2 h

Sintered at 1500 °C for 2 h				
Sample code	Sample number	Green weight (g)	Sintered weight (g)	Mass loss (%)
E4H	1	2.0774	2.0846	-0.35
	2	2.1264	2.1404	-0.66
E6H	1	2.0526	2.0415	0.54
	2	2.0270	2.0195	0.37
E8H	1	2.0513	2.0347	0.81
	2	2.0219	2.0092	0.63
E10H	1	3.4462	3.3928	1.55
	2	3.5544	3.5000	1.53
E16H	1	3.4991	3.4247	2.13
	2	3.4663	3.3925	2.13
H10H	1	2.0275	1.9666	3.00
	2	2.0230	1.9693	2.65
H16H	1	2.0389	1.9603	3.86
	2	2.0015	1.9298	3.58
Sintered at 1550 °C for 2 h				
Sample code	Sample number	Green weight (g)	Sintered weight (g)	Mass loss (%)
E4H	1	2.0882	2.0824	0.28
	2	2.0718	2.0751	-0.16
E6H	1	2.0202	2.0082	0.59
	2	2.0654	2.0577	0.37
E8H	1	2.0486	2.0286	0.98
	2	2.0245	2.0066	0.88
E10H	1	3.4544	3.3984	1.62
	2	3.5472	3.4893	1.63
E16H	1	3.4993	3.4233	2.17
	2	3.5402	3.4651	2.12
H10H	1	1.9820	1.9259	2.83
	2	2.0300	1.9708	2.92
H16H	1	2.0767	1.9982	3.78
	2	2.0310	1.9539	3.80

Table D-1 (cont.)

Sintered at 1600 °C for 2 h				
Sample code	Sample number	Green weight (g)	Sintered weight (g)	Mass loss (%)
E4H	1	2.1035	2.0929	0.50
	2	2.1237	2.1240	-0.01
E6H	1	2.0127	1.9986	0.70
	2	2.0139	2.0040	0.49
E8H	1	2.0662	2.0452	1.02
	2	2.0338	2.0168	0.84
E10H	1	3.5112	3.4465	1.84
	2	3.4934	3.4327	1.74
E16H	1	3.515	3.4404	2.12
	2	3.5299	3.4569	2.07
H10H	1	2.0400	1.9791	2.99
	2	2.0453	1.9876	2.82
H16H	1	2.0296	1.9523	3.81
	2	2.0318	1.9554	3.76
Sintered at 1650 °C for 2 h				
Sample code	Sample number	Green weight (g)	Sintered weight (g)	Mass loss (%)
E4H	1	2.0822	2.0712	0.53
	2	2.1395	2.1350	0.21
E6H	1	2.0297	2.0163	0.66
	2	2.0573	2.0466	0.52
E8H	1	2.0519	2.0311	1.01
	2	2.0323	2.0145	0.88
E10H	1	3.5149	3.4486	1.89
	2	3.5623	3.4939	1.92
E16H	1	3.5482	3.4665	2.30
	2	3.5173	3.4318	2.43
H10H	1	2.0343	1.9726	3.03
	2	2.0020	1.9449	2.85
H16H	1	2.0106	1.9341	3.80
	2	2.0195	1.9427	3.80
Sintered at 1700 °C for 2 h				
Sample code	Sample number	Green weight (g)	Sintered weight (g)	Mass loss (%)
E4H	1	2.0327	2.0206	0.60
	2	2.0633	2.0601	0.16
E6H	1	2.0149	1.9995	0.76
	2	2.0371	2.0264	0.53
E8H	1	2.0363	2.0129	1.15
	2	2.0158	1.9956	1.00
E10H	1	3.4972	3.4295	1.94
	2	3.5629	3.4989	1.80
E16H	1	3.5354	3.4531	2.33
	2	3.5733	3.4938	2.22
H10H	1	2.0468	1.9869	2.93
	2	2.0112	1.9538	2.85
H16H	1	1.9981	1.9227	3.77
	2	2.0229	1.9471	3.75

Table D-2 Water absorption, apparent porosity and density of Si_3N_4 specimens sintered in air atmosphere furnace at 1500, 1550, 1600, 1650 and 1700 °C for 2 h

Sintered at 1500 °C for 2 h								
Sample code	Sample number	D (g)	S (g)	W (g)	W.A. (%)	A.P. (%)	B.D. (g/cm^3)	R.D. (%)
E4H	1	2.0846	1.4001	2.1750	4.34	11.67	2.68	83.23
	2	2.1404	1.4426	2.2424	4.77	12.75	2.67	82.80
E6H	1	2.0415	1.3569	2.0443	0.14	0.41	2.96	91.91
	2	2.0195	1.3376	2.0235	0.20	0.58	2.93	91.12
E8H	1	2.0347	1.3537	2.0360	0.06	0.19	2.97	92.58
	2	2.0092	1.3325	2.0111	0.09	0.28	2.95	91.92
E10H	1	3.393	2.2637	3.4089	0.47	1.39	2.95	92.87
	2	3.4998	2.3342	3.5239	0.69	2.03	2.93	92.21
E16H	1	3.4247	2.3356	3.4263	0.05	0.15	3.13	98.73
	2	3.3924	2.3173	3.3968	0.13	0.41	3.13	98.82
H10H	1	1.9666	1.3248	1.9674	0.04	0.12	3.05	96.51
	2	1.9693	1.3238	1.9709	0.08	0.25	3.03	95.97
H16H	1	1.9603	1.3177	1.9611	0.04	0.12	3.04	96.70
	2	1.9298	1.2974	1.9312	0.07	0.22	3.03	96.63
Sintered at 1550 °C for 2 h								
Sample code	Sample number	D (g)	S (g)	W (g)	W.A. (%)	A.P. (%)	B.D. (g/cm^3)	R.D. (%)
E4H	1	2.0824	1.3856	2.0911	0.42	1.23	2.94	91.32
	2	2.0751	1.3779	2.0879	0.62	1.80	2.91	90.43
E6H	1	2.0082	1.3690	2.0089	0.03	0.11	3.13	97.13
	2	2.0577	1.3999	2.0586	0.04	0.14	3.11	96.68
E8H	1	2.0286	1.3879	2.0293	0.03	0.11	3.15	98.19
	2	2.0066	1.3699	2.0075	0.04	0.14	3.14	97.70
E10H	1	3.3985	2.3165	3.4139	0.45	1.40	3.09	97.07
	2	3.4889	2.3794	3.5072	0.52	1.62	3.08	96.97
E16H	1	3.4232	2.3377	3.4291	0.17	0.54	3.13	98.63
	2	3.4647	2.3657	3.4721	0.21	0.67	3.12	98.47
H10H	1	1.9259	1.2958	1.9266	0.04	0.11	3.04	96.28
	2	1.9708	1.3242	1.9715	0.04	0.11	3.03	96.02
H16H	1	1.9982	1.3505	1.9991	0.05	0.14	3.07	97.77
	2	1.9539	1.3180	1.9549	0.05	0.16	3.06	97.36

Table D-2 (cont.)

Sintered at 1600 °C for 2 h								
Sample code	Sample number	D (g)	S (g)	W (g)	W.A. (%)	A.P. (%)	B.D. (g/cm^3)	R.D. (%)
E4H	1	2.0929	1.4176	2.0961	0.15	0.47	3.07	95.44
	2	2.1240	1.4336	2.1264	0.11	0.35	3.05	94.86
E6H	1	1.9986	1.3649	1.9992	0.03	0.09	3.14	97.51
	2	2.0040	1.3672	2.0046	0.03	0.09	3.13	97.30
E8H	1	2.0452	1.3984	2.0461	0.04	0.14	3.15	98.03
	2	2.0168	1.3732	2.0181	0.06	0.20	3.12	97.09
E10H	1	3.4193	2.3359	3.4261	0.20	0.62	3.13	98.31
	2	3.4326	2.3443	3.4479	0.45	1.39	3.10	97.50
E16H	1	3.4401	2.3513	3.4446	0.13	0.41	3.14	98.94
	2	3.4564	2.3653	3.4649	0.25	0.77	3.13	98.84
H10H	1	1.9791	1.3369	1.9799	0.04	0.12	3.07	97.07
	2	1.9876	1.3407	1.9886	0.05	0.15	3.06	96.75
H16H	1	1.9523	1.3177	1.9531	0.04	0.13	3.06	97.51
	2	1.9554	1.3132	1.9562	0.04	0.12	3.03	96.51
Sintered at 1650 °C for 2 h								
Sample code	Sample number	D (g)	S (g)	W (g)	W.A. (%)	A.P. (%)	B.D. (g/cm^3)	R.D. (%)
E4H	1	2.0712	1.4059	2.0729	0.08	0.25	3.09	96.08
	2	2.1350	1.4476	2.1366	0.07	0.23	3.09	95.87
E6H	1	2.0163	1.3776	2.0171	0.04	0.13	3.14	97.58
	2	2.0466	1.3958	2.0478	0.06	0.18	3.13	97.15
E8H	1	2.0311	1.3882	2.0331	0.10	0.31	3.14	97.78
	2	2.0145	1.3750	2.0154	0.04	0.15	3.13	97.66
E10H	1	3.4482	2.3573	3.4578	0.28	0.87	3.12	98.26
	2	3.4933	2.3856	3.5013	0.23	0.72	3.12	98.18
E16H	1	3.4662	2.372	3.4706	0.13	0.40	3.15	99.25
	2	3.4317	2.3488	3.4381	0.19	0.59	3.14	99.10
H10H	1	1.9726	1.3321	1.9734	0.04	0.14	3.07	97.00
	2	1.9449	1.3109	1.9459	0.05	0.18	3.05	96.59
H16H	1	1.9341	1.2999	1.9349	0.04	0.13	3.04	96.67
	2	1.9427	1.3035	1.9455	0.14	0.44	3.02	96.04

Table D-2 (cont.)

Sintered at 1700 °C for 2 h								
Sample code	Sample number	D (g)	S (g)	W (g)	W.A. (%)	A.P. (%)	B.D. (g/cm^3)	R.D. (%)
E4H	1	2.0206	1.3740	2.0230	0.12	0.37	3.10	96.33
	2	2.0601	1.3977	2.0632	0.15	0.47	3.08	95.78
E6H	1	1.9995	1.3648	2.0015	0.10	0.31	3.13	97.19
	2	2.0264	1.3810	2.0285	0.10	0.32	3.12	96.86
E8H	1	2.0129	1.3759	2.0149	0.10	0.31	3.14	97.79
	2	1.9956	1.3616	1.9968	0.06	0.18	3.13	97.53
E10H	1	3.4295	2.342	3.4345	0.15	0.46	3.13	98.44
	2	3.499	2.3875	3.5017	0.08	0.24	3.13	98.48
E16H	1	3.4535	2.3616	3.4556	0.06	0.19	3.15	99.30
	2	3.4937	2.3862	3.4987	0.14	0.45	3.13	98.79
H10H	1	1.9869	1.3413	1.9886	0.09	0.25	3.06	96.80
	2	1.9538	1.3166	1.9544	0.03	0.09	3.05	96.61
H16H	1	1.9227	1.2913	1.9237	0.05	0.16	3.03	96.49
	2	1.9471	1.3054	1.9478	0.04	0.11	3.02	96.19

Note:
D = Dry weight
S = Suspended weight in water
W = Saturated weight
W.A. = Water absorption
A.P. = Apparent porosity
B.D. = Bulk density
R.D. = Relative density

Table D-3 Mass loss of Si_3N_4 specimens sintered in N_2 atmosphere furnace at 1750 and 1800 °C for 2 h

Sintered at 1750 °C for 2 h				
Sample code	Sample number	Green weight (g)	Sintered weight (g)	Mass loss (%)
E4H	1	4.4841	4.3732	2.47
	2	4.5209	4.3820	3.07
E6H	1	4.4690	4.3456	2.76
	2	4.5372	4.3861	3.33
E8H	1	4.5387	4.3886	3.31
	2	4.5157	4.3722	3.18
	3	4.5388	4.3815	3.47
Sintered at 1800 °C for 2 h				
Sample code	Sample number	Green weight (g)	Sintered weight (g)	Mass loss (%)
E4H	1	4.5104	4.3254	4.10
	2	4.5033	4.2553	5.51
E6H	1	4.5157	4.3087	4.58
	2	4.4473	4.1825	5.95
E8H	1	4.5322	4.2945	5.24
	2	4.5540	4.3448	4.59
	3	4.4979	4.2599	5.29

Table D-4 Water absorption, apparent porosity and density of Si_3N_4 specimens sintered in N_2 gas furnace at 1750 and 1800 °C for 2 h

Sintered at 1750 °C for 2 h								
Sample code	Sample number	D (g)	S (g)	W (g)	W.A. (%)	A.P. (%)	B.D. (g/cm^3)	R.D. (%)
E4H	1	4.3732	2.9944	4.3773	0.09	0.30	3.15	97.87
	2	4.3820	3.0030	4.3859	0.09	0.28	3.16	98.07
E6H	1	4.3456	2.9814	4.3498	0.10	0.31	3.16	98.28
	2	4.3861	3.0099	4.3905	0.10	0.32	3.17	98.32
E8H	1	4.3886	3.0138	4.3929	0.10	0.31	3.17	98.79
	2	4.3722	3.0021	4.3777	0.13	0.40	3.17	98.67
	3	4.3815	3.0091	4.3864	0.11	0.36	3.17	98.76
Sintered at 1800 °C for 2 h								
Sample code	Sample number	D (g)	S (g)	W (g)	W.A. (%)	A.P. (%)	B.D. (g/cm^3)	R.D. (%)
E4H	1	4.3254	2.9859	4.3302	0.11	0.36	3.21	99.58
	2	4.2553	2.9202	4.2613	0.14	0.45	3.16	98.20
E6H	1	4.3087	2.9587	4.3160	0.17	0.54	3.16	98.24
	2	4.1825	2.8751	4.1888	0.15	0.48	3.17	98.53
E8H	1	4.2945	2.9516	4.3005	0.14	0.44	3.17	98.84
	2	4.3448	2.9845	4.3504	0.13	0.41	3.17	98.75
	3	4.2599	2.9268	4.2657	0.14	0.43	3.17	98.77

Note: D = Dry weight
S = Suspended weight in water
W = Saturated weight
W.A. = Water absorption
A.P. = Apparent porosity
B.D. = Bulk density
R.D. = Relative density

Appendix E

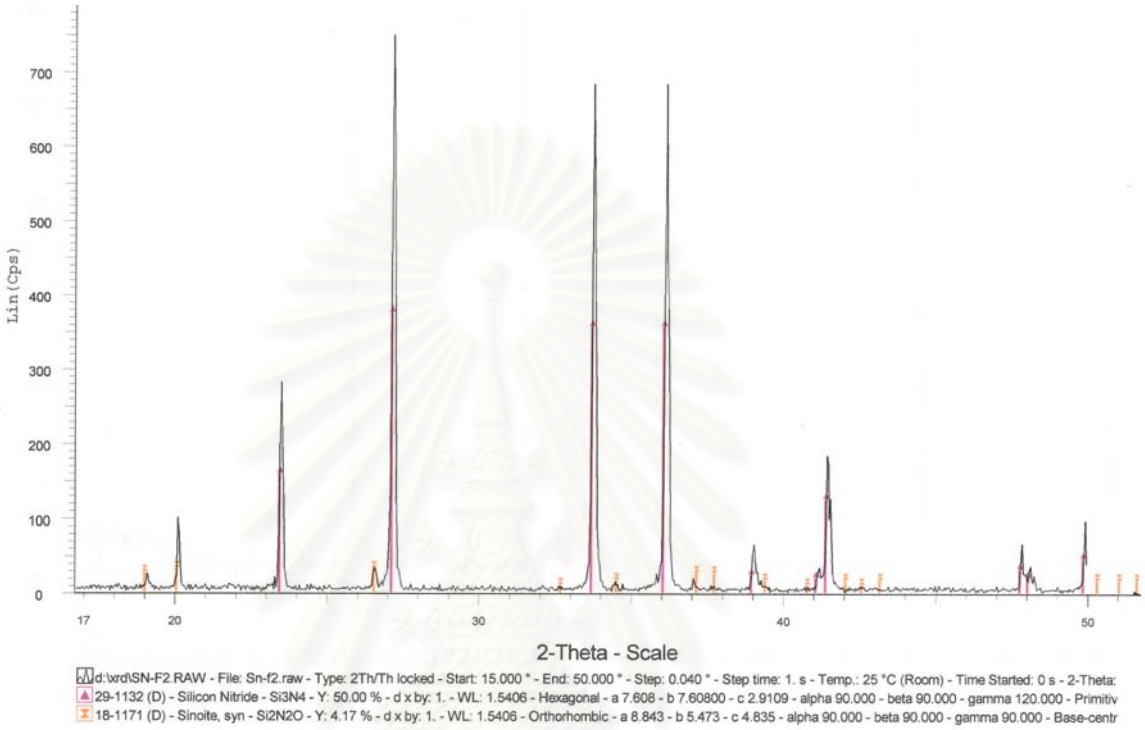

Fig E-1 X-ray diffraction pattern of Si_3N_4 raw powder (SN-F2)

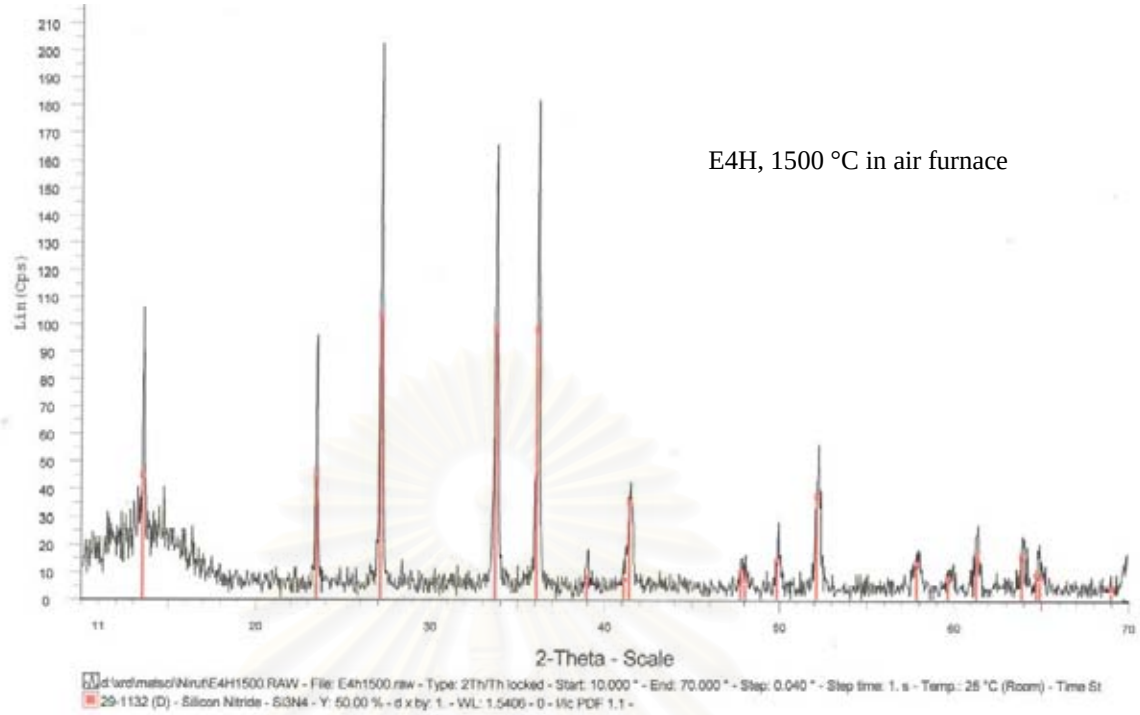

E4H, 1500 °C in air furnace

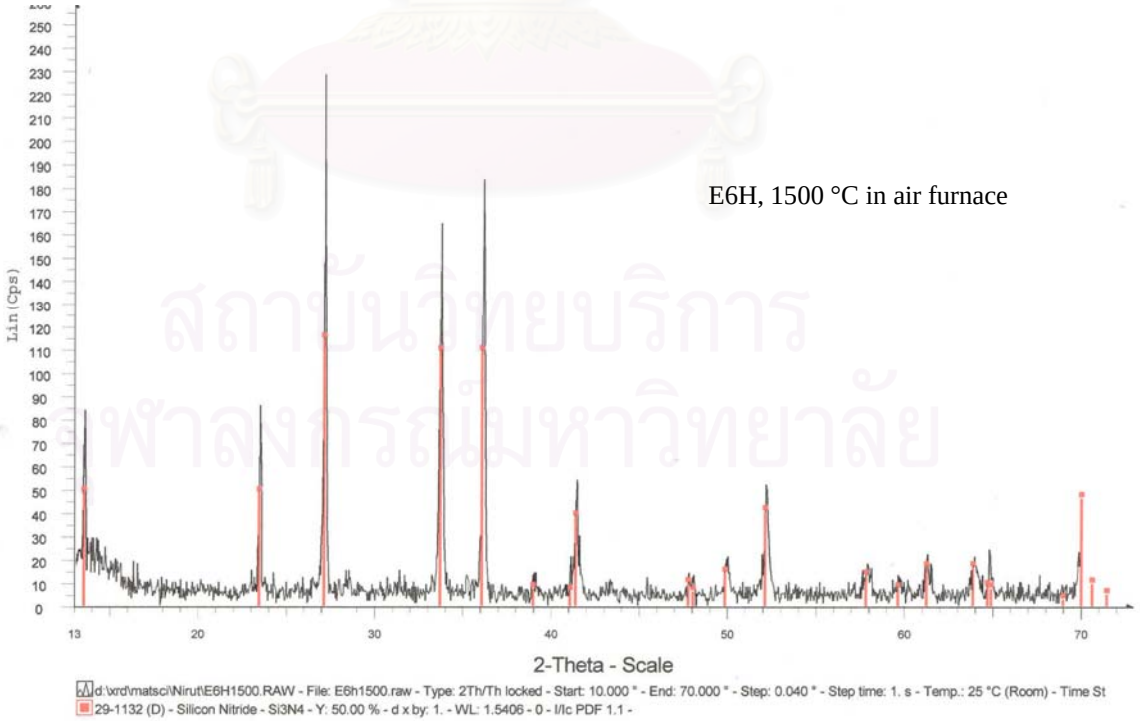

E6H, 1500 °C in air furnace

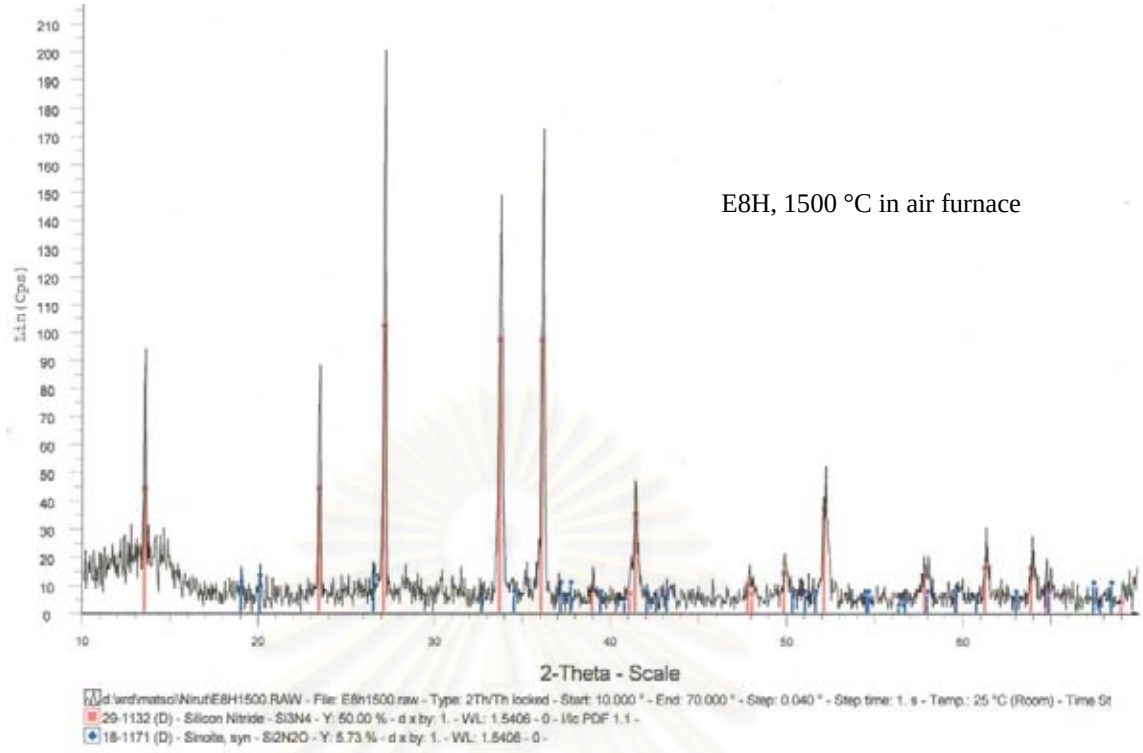

E8H, 1500 °C in air furnace

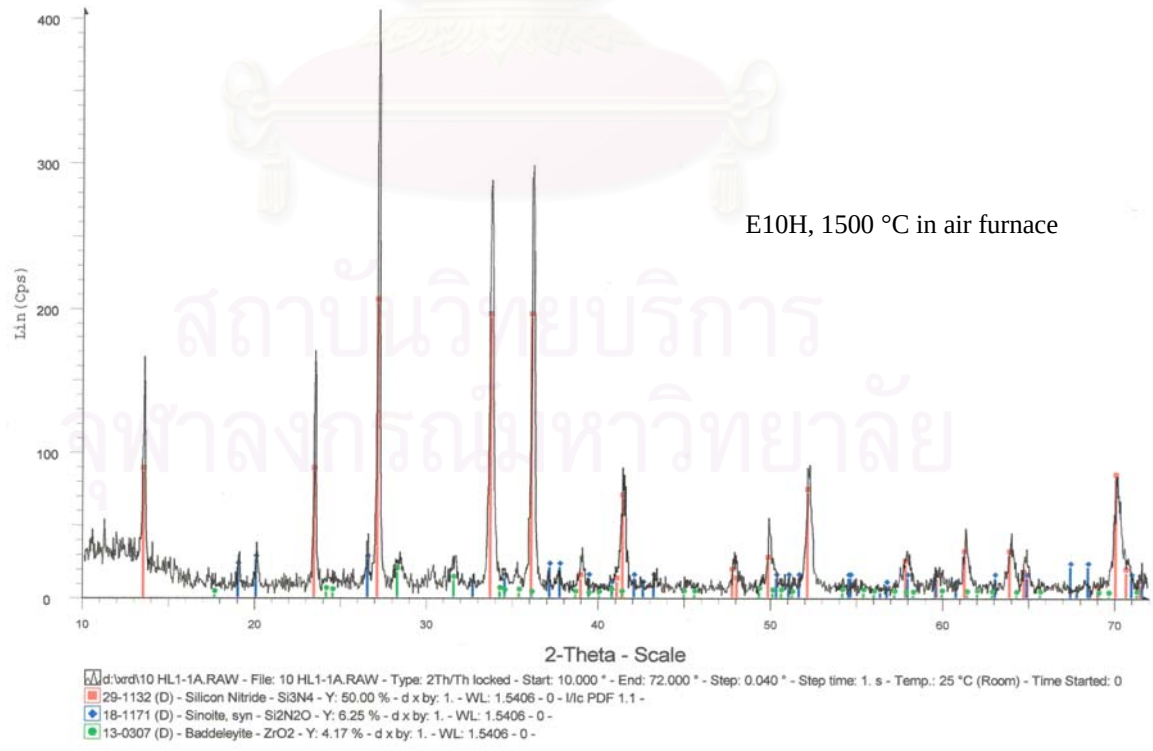

E10H, 1500 °C in air furnace

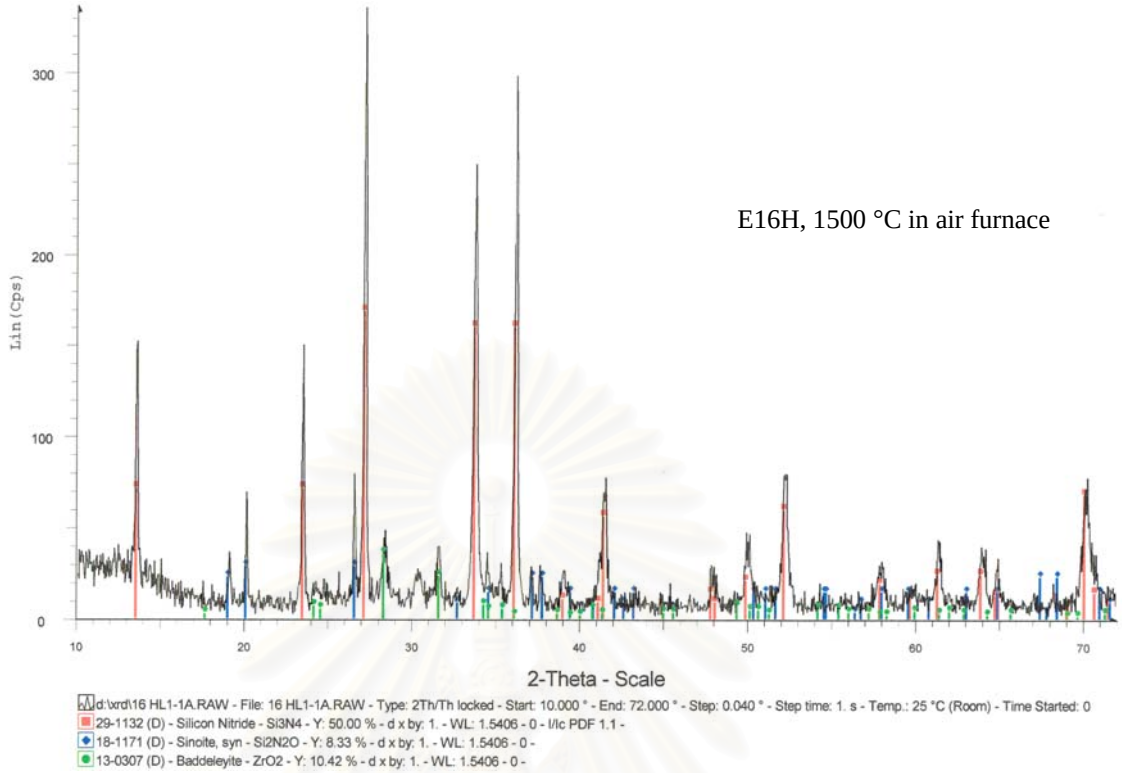

E16H, 1500 °C in air furnace

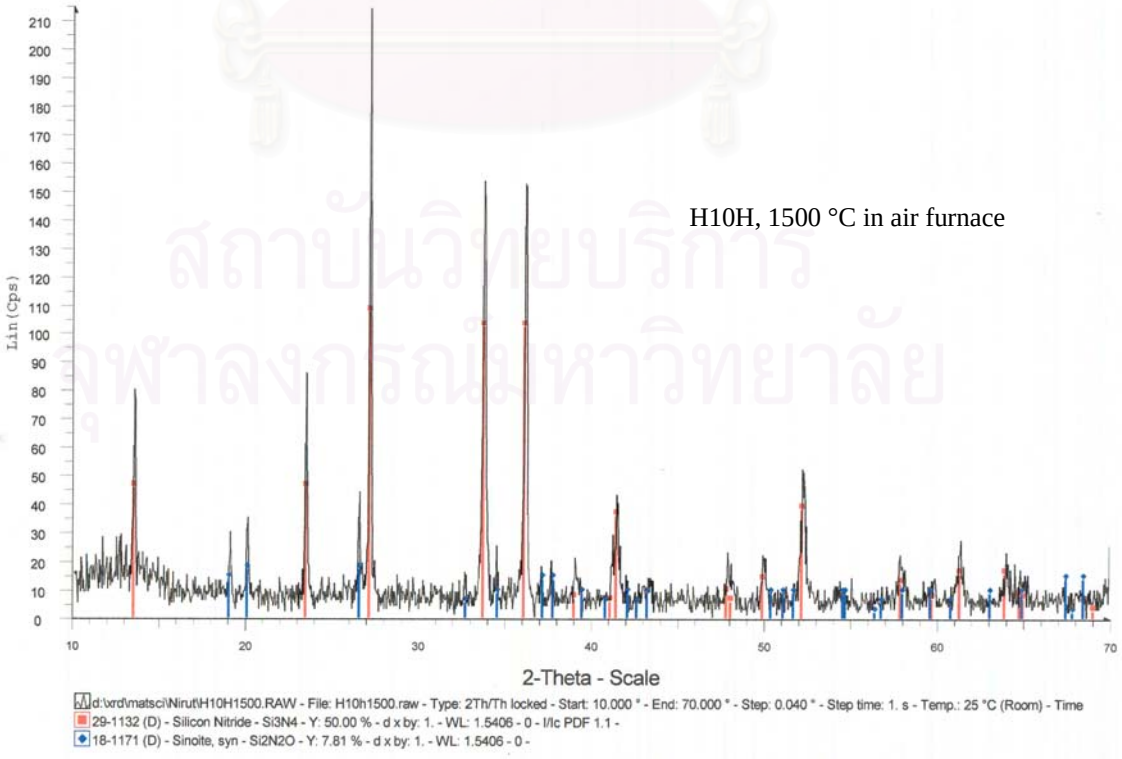

H10H, 1500 °C in air furnace

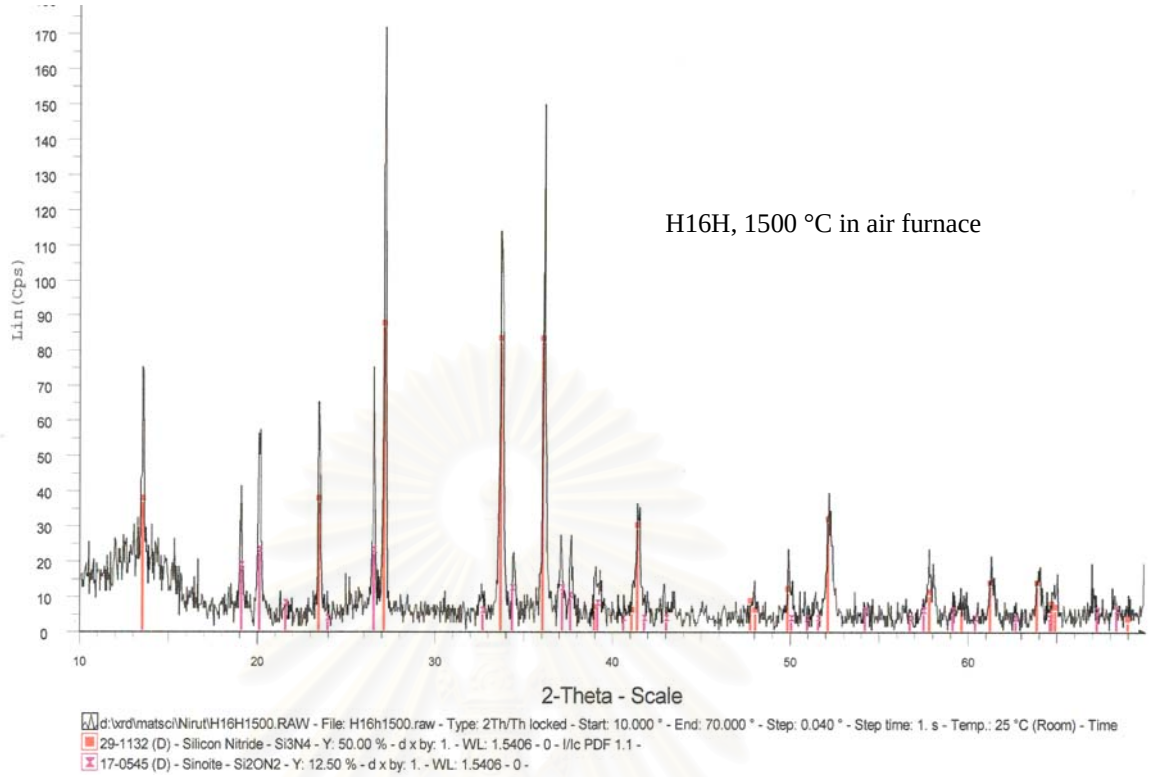

H16H, 1500 °C in air furnace

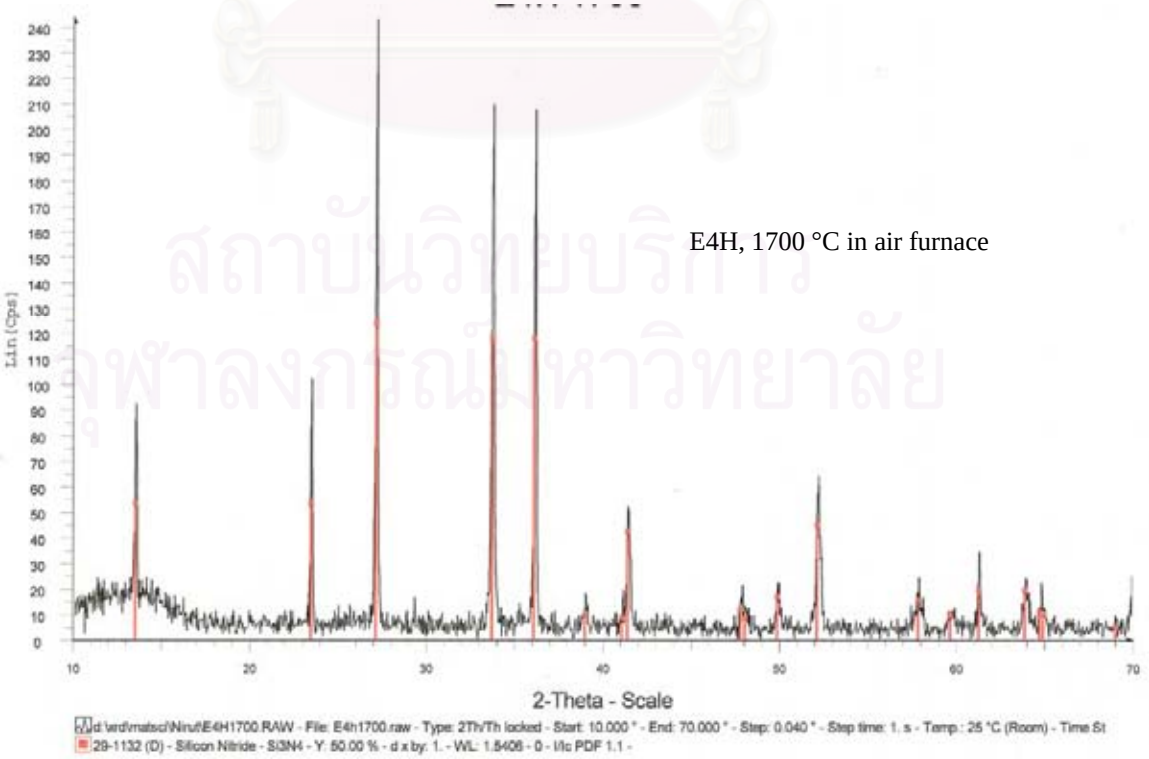

E4H, 1700 °C in air furnace

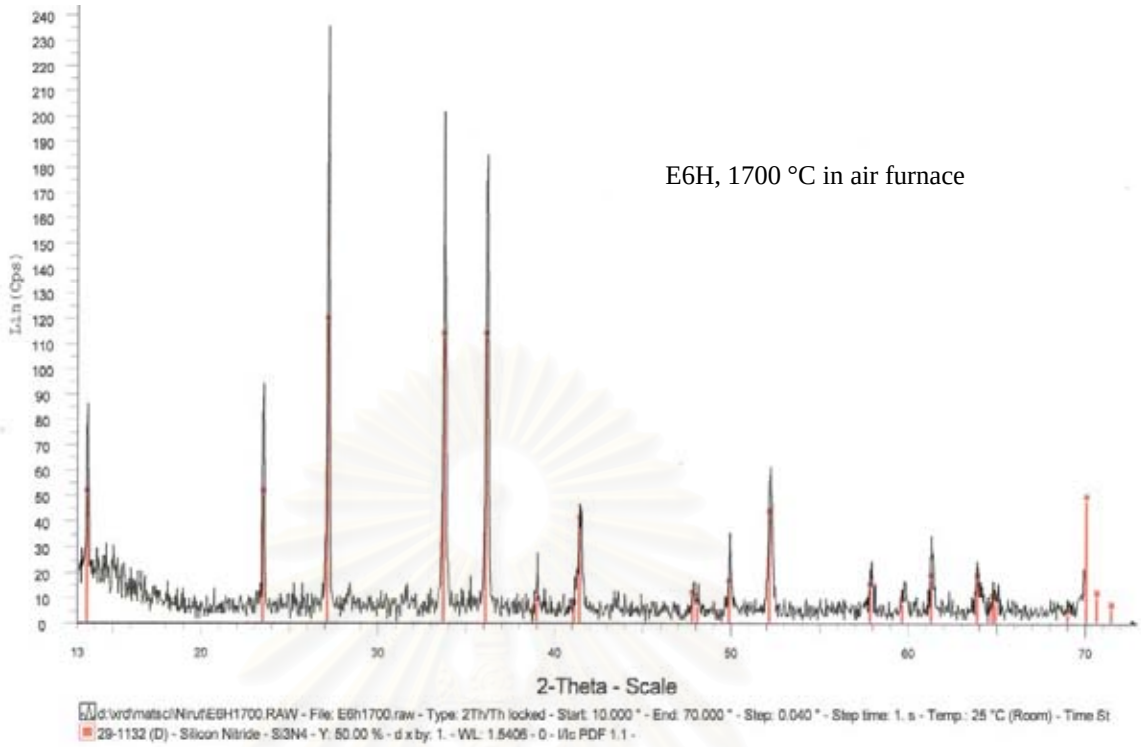

E6H, 1700 °C in air furnace

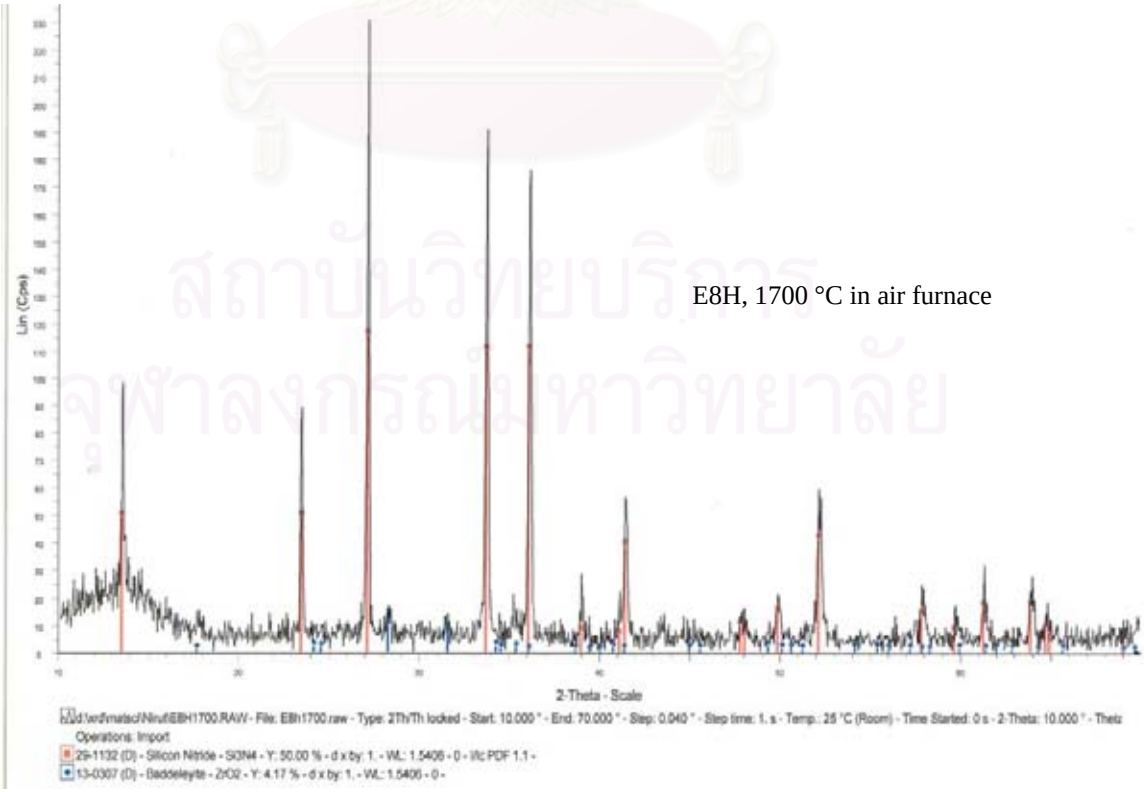

E8H, 1700 °C in air furnace

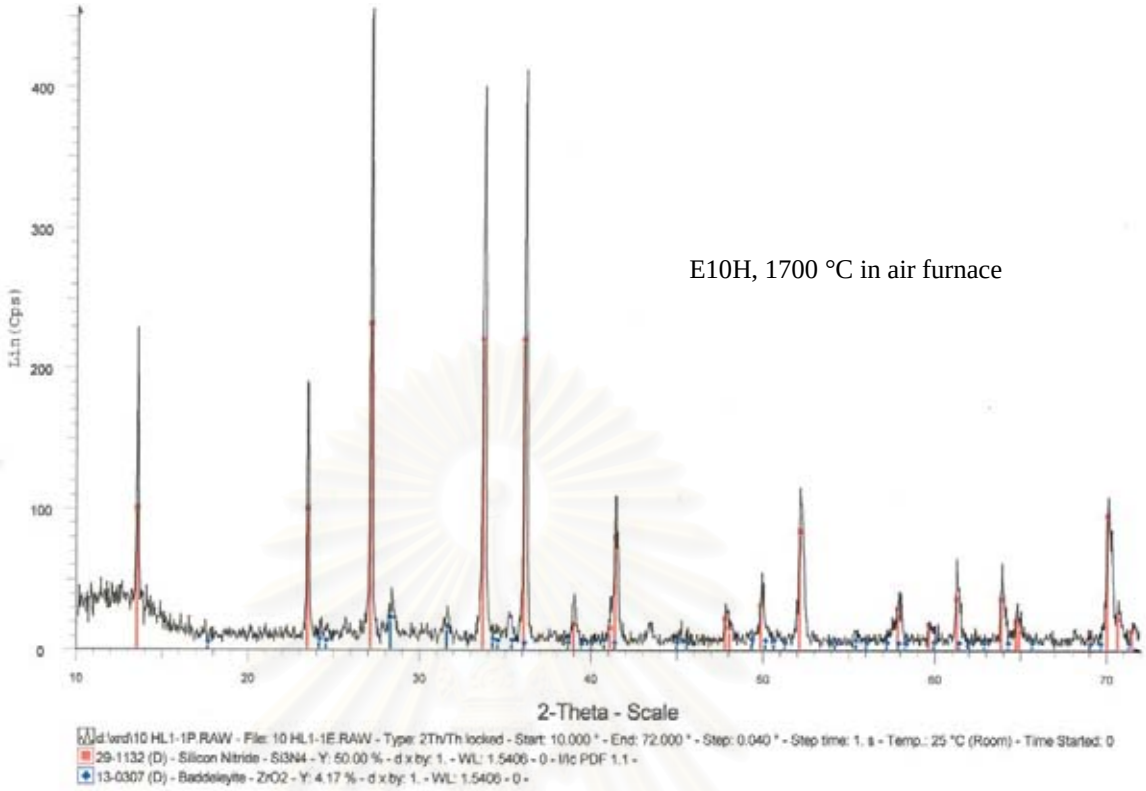

E10H, 1700 °C in air furnace

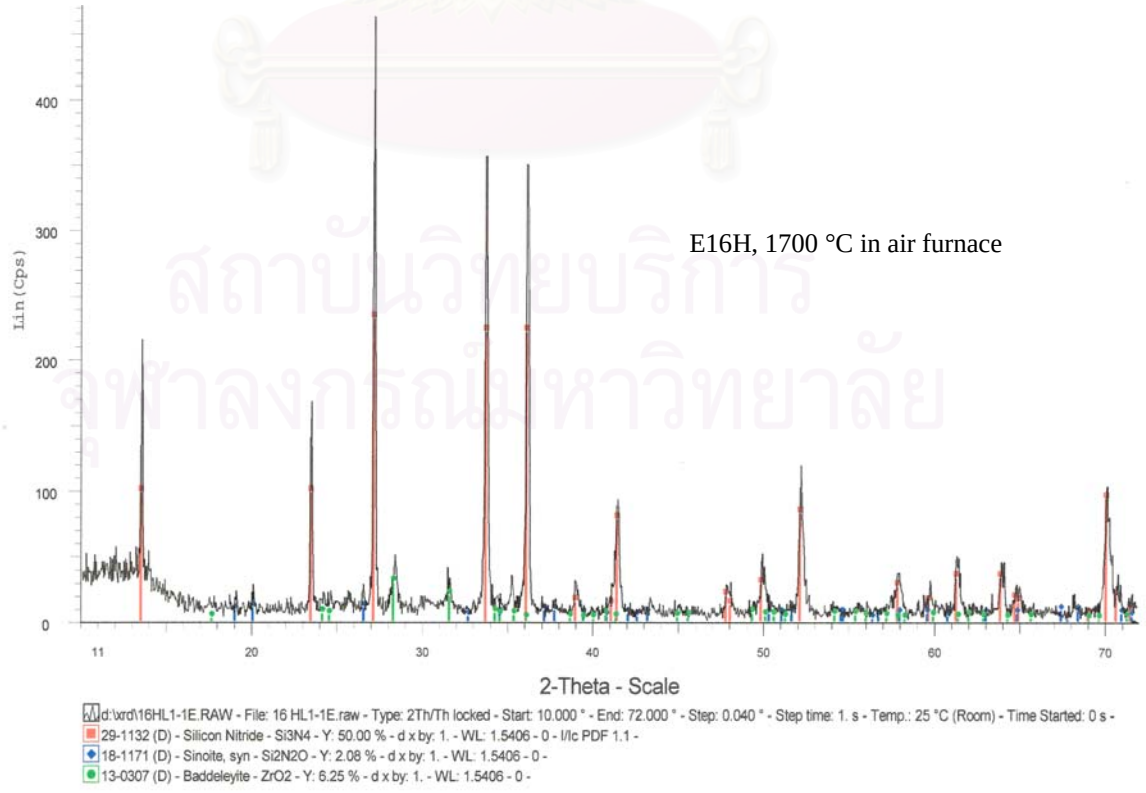

E16H, 1700 °C in air furnace

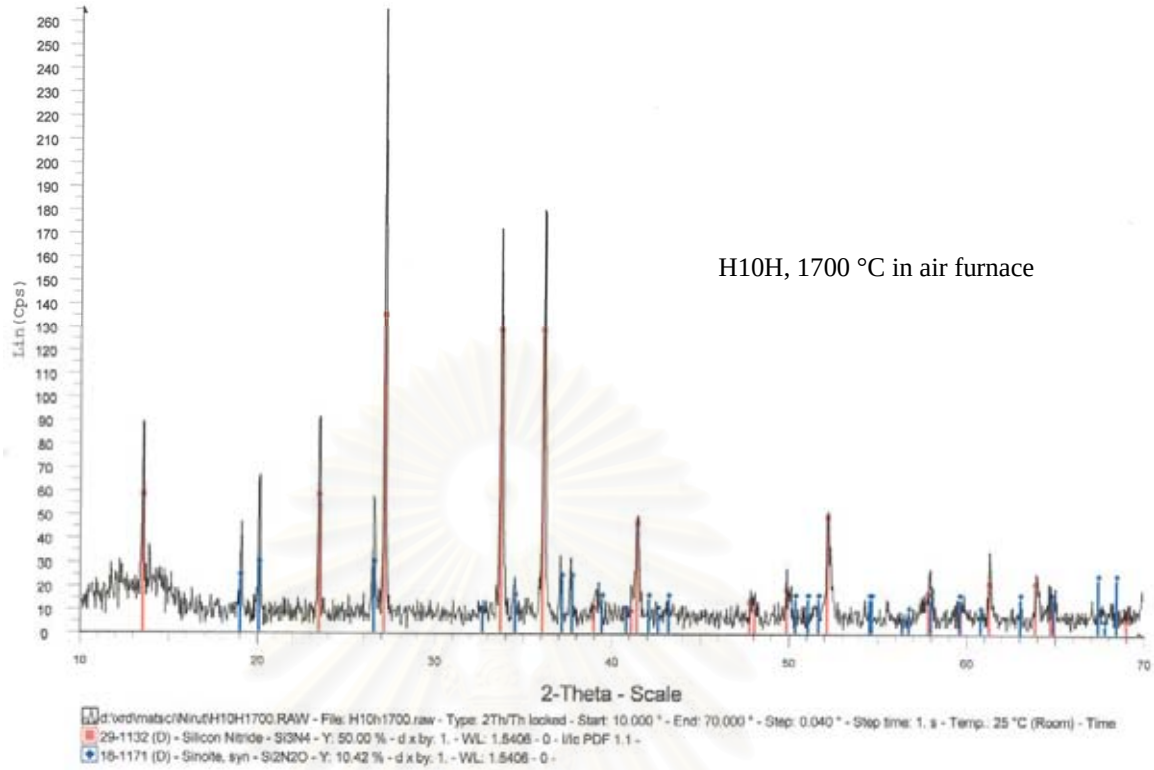

H10H, 1700 °C in air furnace

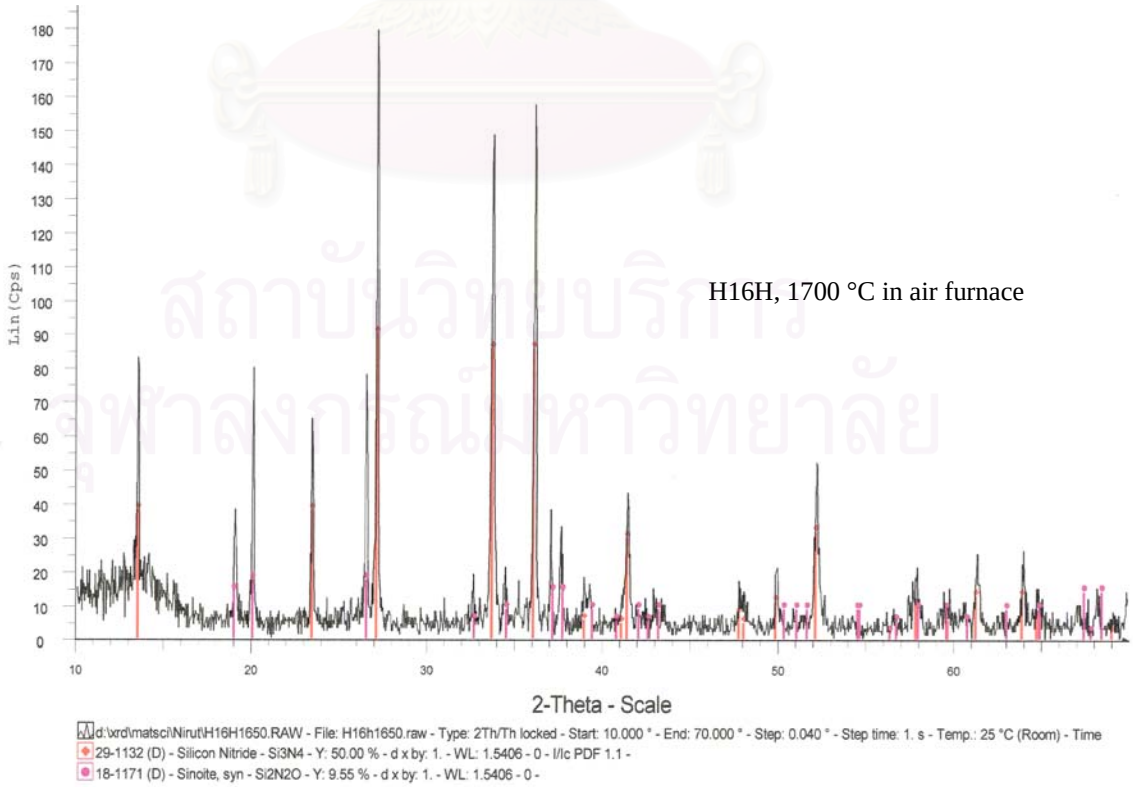

H16H, 1700 °C in air furnace

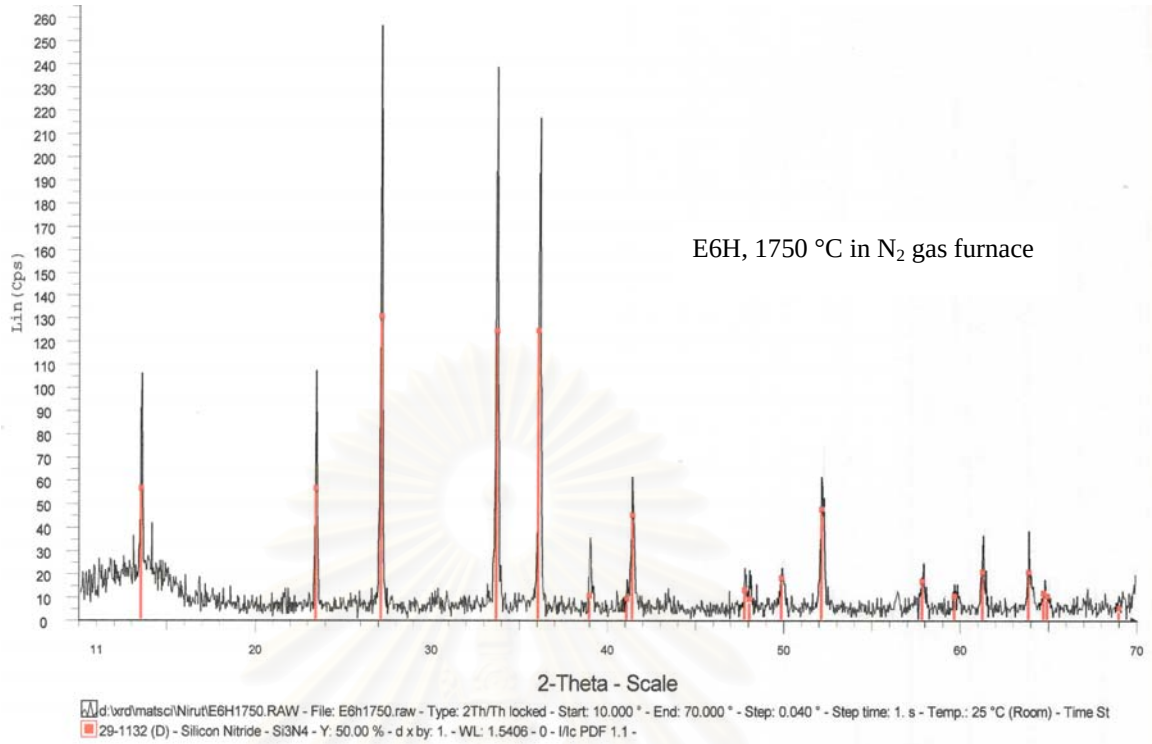

E6H, 1750 °C in N_2 gas furnace

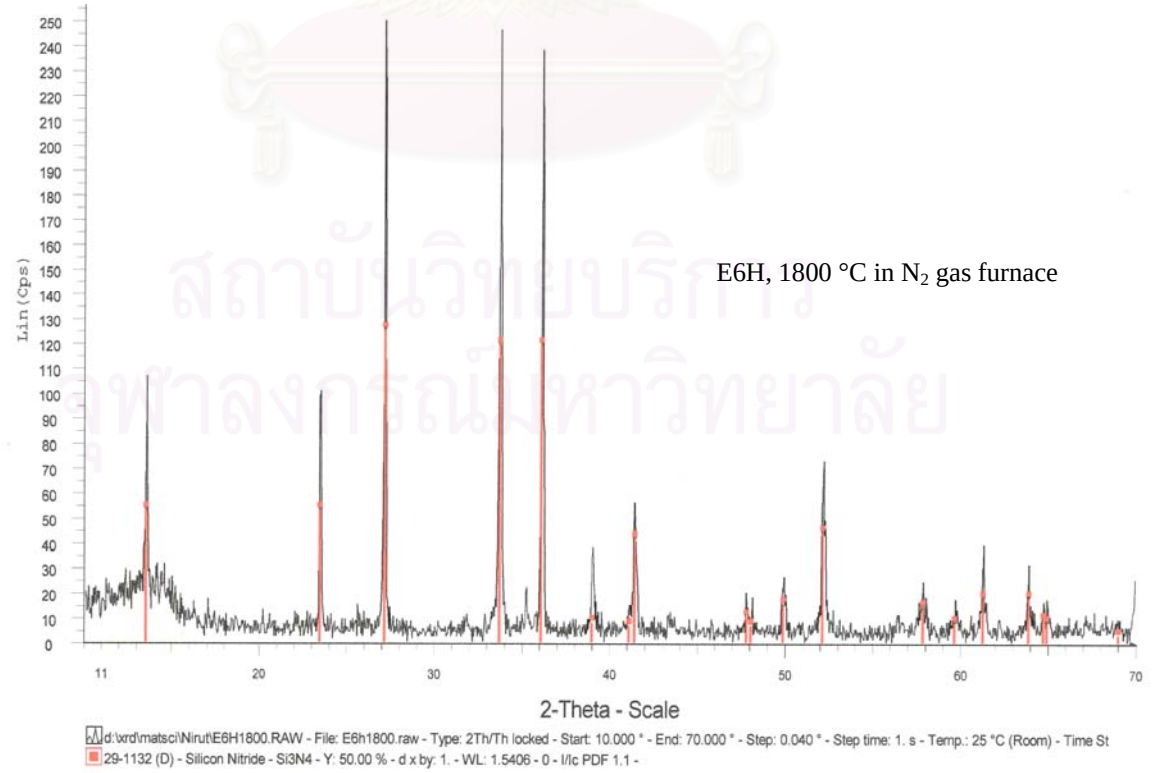

E6H, 1800 °C in N_2 gas furnace

Appendix F

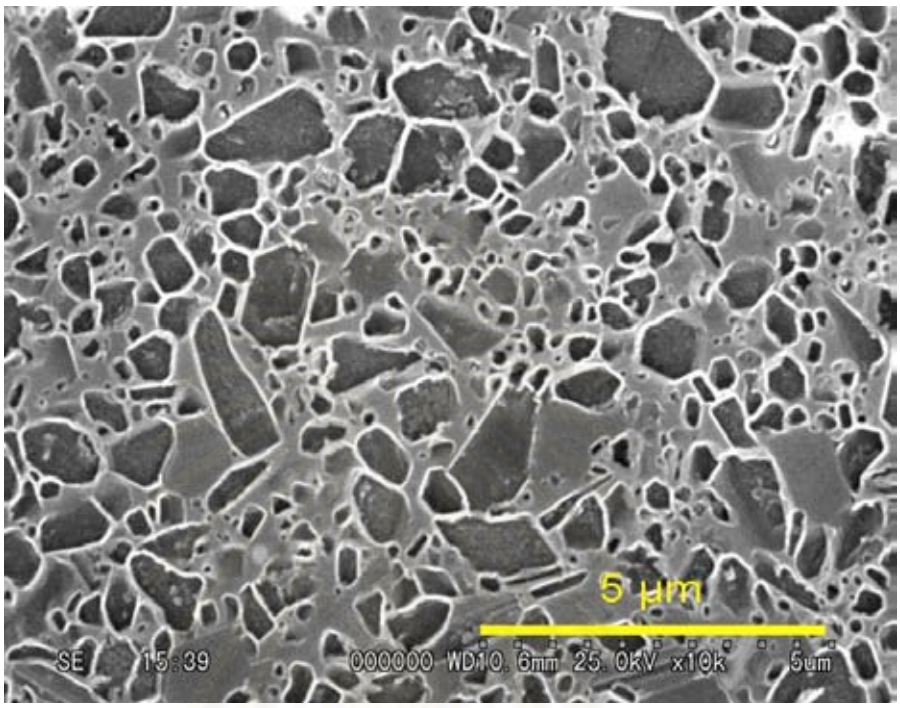

(a)

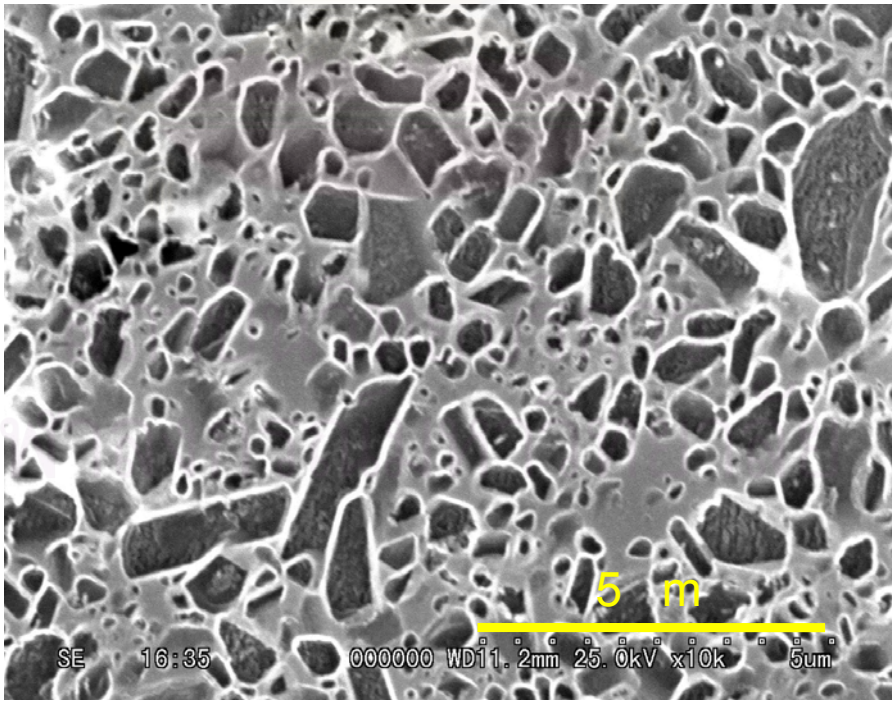

(b)

Fig F-1 SEM micrograph of E8H specimens sintered in air furnace at various temperatures; (a) 1550 °C, (b) 1600 °C

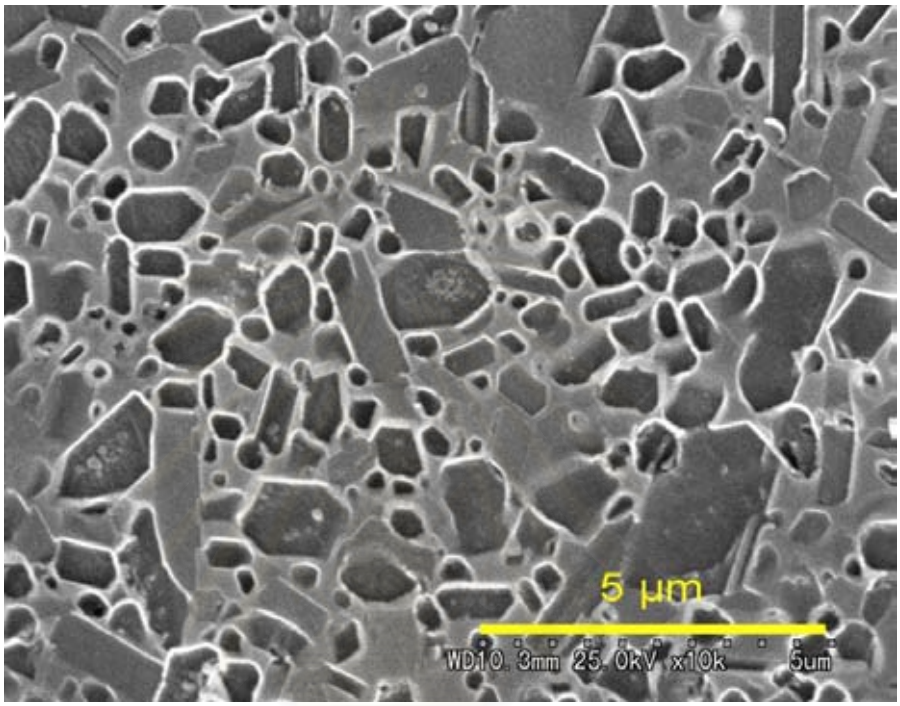

(c)

Fig F-1 (cont.) SEM micrograph of E8H specimens sintered in air furnace at various temperature; (c) 1700 °C

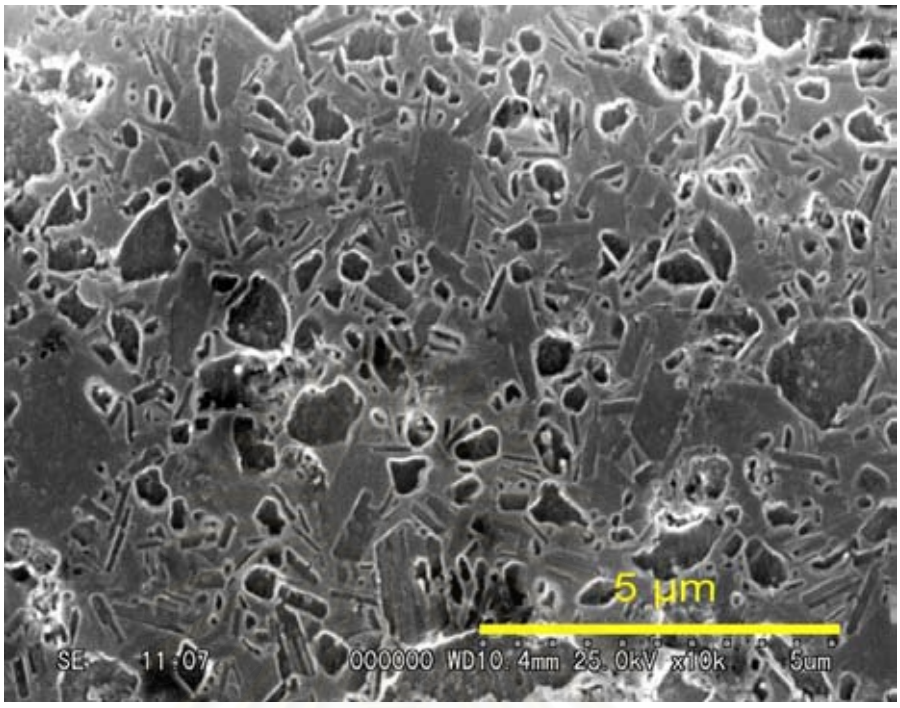

(a)

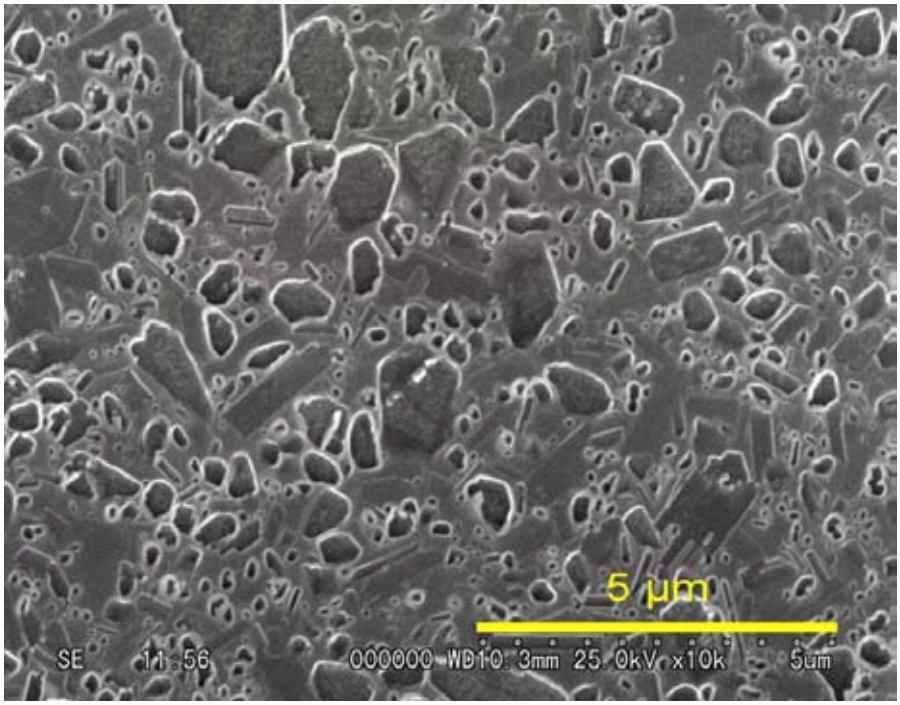

(b)

Fig F-2 SEM micrograph of H16H specimens sintered in air furnace at various temperature; (a) 1550 °C, (b) 1600 °C

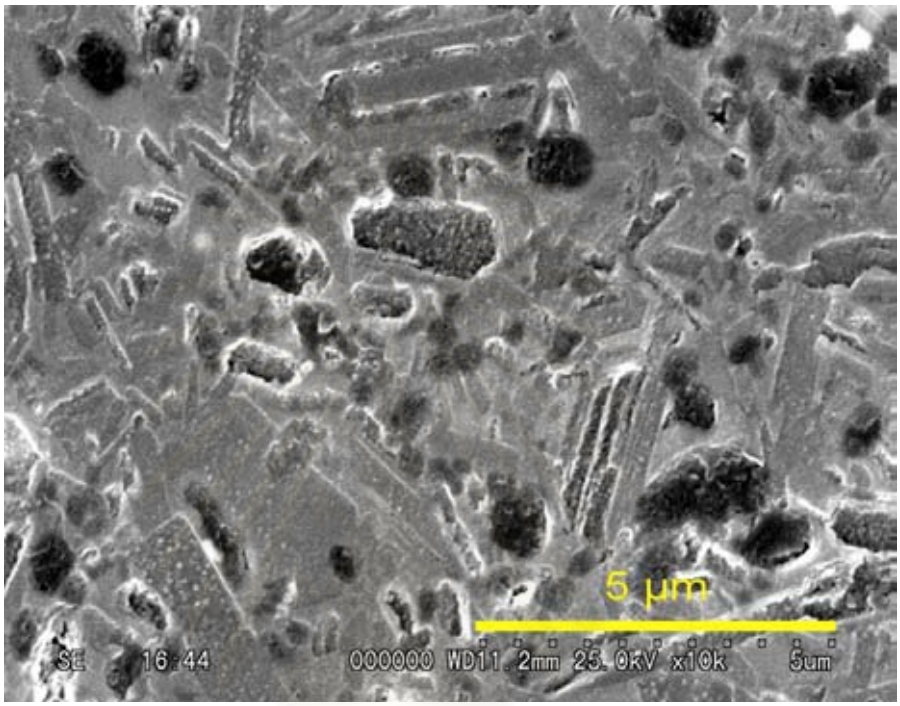

(c)

Fig F-2 (cont.) SEM micrograph of H16H specimens sintered in air furnace at various temperature; (c) 1700 °C

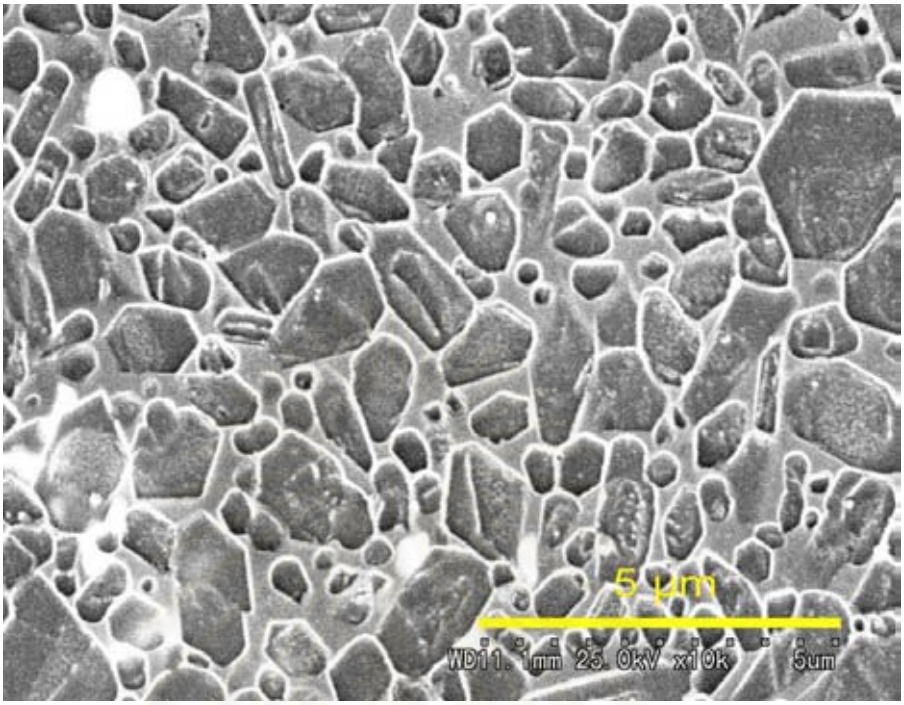

(a)

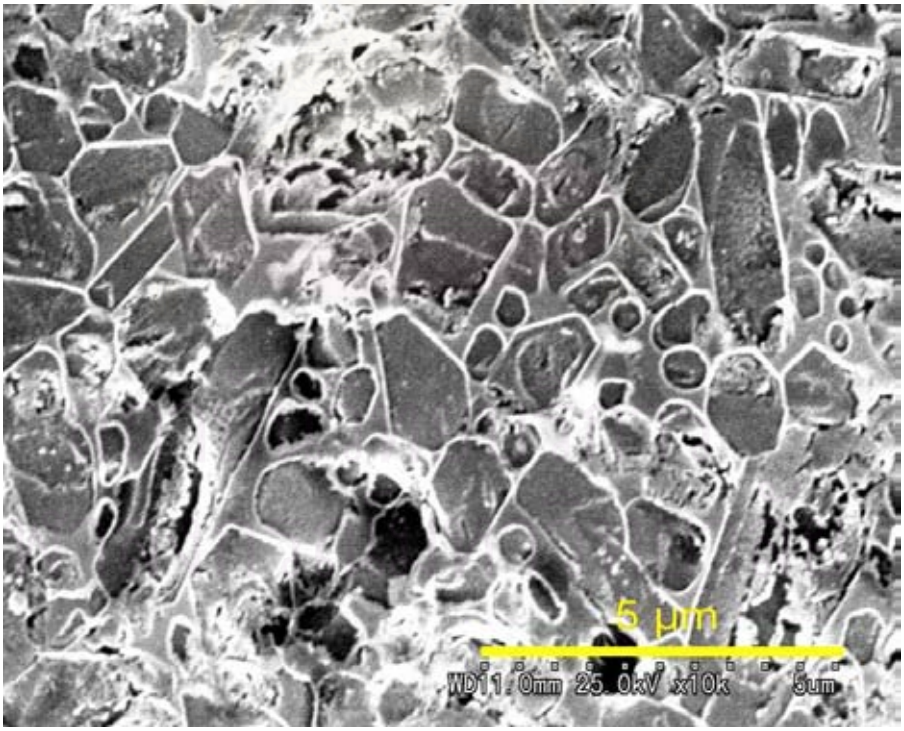

(b)

Fig F-3 SEM micrograph of E4H specimens sintered in N_2 gas furnace; (a) 1750 °C, (b) 1800 °C

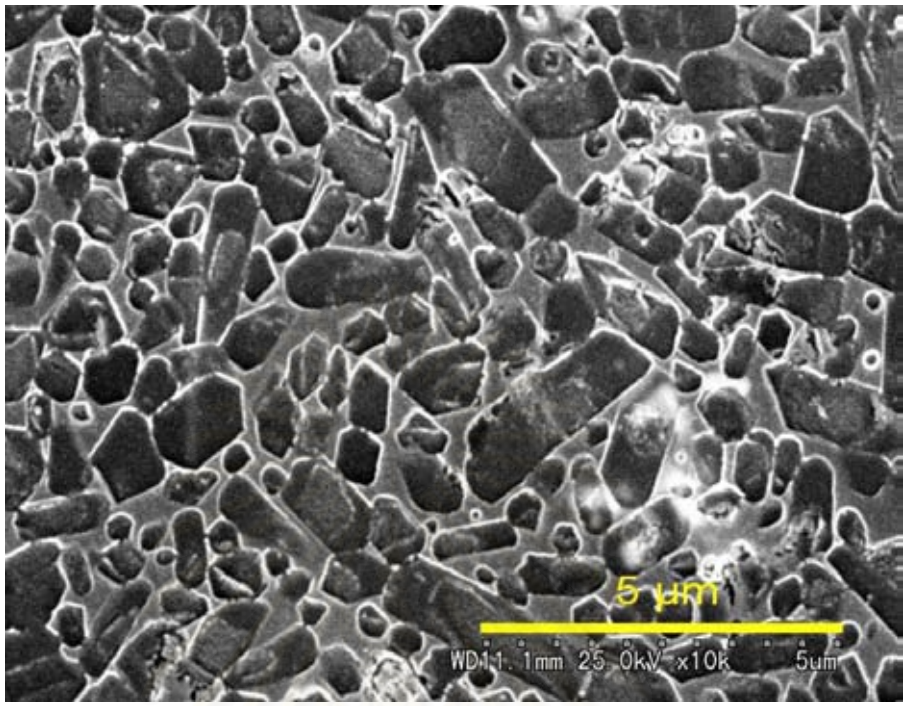

(a)

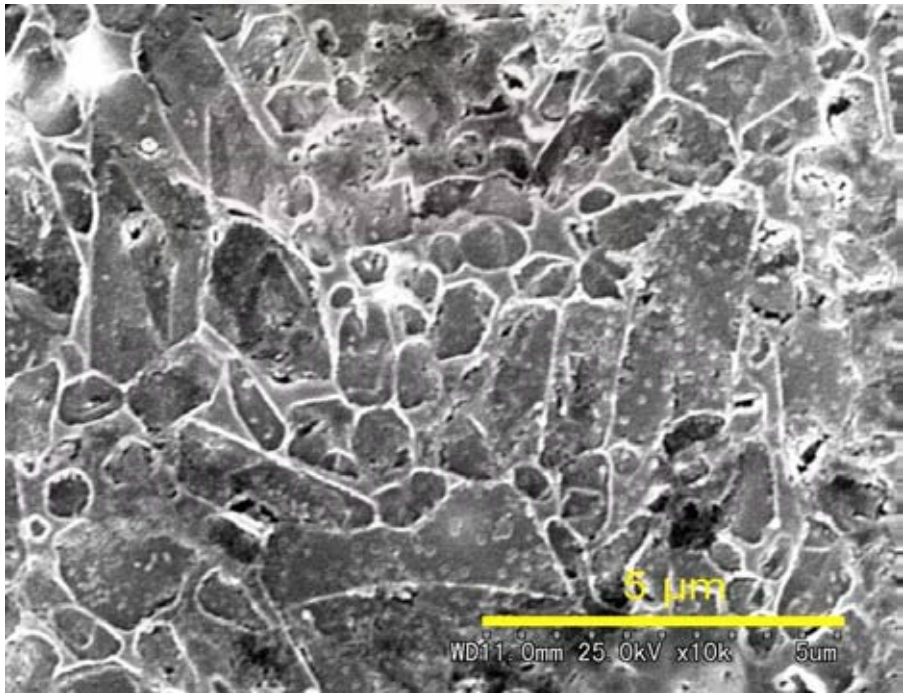

(b)

Fig F-4 SEM micrograph of E6H specimens sintered in N_2 gas furnace; (a) 1750 °C, (b) 1800 °C

Appendix G

Table G-1 Results of fracture toughness (K_{IC}) and Vickers hardness (Hv) of sintered specimens at 1700 ^{O}C for 2 h, in air furnace.

Sample code	Sample No. (Piece)	2a (μm)	C (μm)	Hv (GPa)	K_{IC} (MPa $m^{1/2}$)
E4H	1	119.33	125.90	12.8	6.1
	2	118.76	122.06	12.9	6.3
	3	119.76	129.74	12.7	5.8
	4	120.86	127.55	12.5	6.0
	5	120.31	141.37	12.6	5.1
Average				12.7	5.9
S.D.				0.2	0.4
E6H	1	117.76	122.52	13.1	6.2
	2	120.45	125.46	12.5	6.1
	3	118.05	120.39	13.1	6.4
	4	117.36	127.46	13.2	5.8
	5	118.64	129.60	12.9	5.8
Average				13.0	6.1
S.D.				0.3	0.3
E8H	1	121.05	138.25	12.4	5.3
	2	120.86	133.25	12.5	5.6
	3	118.83	135.44	12.9	5.4
	4	118.98	135.18	12.8	5.4
	5	119.62	134.37	12.7	5.5
Average				12.7	5.5
S.D.				0.2	0.1

Table G-2 Results of fracture toughness (K_{IC}) and Vickers hardness (Hv) of sintered specimens at 1750 ^{O}C for 2 h, in N_2 furnace.

Sample code	Sample No. (Piece)	2a (μm)	C (μm)	Hv (GPa)	K_{IC} (MPa $m^{1/2}$)
E4H	1	117.45	113.30	13.2	7.0
	2	116.93	113.01	13.3	7.0
	3	116.36	112.67	13.4	7.0
	4	116.17	107.45	13.5	7.5
	5	117.00	130.88	13.3	5.6
Average				13.3	6.8
S.D.				0.1	0.7
E6H	1	113.90	122.46	14.0	6.0
	2	115.64	113.58	13.6	6.8
	3	115.14	114.60	13.7	6.7
	4	115.17	117.19	13.7	6.5
	5	115.45	121.20	13.6	6.2
Average				13.7	6.5
S.D.				0.2	0.3
E8H	1	116.74	130.31	13.3	5.6
	2	116.00	119.38	13.5	6.4
	3	116.67	120.52	13.4	6.3
	4	117.38	121.85	13.2	6.3
	5	115.86	126.30	13.5	5.9
Average				13.4	6.1
S.D.				0.1	0.3

Table G-3 Results of fracture toughness (K_{IC}) and Vickers hardness (Hv) of sintered specimens at 1800 ^{O}C for 2 h, in N_2 furnace.

Sample code	Sample No. (Piece)	2a (μm)	C (μm)	Hv (GPa)	K_{IC} (MPa $m^{1/2}$)
E4H	1	115.98	115.05	13.5	6.7
	2	113.64	110.39	14.1	7.0
	3	115.29	115.94	13.7	6.6
	4	115.31	130.65	13.7	5.5
	5	117.64	110.90	13.1	7.2
Average				13.6	6.6
S.D.				0.3	0.7
E6H	1	115.05	114.27	13.7	6.8
	2	114.91	122.22	13.8	6.1
	3	114.95	130.92	13.8	5.5
	4	114.25	106.37	13.9	7.5
	5	115.09	119.86	13.7	6.3
Average				13.8	6.4
S.D.				0.1	0.7
E8H	1	114.39	114.17	13.9	6.7
	2	121.04	113.94	12.4	7.1
	3	115.52	112.55	13.6	6.9
	4	115.66	116.09	13.6	6.6
	5	115.05	115.78	13.7	6.6
Average				13.5	6.8
S.D.				0.6	0.2

Calculation results of specimens sintered in air and N_2 atmosphere furnace

The calculation results of biaxial flexural strength were calculated using the equation as follows:

$$S = \frac{-0.2387P \times (X - Y)}{d^2}$$

Table G-4 Calculation results of biaxial flexural strength (S) of specimens sintered at 1650 °C for 2 h, in air furnace

Sample code	Sample number	Diameter (mm)	Thickness (mm)	X	Y	d^2 (mm^2)	P (N)	S (MPa)
E10H	1	26.84	1.321	-4.121	1.723	1.745	292.2	234
	2	26.84	1.321	-4.121	1.723	1.745	274.8	220
	3	26.84	1.321	-4.121	1.723	1.745	250.4	200
	4	26.84	1.321	-4.121	1.723	1.745	241.3	193
	5	26.84	1.321	-4.121	1.723	1.745	251.8	201
	6	26.84	1.321	-4.121	1.723	1.745	387.6	310
	7	26.84	1.321	-4.121	1.723	1.745	263.8	211
	8	26.84	1.321	-4.121	1.723	1.745	245.7	196
	9	26.84	1.321	-4.121	1.723	1.745	259.4	207
Average								219
S.D.								36

Table G-5 Calculation results of biaxial flexural strength (S) of specimens sintered at 1700 °C for 2 h, in air furnace

Sample code	Sample number	Diameter (mm)	Thickness (mm)	X	Y	d^2 (mm^2)	P (N)	S (MPa)
E4H	1	27.88	1.475	-4.215	1.581	2.176	358.8	228
	2	27.88	1.475	-4.215	1.581	2.176	409.5	260
	3	27.95	1.466	-4.222	1.570	2.149	319.3	205
	4	28.18	1.474	-4.242	1.541	2.173	431.4	274
	5	27.95	1.475	-4.219	1.576	2.176	370.8	236
	6	27.95	1.461	-4.222	1.570	2.135	345.0	223
Average								238
S.D.								25
E6H	1	27.75	1.456	-4.167	1.602	2.120	342.9	223
	2	27.68	1.475	-4.197	1.608	2.176	408.6	260
	3	27.63	1.471	-4.192	1.616	2.164	521.3	334
	4	27.73	1.471	-4.201	1.602	2.164	419.8	269
	5	27.93	1.462	-4.219	1.576	2.137	351.7	228
Average								263
S.D.								45
E8H	1	27.73	1.472	-4.201	1.602	2.167	393.5	252
	2	27.55	1.469	-4.186	1.624	2.158	374.8	241
	3	27.50	1.468	-4.181	1.632	2.155	306.9	198
	4	27.55	1.466	-4.186	1.624	2.149	352.7	228
	5	27.48	1.460	-4.179	1.635	2.132	424.6	276
	6	27.48	1.433	-4.179	1.635	2.053	474.0	320
Average								252
S.D.								42

Table G-6 Calculation results of biaxial flexural strength (S) of specimens sintered at 1750 °C and 1800 °C for 2 h, in air furnace

Sintering at 1750 °C for 2 h								
Sample code	Sample number	Diameter (mm)	Thickness (mm)	X	Y	d^2 (mm^2)	P (N)	S (MPa)
E4H	1	26.90	2.407	-4.126	1.715	5.794	1647.0	396
	2	26.62	2.415	-4.100	1.755	5.832	1734.0	416
Average								406
S.D.								14
E6H	1	26.62	2.474	-4.100	1.755	6.121	1585.0	362
	2	26.70	2.475	-4.108	1.743	6.126	1285.0	293
Average								327
S.D.								49
E8H	1	27.15	2.408	-4.149	1.680	5.798	1343.0	322
	2	26.70	2.443	-4.108	1.743	5.968	1751.0	410
	3	27.00	2.405	-4.135	1.701	5.784	1050.0	253
Average								328
S.D.								79
Sintering at 1800 °C for 2 h								
Sample code	Sample number	Diameter (mm)	Thickness (mm)	X	Y	d2 (mm2)	P (N)	S (MPa)
E4H	1	26.98	2.369	-4.133	1.704	5.612	1369.0	340
	2	26.80	2.362	-4.117	1.729	5.579	1097.0	274
Average								307
S.D.								46
E6H	1	26.65	2.427	-4.103	1.750	5.890	1205.0	286
	2	26.56	2.357	-4.094	1.763	6.126	1039.0	237
Average								261
S.D.								34
E8H	1	26.42	2.450	-4.081	1.784	6.003	1683.0	393
	2	26.52	2.383	-4.091	1.769	5.679	1836.0	452
	3	26.48	2.413	-4.087	1.775	5.823	1354.0	325
Average								390
S.D.								63

Appendix H

Properties of TOSHIBA's specimen (standard bar)

1. Chemical composition

Composition (mass %)				
Si_3N_4	$MgAl_2O_4$	SiC	SiO_2	TiO_2
88.9	4.3	5.0	0.9	0.9

2. Estimated real density: 3.23 g/cm^3

   Densities of Si_3N_4, $MgAl_2O_4$, SiC, SiO_2, and TiO_2 are 3.21, 3.60, 3.22, 2.20 and 4.25 g/cm^3, respectively.

3. Bulk density and relative density

   Measured bulk density was 3.19 g/cm^3. Then, relative density is 98.8 %

4. Vickers' Hardness

   16.8 GPa

5. Fracture Toughness

   5.4 (MPa.m$^{1/2}$)

6. Young's Modulus, E = 300 GPa.

BIOGRAPHY

Mr. Nirut Wangmooklang was born in Nakhonratchasima on 24th November 1977. He was received a Bachelor's Degree in Chemistry from Faculty of Science and Technology, Rajabhat Institute Bansomdejchaopraya in 2001. During his Bachelor study, he was also working at Siam Research and Development Co. Ltd. After working for 3 years, he continued studying in Master's Degree in the field of Ceramic Technology at Chulalongkorn University and graduated in April 2004.